

Towards a Generalized Framework for the Analysis of Solar Cell Performance based on the Principle of Detailed Balance

Beatrix Johanna Blank

Energie & Umwelt / Energy & Environment

Band / Volume 522

ISBN 978-3-95806-514-7

Forschungszentrum Jülich GmbH
Institut für Energie- und Klimaforschung
IEK-5 Photovoltaik

Towards a Generalized Framework for the Analysis of Solar Cell Performance based on the Principle of Detailed Balance

Beatrix Johanna Blank

Schriften des Forschungszentrums Jülich
Reihe Energie & Umwelt / Energy & Environment

Band / Volume 522

ISSN 1866-1793

ISBN 978-3-95806-514-7

Bibliografische Information der Deutschen Nationalbibliothek.
Die Deutsche Nationalbibliothek verzeichnet diese Publikation in der
Deutschen Nationalbibliografie; detaillierte Bibliografische Daten
sind im Internet über <http://dnb.d-nb.de> abrufbar.

Herausgeber und Vertrieb: Forschungszentrum Jülich GmbH
Zentralbibliothek, Verlag
52425 Jülich
Tel.: +49 2461 61-5368
Fax: +49 2461 61-6103
zb-publikation@fz-juelich.de
www.fz-juelich.de/zb

Umschlaggestaltung: Grafische Medien, Forschungszentrum Jülich GmbH

Druck: Grafische Medien, Forschungszentrum Jülich GmbH

Copyright: Forschungszentrum Jülich 2020

Schriften des Forschungszentrums Jülich
Reihe Energie & Umwelt / Energy & Environment, Band / Volume 522

D 82 (Diss. RWTH Aachen University, 2019)

ISSN 1866-1793
ISBN 978-3-95806-514-7

Vollständig frei verfügbar über das Publikationsportal des Forschungszentrums Jülich (JuSER)
unter www.fz-juelich.de/zb/openaccess.



This is an Open Access publication distributed under the terms of the [Creative Commons Attribution License 4.0](https://creativecommons.org/licenses/by/4.0/), which permits unrestricted use, distribution, and reproduction in any medium, provided the original work is properly cited.

” *Nothing in life is to be feared, it is only to be understood. Now is the time to understand more, so that we may fear less.*

— **Marie Curie**

Contents

Kurzfassung	1
Abstract	5
1 Introduction	7
2 Theoretical Background	13
2.1 Working Principle of Solar Cells	13
2.1.1 Band Diagram	14
2.1.2 Charge Separation in Organic Solar Cells	14
2.1.3 Current-Voltage Characteristic	16
2.2 Shockley-Queisser Model - The Ideal Solar Cell	18
2.3 Würfel's Generalization of Planck's Law	19
2.4 Opto-Electronic Reciprocity	19
2.5 Electron Transfer Theories	20
2.5.1 Miller-Abrahams Model	21
2.5.2 Marcus Theory	21
3 The Solar Cell Described by External Parameters	25
3.1 Quantifying Voltage Losses	26
3.1.1 Challenges and Limitations	28
3.2 Generalization Across Different Technologies	31
3.2.1 Distribution of Shockley-Queisser Band Gap Energies	33
3.2.2 Photovoltaic Band Gap Definition	34
3.2.3 Radiative Ideality Factors $n_{\text{rad}} > 1$	38
3.3 Application to Various Photovoltaic Technologies	40

3.4	Voltage vs. Efficiency Losses	44
3.5	Summary and Outlook	45
4	Efficiency Limits of New Absorber Materials	47
4.1	From Internal to External Parameters	48
4.1.1	Model - Consistent with Detailed Balance	49
4.1.2	State-of-the-Art Model by Yu and Zunger	54
4.2	Model Comparison	56
4.2.1	Impact of Thickness on Conversion Efficiency	58
4.2.2	Impact of the Internal Luminescence Quantum Efficiency on the Maximum Conversion Efficiency	62
4.2.3	Impact of the Refractive Index on the Maximum Conversion Efficiency	65
4.2.4	Towards a Meaningful Selection Metric	67
4.3	Selection Metric for Photovoltaic Absorber Materials Screen- ing	68
4.3.1	Recipe for Calculating Efficiency Limits	68
4.3.2	Application to Calculated Material Properties	69
4.3.3	Limitations and Outlook	73
4.4	Summary	74
5	The Organic Solar Cell Described by Internal Parameters	77
5.1	Introduction to the Rate Model	78
5.2	Occupation Probability of Charge Transfer States	83
5.2.1	Occupation According to Miller-Abrahams Transfer Rates	85
5.2.2	Occupation According to Marcus Transfer Rates	88
5.3	Superposition of Electro- and Photoluminescence	93
5.4	Opto-Electronic Reciprocity	94
5.5	Collection Efficiency	97
5.5.1	Definition of the Capture, Transfer and Collection Efficiency	99
5.5.2	Analysis of the Transfer Efficiency	102
5.5.3	Analysis of the Capture Efficiency	104
5.6	Summary and Outlook	109
6	Conclusion and Outlook	113

Bibliography	117
Appendix	129
List of Symbols	131
List of Publications	137
Acknowledgements	139

Kurzfassung

Die theoretische Grundlage dieser Arbeit bildet das Prinzip der detaillierten Bilanz. Es besagt, dass im thermodynamischen Gleichgewicht alle mikroskopischen Prozesse im Gleichgewicht mit ihren entsprechenden entgegengerichteten Prozessen sind. Für Solarzellen im thermodynamischen Gleichgewicht bedeutet dies zum Beispiel, dass die gleiche Anzahl von Photonen absorbiert und emittiert werden. Shockley und Queisser benutzen dieses Prinzip, um ein theoretisches Effizienzlimit einer Solarzelle mit einer bestimmten Bandlückenenergie zu berechnen. Für diese idealisierte Solarzelle nehmen sie an, dass alle Photonen mit Energien größer als diese Bandlückenenergie absorbiert werden und unterhalb der Bandlückenenergie die Absorption gleich null ist. Echte Materialien zeigen jedoch keine derart scharfe Absorptionskante. Für die verschiedenen Solarzellentechnologien gibt es unterschiedliche Konventionen die Bandlückenenergie zu bestimmen. Die auf diese Weise bestimmte Bandlückenenergie wird dann beispielsweise benutzt, um die Verlustmechanismen einer Solarzelle im Vergleich zu der idealen Solarzelle nach Shockley und Queisser zu quantifizieren.

In dieser Arbeit wird eine Vorgehensweise zur einheitlichen Bestimmung der Bandlückenenergie für alle Solarzellentechnologien vorgestellt, die auf der Theorie von Shockley und Queisser basiert. Diese Methode beruht auf der mathematischen Definition einer Verteilung von Bandlückenenergien, die einzig aus der externen Quanteneffizienz der Solarzelle berechnet wird. Diese sogenannte Shockley-Queisser-Bandlücke wird dann benutzt, um Spannungsverluste im Vergleich zur

idealen Solarzelle zu berechnen. Da die Shockley-Queisser-Bandlücke nicht von internen Materialeigenschaften bestimmt wird, ermöglicht diese externe Definition der Bandlückenenergie den konsistenten Vergleich von Verlustmechanismen für alle Solarzelltechnologien.

Um das Effizienzlimit basierend auf internen Materialeigenschaften des Absorbers zu berechnen, müssen externe Solarparameter, z.B. der Kurzschlussstrom, mit internen Materialeigenschaften, z.B. dem komplexen Brechungsindex, verknüpft werden. Diese Materialeigenschaften können sowohl mittels first-principle Simulationen als auch experimentell ermittelt werden. Das aktuelle Modell von Yu und Zunger, das aus Absorptionsspektren des Absorbermaterials ein Effizienzlimit einer entsprechenden Solarzelle berechnet, ist jedoch nicht kompatibel mit dem Prinzip der detaillierten Bilanz. In der vorliegenden Arbeit wird gezeigt, dass auch der Brechungsindex berücksichtigt werden muss, um Kompatibilität mit dem Prinzip der detaillierten Bilanz herzustellen. Ein entsprechendes Modell wird aufgestellt und eine Selektionsmetrik für computerbasiertes Vorab-Materialscreening wird entwickelt. Diese Selektionsmetrik wird dann auf verschiedene Materialdaten angewandt. Das in dieser Arbeit ermittelte Effizienzlimit unterscheidet sich bis zu 20 Prozent vom aktuell gebräuchlichen Modell.

Nachdem die Solarzelle zunächst nur aus externer Sicht beschrieben wurde und ein Modell vorgestellt wurde, um interne mit externen Parametern zu verknüpfen, werden zuletzt ausschließlich interne Prozesse der organischen Solarzelle betrachtet. Wegen der für organische Materialien typischerweise niedrigen Dielektrizitätskonstante sind die Elektron-Lochpaare stark gebunden und werden als Exzitonen bezeichnet. Um Exzitonen effizient zu teilen, ist ein weiterer elektronischer Zustand nötig, der Charge-Transfer-Komplex. Basierend auf dem Prinzip der detaillierten Bilanz wird ein 0-dimensionales Ratenmodell beschrieben, welches diesen zusätzlichen Zustand berücksichtigt. Es wird gezeigt, dass für dieses Modell die Superposition der Elektro- und Photolumineszenz sowie das opto-elektronische Reziprozitätstheorem

der Solarzelle gültig sind, solange keine Sättigungseffekte auftreten. Die Besetzungsverteilung des Charge-Transfer-Komplexes sowie die Sammlungseffizienz der Ladungsträger wird im Detail betrachtet für Transferraten, die sowohl entsprechend des Miller-Abrahams Modells als auch basierend auf der Marcus Theorie beschrieben werden.

Abstract

The principle of detailed balance forms the basis of the present thesis. It states that all microscopic processes in thermodynamic equilibrium are equal to their respective counter processes. For solar cells in thermodynamic equilibrium, for example, as many photons get absorbed by the cell as are emitted. Shockley and Queisser used this principle to determine a theoretical conversion efficiency limit for a solar cell with a given band gap energy, using additionally the assumption that all photons with energies higher than the band gap energy are absorbed and that there is zero absorption below the band gap energy. This so-called step-function in absorption is one of the idealizations of the model as no material shows this kind of sharp absorption edge. There are different conventions on how to quantify the band gap energy, each of which is preferentially used in different solar cell technology communities. This band gap energy, for instance, is used to quantify losses that occur in the solar cell with respect to the ideal solar cell after Shockley and Queisser.

This thesis introduces a procedure based on the theory of Shockley and Queisser to determine the band gap energy that is applicable to all technologies. It is derived from a mathematical definition of a distribution of band gap energies that is calculated solely from the external quantum efficiency of the solar cell. This so-called Shockley-Queisser band gap energy is then used to quantify voltage loss mechanisms with respect to the ideal case. Because the Shockley-Queisser band gap energy is not determined from internal material properties, it allows

for the comparison of these loss mechanisms consistently throughout all solar cell technologies.

In contrast, to determine the efficiency potential of theoretical materials generated via first-principle calculations it is necessary to deduce external solar cell parameters such as the short-circuit current from internal material properties such as the complex refractive index. The state-of-the-art model by Yu and Zunger used to determine efficiency limits from computationally or experimentally derived absorption spectra, however, is not compatible with the principle of detailed balance. In the present thesis it is shown that the refractive index must be taken into account in order to achieve compatibility with the principle of detailed balance. A consistent model is described and a selection metric for computational high-throughput materials screening is developed. This selection metric is then applied to a variety of materials. The efficiency potential is shown to differ from the state-of-the-art model by up to 20 %.

After looking at the solar cell solely from the outside and establishing a model that connects internal and external parameters, the final topic in the thesis is dedicated to modelling the organic solar cell exclusively by internal means. Due to the low dielectric constants typical of organic materials, the generated electron-hole pairs are found as strongly bound excitons. To efficiently split these excitons an additional state is needed, namely the charge transfer state. Based on the principle of detailed balance a 0-dimensional rate model is described that accounts for this extra electronic state. It is shown that for this model both the superposition of electro and photoluminescence and the opto-electronic reciprocity theorem by Rau hold under non-saturation conditions. The occupation of the charge transfer state as well as the collection efficiency are thoroughly discussed for the transfer rate models according to both the Miller-Abrahams and Marcus theory.

Introduction

“ *Classical thermodynamics ... is the only physical theory of universal content which I am convinced ... will never be overthrown.*

— **Albert Einstein**

The laws of thermodynamics are undoubtedly one of the most important laws in physics and have led to innumerable discussions not only among physicists but also among other natural scientists, philosophers and economists.¹⁻¹¹ Thermodynamics sets physical processes an efficiency limit, and because everything is based on physical processes – as a physicist I am allowed to have this opinion – it inevitably leads to the question as to whether thermodynamics sets a limit to everything we know in this world.

Life would not be possible if it were not for the second law of thermodynamics. How could we survive, if our blood would all a sudden accumulate in our small toe? Or if all the heat on Earth would accumulate in our living room? The second law forbids this spontaneous accumulation of heat or blood cells. It states that in absence of an external influence on the system every gradient of a physical variable, e.g. temperature, pressure or concentration, becomes minimal over time or as Boltzmann¹² expresses it: every system tends towards its most probable state. This state is the state of thermodynamic equilibrium, where the principle of detailed balance holds, i.e. every process is counterbalanced by its reverse process. However, this state is equal to

death. In other words, we need gradients in our body to be alive. If our blood pressure would be equal everywhere in our body it would stop circulating. Therefore, the second law of thermodynamics allows for life but at the same time promotes its inevitable death. This has been an argument for biologist, evolutionist and some philosophers to argue that the second law is flawed and does not hold for living organisms.⁵ Their arguments neglect, however, that living organisms need an external source of energy to survive, to fight every moment against its tendency towards thermodynamic equilibrium.^{13,14} For plants, that external source of energy is sunlight and plants in turn provide energy for animals. To conclude, according to the laws of thermodynamics life without an external energy source would not be possible. On Earth, this energy source is the sun's light.

An analogous conclusion has been drawn in the field of economics. Georgescu-Roegen⁷ is widely considered to be the most influential writer to address the importance of thermodynamics in economics. He and other economists argued that any economic process is a physical process and therefore brings the Earth one step closer to thermodynamic equilibrium - the heat death. Consequently, any economic action on Earth inevitably puts a burden at the expense of future generations.¹⁵⁻¹⁷ Whereas many economists argue that thermodynamics does not (yet) limit our economic growth, but that it is the "fragility of self organized natural cycles that we have to fear"¹⁸ they all come to a similar conclusion: The use of solar energy for economic processes is an absolute prerequisite for a sustainable economic status.¹⁸⁻²¹ The device that converts solar energy into electrical energy and therefore makes solar energy directly usable for industrial purposes is the solar cell.

Unsurprisingly, the efficiency of a solar cell itself is limited by thermodynamics. The first scientists to determine an efficiency limit for solar cells based on thermodynamic principles were Shockley and Queisser in the early 1950s.²² They concluded that the maximal conversion efficiency for any solar cell cannot exceed 30 %. For more than a decade

the relevance and potential of this paper remained unnoticed with less than 20 citations per year. Nevertheless, it eventually became one of the highest cited articles in the field of photovoltaics, reaching up to 30.000 citations a year. Shockley and Queisser idealized the solar cell by assuming perfect absorption above a certain threshold energy, the band gap energy, and perfect carrier collection, i.e. every generated electron-hole pair is collected at the contacts. While the simplicity of their approach is captivating, this simplicity is both its strength and weakness at the same time. According to their assumptions, the solar cell has to be infinitely thick (perfect absorption) and yet infinitely thin (perfect charge carrier collection), conditions which cannot be satisfied by any real device.

A generalization of the Shockley-Queisser model for real devices is provided by the opto-electronic reciprocity relation by Rau.²³ Here instead of perfect absorption and collection, the real quantum efficiency of a solar cell is used. The quantum efficiency is defined as the number of charge carriers that are collected per impinging photon as a function of energy. It connects the quantum efficiency with the luminescence efficiency, i.e. the efficiency of the same device operated as a light emitting diode. This reciprocity between absorption and emittance is derived by a linear extrapolation from thermodynamic equilibrium using what is already known under equilibrium: the principle of detailed balance holds.

The idea of a thermodynamic limit, the extrapolation from detailed balance to steady-state condition and the objection of finding a common framework for all solar cell technologies, as provided by the Shockley-Queisser model, are the central ingredients of the current thesis. The Shockley-Queisser model is nowadays excessively used to evaluate a solar cell's performance by quantifying the difference between the real device and the idealized solar cell's efficiency or voltage. However, inevitably the question arises as to how to determine the band gap of the idealized reference solar cell. In principle the band gap is an internal material property with different measurement standards for different

material classes, i.e. solar cell technologies. In the Shockley-Queisser model, however, it is an external parameter of a device. In **Chapter 3**, a new functional definition of the Shockley-Queisser band gap for real devices is developed that follows directly from a generalization of the Shockley-Queisser model and is applicable to all solar cell technologies. This universal method is then readily applied to quantify the voltage and efficiency losses across different solar cell technologies. This method is therefore useful in evaluating the potential for improvement of existing devices.

In contrast, the following chapter concentrates on calculating efficiency limits for not yet existing absorber materials. In the rapidly emerging field of computational high-throughput materials screening for photovoltaic applications, internal material properties are calculated and evaluated for their potential use as a photovoltaic absorber material. A selection metric that provides a mapping from internal material properties to an efficiency limit is developed in **Chapter 4**. In contrast to the state-of-the-art method,²⁴ this selection metric is shown to be consistent with the principle of detailed balance. The newly developed metric connects internal parameters of a material with external parameters of a photovoltaic device in a self consistent way. The introduced selection metric uses the calculated absorption coefficient and the refractive index as input parameters, and it is computationally not demanding. Moreover, it is exemplarily applied to several materials in this thesis.

Last but not least, in **Chapter 5** a rate model is introduced to analyze the inside of organic solar cells. In organic devices light generates strongly bound electron-hole pairs so-called excitons. To efficiently split these excitons into free charges in contrast to inorganic devices an additional electronic state is needed. The rate model is designed to be as simple as possible, yet to include all known important electronic states in organic cells. It is once again based on the linear extrapolation from thermodynamic equilibrium using the principle of detailed balance. The impact of different parameters on the occupation probability and the collection efficiency is investigated in detail using two different

electron transfer theories. Moreover, the validity of the opto-electronic reciprocity for this model is shown for the case of non-saturation of electronic states.

Theoretical Background

“ *A theory must be tempered with reality.* ”

— **Jawaharlal Nehru**
(1st Prime Minister of India)

The solar cell is a semiconductor device that converts light into electrical energy. Starting by introducing its basic working principle, the thermodynamic efficiency limit of an ideal solar cell known as the Shockley-Queisser limit is described. The underlying principle is the principle of detailed balance that states that every process is counter-balanced by its reverse process in thermodynamic equilibrium. This principle is also the basis for Würfel’s generalization of Planck’s law and Rau’s opto-electronic reciprocity as outlined in Sections 2.3 and 2.4. The chapter closes with a description of two different electron transfer theories that are most commonly used in solar cell simulations.

2.1 Working Principle of Solar Cells

For many decades solar cells have been subject to intense research and their basic working principle is therefore thoroughly explained in many standard text books.^{25–27} With reference to these text books, the band diagram and the current-voltage characteristic of solar cells will only be briefly introduced without going into detail of underlying physical principles and derivations.

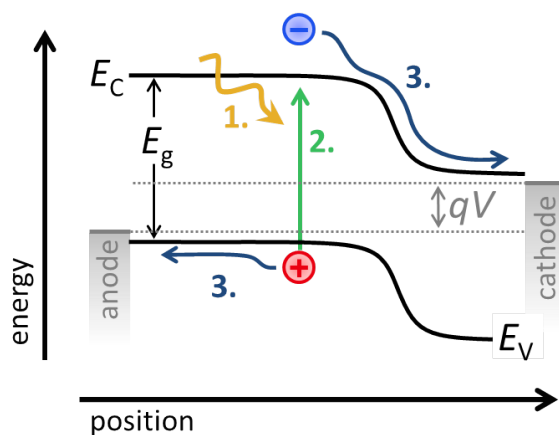


Fig. 2.1 Band diagram of a solar cell. The photon lifts an electron from the valence band with energy E_v into the conduction band with energy E_c . The band gap E_g is defined as $E_c - E_v$. Due to the internal electric field the electrons are collected at the cathode and the holes at the anode with the difference in energy of qV , where V is the applied voltage and q is the elementary charge.

2.1.1 Band Diagram

For a solar cell to convert the energy of a photon into electrical energy the photon has to: 1. enter the cell, 2. be absorbed and generate an electron-hole pair by lifting an electron from the valence band into the conduction band and 3. the electron and hole have to be extracted to the selective contacts. Figure 2.1 shows schematically these three processes in a band diagram. The band gap E_g is defined as the energy difference between the conduction and valence band $E_c - E_v$. The applied voltage is denoted with V and q is the elementary charge.

2.1.2 Charge Separation in Organic Solar Cells

In organic solar cells, the conduction band is the lowest unoccupied molecular orbital (LUMO) and the valence band is the highest occupied

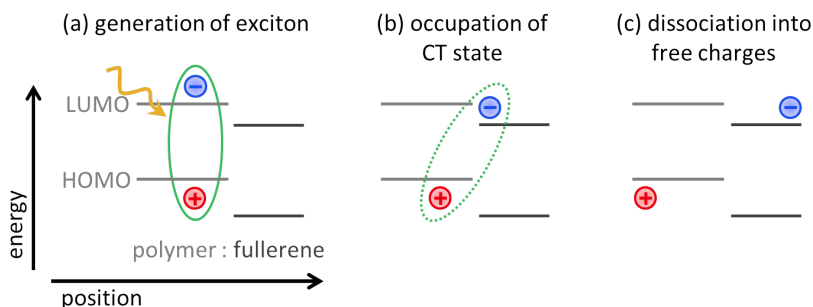


Fig. 2.2 Charge generation and separation in organic polymer:fullerene solar cells. The role of the conduction band is played by the lowest unoccupied molecular orbital (LUMO) and the role of the valence band by the highest occupied molecular orbital (HOMO).

molecular orbital (HOMO) of the organic semiconductor. If a photon lifts an electron from the HOMO into the LUMO an electron-hole pair is generated. However, this electron-hole pair is strongly bound because of the typically low dielectric constant in organic semiconductors and is called exciton.

To split an exciton a state is needed that is energetically favorable but at the same time separates the exciton spatially to decrease the attraction between the electron and the hole. This state is called charge transfer (CT) state. The efficiency of an organic solar cell is therefore directly connected to the CT state and its ability to split excitons efficiently. In chapter 5 a rate model is developed to simulate the characteristics of the CT state and discuss the effect of the involved kinetics on the charge collection efficiency in organic cells.

The charge transfer state is often realized by a two-material system where the electron jumps onto a second material while the hole remains in the material where it was generated. This process of charge separation is shown exemplarily for a polymer:fullerene solar cell in Figure 2.2.

2.1.3 Current-Voltage Characteristic

The electrical energy in our homes is supplied by the combination of electric current J and electric potential, i.e. voltage V . The basic current-voltage (JV) characteristic of an solar cell under illumination is described as

$$J = J_{sc} - J_0 \left[\exp\left(\frac{qV}{n_{id}kT_c}\right) - 1 \right]. \quad (2.1)$$

The net total electrical current J of the solar cell is equal to the generated photo current J_{sc} minus the diode current. The diode current follows the Shockley diode equation with the elementary charge q , Boltzmann constant k and the cell's temperature T_c . The ideality factor n_{id} of a cell is equal to unity for voltage-independent charge carrier collection and band-to-band recombination limited by minority carriers.

Saturation Current The saturation current J_0 is a measure of the recombination loss in the solar cell. This loss can be split into a radiative loss term J_0^{rad} and an non-radiative loss term J_0^{nrad} ,

$$J_0 = J_0^{\text{rad}} + J_0^{\text{nrad}}.$$

The radiative saturation current J_0^{rad} is the radiative emission current of the cell in thermodynamic equilibrium. Planck's law^{28,29} states that the spectrum that is emitted of a black body with constant and uniform temperature T that is in thermodynamic equilibrium with its environment is described by the black body radiation $\phi_{\text{bb}}(E_\gamma, T) = 2E_\gamma^2 h^{-3} c^{-2} [\exp(E_\gamma/kT) - 1]^{-1}$, where h denotes the Planck constant and c is the velocity of light in vacuum. According to Kirchoff's law³⁰ the absorptance A and emissivity as a function of angle and energy are equal. In thermodynamic equilibrium, the total emission of an arbitrary body is therefore equal to $A \phi_{\text{bb}}$ and hence the radiative saturation current is given by

$$J_0^{\text{rad}} = q \int_0^\infty A(E_\gamma) \phi_{\text{bb}}(E_\gamma) dE_\gamma. \quad (2.2)$$

Short-Circuit Current The generated photo current J_{sc} under short-circuit can be written as

$$J_{sc} = q \int_0^{\infty} Q_e^{PV}(E_\gamma) \phi_{sun}(E_\gamma) dE_\gamma. \quad (2.3)$$

This expression for J_{sc} follows directly from the definition of the external photovoltaic quantum efficiency Q_e^{PV} . The external quantum efficiency is defined as the number of charge carriers N_{e-} that are generated and collected at the contacts under short-circuit when a certain number of photons N_{ph} with energy E_γ impinge onto the cell divided by N_{ph} , i.e. $Q_e^{PV}(E_\gamma) = N_{e-}/N_{ph}(E_\gamma)$. The spectrum ϕ_{sun} denotes the number of impinging photons per energy interval and time.

Open-Circuit Voltage The voltage for which the recombination current is equal to the generation current, i.e. $J = 0$, is called the open-circuit voltage V_{oc} . Solving the diode equation (2.1) for V_{oc} yields

$$V_{oc} = \frac{n_{id}kT}{q} \ln \left(\frac{J_{sc}}{J_0} + 1 \right) \approx \frac{n_{id}kT}{q} \ln \left(\frac{J_{sc}}{J_0} \right). \quad (2.4)$$

The approximation is justified because for any reasonably performing solar cell is $J_{sc} \gg J_0$.

Conversion Efficiency The conversion efficiency η is defined as the quotient of the maximum power output P_{max} and the total photon energy P_{sun} impinging on the solar cell

$$\eta = P_{max}/P_{sun}. \quad (2.5)$$

The maximum power output P_{max} of a solar cell is equal to the maximum of the current-voltage product JV .

2.2 Shockley-Queisser Model - The Ideal Solar Cell

Shockley and Queisser were the first to determine thermodynamic efficiency limits of solar cells based on the principle of detailed balance.²² To define a conversion limit Shockley and Queisser (SQ) assume perfect absorption: all photons impinging on the solar cell with a minimum threshold energy, the band gap energy E_g , are absorbed whereas photons below that energy do not interact with the solar cell. Mathematically, the absorptance $A_{\text{SQ}}(E_\gamma)$ in the SQ model is a step-function defined as $A_{\text{SQ}}(E_\gamma) = 0$ for $E_\gamma \leq E_g$, and $A_{\text{SQ}}(E_\gamma) = 1$ for $E_\gamma > E_g$. Moreover, each absorbed photon generates exactly one-electron hole pair with electrical potential energy E_g and all generated electron-hole pairs are collected under short-circuit, i.e. $Q_{e,\text{SQ}}^{\text{PV}} = A_{\text{SQ}}$. Therefore, the generated photo current is according to the SQ model

$$\begin{aligned} J_{\text{sc}}^{\text{SQ}} &= q \int_0^\infty A_{\text{SQ}}(E_\gamma) \phi_{\text{sun}}(E_\gamma) dE_\gamma \\ &= q \int_{E_g}^\infty \phi_{\text{sun}}(E_\gamma) dE_\gamma. \end{aligned} \quad (2.6)$$

In the original publication, the spectrum of the sun ϕ_{sun} is approximated by the black body spectrum ϕ_{bb} at temperature $T = 6000$ K. However, nowadays it is most common to use the standard AM1.5g³¹ spectrum instead which is also used in this thesis.

Because the radiative recombination is the only allowed recombination path in the SQ model and every generated photon leaves the solar cell without being reabsorbed, the radiative saturation current can be calculated via

$$\begin{aligned} J_0^{\text{SQ}} &= q \int_0^\infty A_{\text{SQ}}(E_\gamma) \phi_{\text{bb}}(E_\gamma, T = T_c) dE_\gamma \\ &= q \int_{E_g}^\infty \phi_{\text{bb}}(E_\gamma, T = T_c) dE_\gamma. \end{aligned} \quad (2.7)$$

Using the diode equation (2.1) of a solar cell with $n_{id} = 1$ and the definition of the conversion efficiency (2.5) the SQ efficiency limit η^{SQ} is calculated via

$$\eta^{SQ} = \frac{\max_V \left[V \left(J_{sc}^{SQ} - J_0^{SQ} \left[\exp \left(\frac{qV}{kT} \right) - 1 \right] \right) \right]}{\int_0^\infty E_\gamma \phi_{sun}(E_\gamma) dE_\gamma}. \quad (2.8)$$

Note that the diode equation for an ideal solar cell is not an assumption of the SQ model but can be derived by combining the SQ model and Würfel's³² generalization of Planck's law for semiconductors under non-equilibrium.³³ Würfel's law is introduced in the next section.

2.3 Würfel's Generalization of Planck's Law

Würfel's generalization of Planck's law states that the absorptance A and the emission ϕ_{em} of a semiconductor are linked via

$$\phi_{em}(E_\gamma) = A(E_\gamma) \phi_{bb}(E_\gamma) \left[\exp \left(\frac{\mu_\gamma}{kT} \right) - 1 \right], \quad (2.9)$$

where μ_γ is the chemical potential of radiation.^{32,34,35} For an ideal solar cell with flat quasi Fermi levels and uniform temperature μ_γ is equal to qV . An inherent assumption of this generalization is the linear extrapolation of thermal equilibrium to a non-equilibrium situation.

2.4 Opto-Electronic Reciprocity

Würfel's law links the absorptance to the emission of a semiconductor without considering the spatial dimension of the device and therefore the transport of charge carriers. Rau²³ extended Würfel's law by combining it with a reciprocity theorem for transport in pn-junctions. This transport reciprocity theorem of Donolato³⁶ connects the injection of

carriers in the dark to the extraction of carriers under illumination. Just like the SQ limit, the Donolato theorem is also a direct consequence of the principle of detailed balance. With this the external quantum efficiency Q_e^{PV} is linked to the luminescence of a solar cell ϕ_{em} via Rau's opto-electronic reciprocity theorem²³ as follows

$$\phi_{\text{em}}(E_\gamma) = Q_e^{\text{PV}}(E_\gamma)\phi_{\text{bb}}(E_\gamma) \left[\exp\left(\frac{qV}{kT}\right) - 1 \right]. \quad (2.10)$$

This relation has been experimentally verified for a number of solar cell technologies.^{37–40} However, because the reciprocity relation is derived from a linear extrapolation from thermodynamic equilibrium it does not hold for solar cells with non-negligible non-linear effects, such as saturation effects or voltage-dependent collection efficiencies. These effects cause ideality factors that deviate from unity. Experimentally, a violation of the opto-electronic reciprocity has been analyzed, for example, for amorphous silicon solar cells.^{41,42}

2.5 Electron Transfer Theories

In the following, the two most common theories on electron transfer are introduced. The physicists Miller and Abrahams⁴³ developed their model on electron transfer rates to describe the impurity conductance in semiconductors and around the same time the chemist Marcus⁴⁴ published his theory to explain electron transfer rates in chemical reactions. Nowadays, both theories are used to model electron transfer rates in inorganic and organic solar cells.^{45–51} Moreover, they are compatible with the principle of detailed balance, i.e. they lead to the Fermi-Dirac distribution for occupied states in thermodynamic equilibrium.

2.5.1 Miller-Abrahams Model

In 1960, Miller and Abrahams published their theory on electron transfer explaining the impurity conduction in semiconductors.⁴³ The theory is based on the phonon-assisted tunneling mechanism where the transfer rate to energetically higher states is "punished" by a Boltzmann factor and the rate to energetically lower states is independent of the energy difference between the two involved states. The rate coefficient of the electron transfer from a state with potential energy E_i to a state with energy E_j is given as

$$R = C \cdot \begin{cases} \exp\left(-\frac{E_j - E_i}{kT}\right), & \text{if } E_j > E_i, \\ 1, & \text{else.} \end{cases} \quad (2.11)$$

In the classical Miller-Abrahams Model, the factor C depends on the phonon vibration frequency (also referred to as the attempt-to-escape frequency) and the overlap of the electronic wave functions of the two states.

2.5.2 Marcus Theory

Inspired by Libby's⁵² idea to explain chemical reaction rates by the Franck-Condon principle⁵³⁻⁵⁵ R. A. Marcus developed his electron transfer theory.⁵⁶ He found that in Libby's approach the conservation of energy is violated and searched for a way to fix this problem but at the same time obey the Franck-Condon principle. He developed, reformulated and improved his theory for decades and received for his contributions to the theory on electron transfer the 1992 Nobel Prize in Chemistry.^{44,57,58}

The fast success of Marcus theory is not least build on his capability to find an intuitive visualization of his theory that is depicted in Figure 2.3. For this simple visualization he defined the global reaction coordinate⁴⁴ in the N -dimensional coordinate space of reacting systems that includes

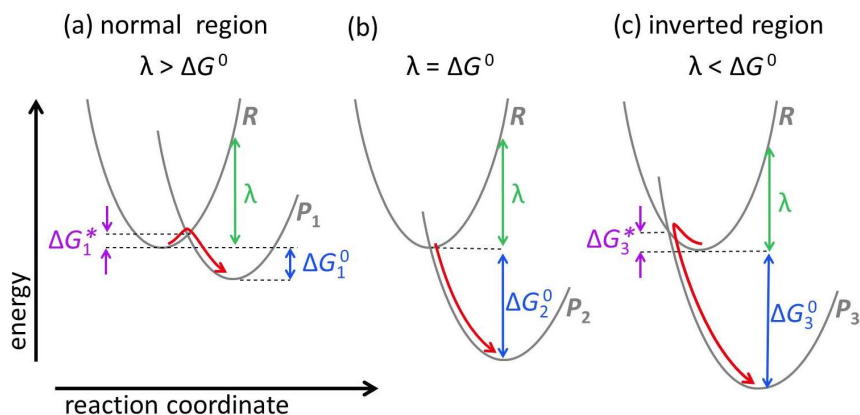


Fig. 2.3 Schematic sketch of Marcus' electron transfer theory. The free energy curves of the reactant R and products P_1 , P_2 and P_3 are quadratic functions of the reaction coordinate. (a) In the normal region, the electron transfer rate increases with increasing $\Delta G^0 = G_R^0 - G_P^0$. (b) For $\lambda = \Delta G^0$, the activation energy ΔG^* is minimal and the transfer rate maximal. (c) In the inverted region, counter intuitively, the electron transfer rate decreases with increasing $\Delta G^0 = G_R^0 - G_P^0$.

the position of atoms, dipole moments and vibrational coordinates to name just a few. This globally defined reaction coordinate is equal to the potential energy difference between the products plus solvent and the reactants plus solvent. Moreover, he applied the "linear response approximation" to his theory in which any change in charge of the reactants leads to a respective proportional change in the dielectric polarization of the solvent. The free energy curves of the reactant R and the product P are consequently simple quadratic functions of the reaction coordinate.

The electron transition occurs at the interception of the free energy curves of R and P and therefore does not violate the Frank-Condon principle. The principle states that the electron transfer is faster than reorganization of nuclear configuration. By simple calculations of the

intersection points of the parabolas gives the activation energy ΔG^* , that is needed for the reactant to reach the point of intersection, as

$$\Delta G^* = \frac{(\lambda - \Delta G^0)^2}{4\lambda}. \quad (2.12)$$

The reorganization energy λ is defined as the energy change in free energy if the reactant were to distort to the equilibrium configuration of the product state without electron transfer. The difference between the free energy in equilibrium configuration of the product G_P^0 and the reactant G_R^0 is denoted as ΔG^0 , i.e. $\Delta G^0 = G_P^0 - G_R^0$.

According to classical transition-state theory by Eyring⁵⁹ or Arrhenius⁶⁰ the rate coefficient of the electron transfer is given as

$$R = C \exp\left(\frac{-\Delta G^*}{kT}\right), \quad (2.13)$$

where term C depends on the nature of the electron transfer reaction. For $\lambda = \Delta G^0$, the rate coefficient R is maximal because the activation energy is $\Delta G^* = 0$ as schematically shown in Figure 2.3b. In the normal region, the electron transfer becomes more likely the bigger the energy difference ΔG^0 between reactant and product is, as intuitively expected. In the inverted region, however, the transfer becomes less likely with increasing energy difference ΔG^0 . This counter-intuitive behavior can readily be seen and understood with the help of Figure 2.3c. In 1960, Marcus explicitly stated the prediction of the inverted region⁴⁴ but it took more than 20 years to provide experimental evidence.⁶¹ Later, Marcus extended his electron charge transfer theory in the dark to photo-absorption and photo-emission processes.⁶² For this purpose the energy difference of the reactant and product ΔG^0 is shifted by the photon energy E_γ .

The Solar Cell Described by External Parameters

” *Users do not care about what is inside the box, as long as the box does what they need done.*

— **Jef Raskin**
(Computer Scientist)

Once a solar cell is fabricated and the efficiency is measured, one realizes that the thermodynamic Shockley-Queisser limit could not be reached by the device. And the question arises where the losses in efficiency have their origin. A very powerful tool for quantifying and distinguishing between different loss mechanisms has been the analysis of open-circuit voltage losses of the device. However, every solar cell technology has its own and oftentimes not so-well-defined standards to determine these losses. This variation complicates a meaningful comparison of different technologies. This chapter introduces a methodology to comparing the losses of various photovoltaic absorber materials by using exclusively external device parameters. In the first section the current approach and its limitation will be described. To make the voltage analysis applicable to a wide range of technologies a definition of photovoltaic band-gap energy via distribution of SQ band-gap energies will be introduced in Section 3.2 and extended the analysis to radiative ideality factors greater than one. In Section 3.3,

this generalized approach is applied to quantify voltage losses to various technologies. At the end, the correlation between voltage and efficiency losses will be discussed. This chapter has partially been published before in *Physical Review Applied*, see *List of Publications*.

3.1 Quantifying Voltage Losses

Following Ross⁶³ and later works^{23,64} the open-circuit voltage of a solar cell can be separated into a radiative open-circuit voltage V_{oc}^{rad} and a non-radiative loss term as

$$\begin{aligned} V_{oc} &= \frac{kT_c}{q} \ln \left(\frac{J_{sc}}{J_0} \right) = \frac{kT_c}{q} \ln \left(\frac{J_{sc}}{J_0^{rad}} \frac{J_0^{rad}}{J_0} \right) \\ &= \frac{kT_c}{q} \ln \left(\frac{J_{sc}}{J_0^{rad}} \right) + \frac{kT_c}{q} \ln \left(\frac{J_0^{rad}}{J_0} \right) = V_{oc}^{rad} + \frac{kT_c}{q} \ln \left(\frac{J_0^{rad}}{J_0} \right) \quad (3.1) \\ &= V_{oc}^{rad} + \frac{kT_c}{q} \ln (Q_e^{LED}), \end{aligned}$$

where Q_e^{LED} denotes the external luminescence or LED (light emitting diode) quantum efficiency.

The combination of Equation (3.1) with Equations (2.10), (2.3) and (2.2)^{37,38,65} allows one to compare non-radiative losses in solar cells across all technologies based on a common theoretical framework and has been used in various publications.^{37,38,40,63–72} However, there are other loss mechanisms that affect V_{oc}^{rad} and for these loss mechanisms such a common theoretical framework across different technologies is still missing.

For the analysis of such loss mechanisms within the radiative limit, a maximal achievable V_{oc} is needed as reference. The obvious choice for this reference is the V_{oc} of an ideal solar cell, the open-circuit voltage according to the SQ model V_{oc}^{SQ} . However, V_{oc}^{SQ} depends solely on the band gap energy E_g and there are different definitions and experimental standards to determine E_g . This inherit problem of a

deeper analysis of losses that limit V_{oc}^{rad} is subject to this thesis and will be thoroughly discussed in the next subsection before a definition of the SQ band gap E_g^{SQ} is developed. This new definition allows for an experimental standard across technologies.

One possibility to quantify losses that directly effect V_{oc}^{rad} is to expand the expression for the open-circuit voltage V_{oc} , Equation (3.1), with the definitions given in Chapter 2

$$V_{oc} = \frac{kT_c}{q} \ln \left(\frac{J_{sc}}{J_0} \right) = \frac{kT_c}{q} \ln \left(\frac{J_{sc}^{SQ}}{J_0^{SQ}} \frac{J_{sc}}{J_{sc}^{SQ}} \frac{J_0^{SQ}}{J_0^{rad}} \frac{J_0^{rad}}{J_0} \right). \quad (3.2)$$

The three last quotients in the argument of the logarithm are well-defined for any solar cell technology and can be associated with a loss term ΔV_{oc}^x according to

$$V_{oc} = V_{oc}^{SQ} - \Delta V_{oc}^{sc} - \Delta V_{oc}^{rad} - \Delta V_{oc}^{nrad}. \quad (3.3)$$

In Equation (3.3), we have with $V_{oc}^{SQ}(E_g^{PV})$ a reference quantity uniquely defined by the photovoltaic band-gap energy E_g^{PV} . For the mathematical definition of $V_{oc}^{SQ}(E_g^{PV})$ see Equation (3.9). Since the open-circuit voltage can be understood as the asymptotic energy turn over per incident photon (i.e., each excess electron-hole pair photogenerated and collected under open-circuit conditions delivers an energy qV_{oc} at the terminals of the device),⁷³ each loss term V_{oc}^x in Equation (3.3) corresponds to an entropy generation term $\sigma_x = q\Delta V_{oc}^x/T$.

The short-circuit loss term $\Delta V_{oc}^{sc} = kT_c/q \ln(J_{sc}^{SQ}/J_{sc})$ results from the difference between the real short-circuit current density J_{sc} and the theoretical value J_{sc}^{SQ} that is defined by a step-function-like external quantum efficiency. As this difference for most solar cells amounts to some ten percent at most, the resulting open-circuit voltage loss is small (though the loss in overall performance might be significant).

In contrast, the radiative loss term $\Delta V_{oc}^{rad} = kT_c/q \ln(J_0^{rad}/J_0^{SQ})$ can amount to hundreds of mV.⁶⁶ This is because an energy shift of the

luminescent emission with respect to the photovoltaic band-gap energy E_g^{PV} leads to a J_0^{rad} that can be orders of magnitude larger than J_0^{SQ} , as can be seen in Figure 3.1.

Finally, the non-radiative loss term $\Delta V_{\text{oc}}^{\text{nrad}} = kT_c/q \ln(J_0/J_0^{\text{rad}})$ corresponds to the difference between the actual V_{oc} of the device and the open-circuit voltage $V_{\text{oc}}^{\text{rad}} = kT_c/q \ln(J_{\text{sc}}/J_0^{\text{rad}})$ in the radiative limit. The difference $\Delta V_{\text{oc}}^{\text{nrad}}$ is related to the external electroluminescence quantum efficiency Q_e^{LED} of the device via^{23,63,64}

$$\Delta V_{\text{oc}}^{\text{nrad}} = -kT_c/q \ln(Q_e^{\text{LED}}). \quad (3.4)$$

This relation has been proven to be extraordinarily useful for the direct, quantitative comparison of different solar cell technologies^{38,40,65–70,72,74} as well as for the analysis of light trapping schemes in photovoltaic devices.^{75–77}

3.1.1 Challenges and Limitations

Even though the voltage loss analysis of solar cells has been widely applied and proven to be a powerful tool to analyze solar cells and ultimately to improve their efficiencies, there are two drawbacks that are worth mentioning and will be addressed in the following. Firstly, the crucial role of the band-gap energy E_g in the analysis. The current approaches for determining the band-gap energy from external parameters leaves room for personal interpretation and depends on the research community, which makes a meaningful comparison of different technologies challenging. Secondly, the necessity of using the opto-electronic reciprocity relation (2.10) to overcome to experimental limitation of the external quantum efficiency measurements for low absorptance. However, the reciprocity relation is not valid for all technologies and has to be verified for each material system beforehand.

Band Gap Definition

The current definition of the band gap E_g and its experimental determination depends strongly on the respective research community. Whereas the definition of E_g for crystalline materials is given by semiconductor theory of solid state physics, the situation is, even from a theoretical point of view, not clear for disordered materials such as amorphous silicon and many organic semiconductors.

Crystalline Semiconductors Crystalline semiconductors like the most commonly used crystalline silicon (c-Si) or high performing III-V semiconductors have a well-defined band-gap energy defined via the concept of periodic Bloch functions.⁷⁸ This energy is given by intrinsic material properties, e.g. the lattice constant. Moreover, the underlying theory can be used to measure the band gap of c-Si very precisely by temperature dependent measurements.⁷⁹

Amorphous Silicon The band gap of amorphous silicon is much harder to define and most commonly one distinguishes between two functional definitions, the mobility band gap and the optical band gap⁸⁰. A standard method to determine the optical band gap is the Tauc plot⁸¹ (see for a more detailed description Section 3.2.2). However, the Tauc plot is ambiguous for many amorphous materials and depends on the chosen energy range for the linear fit as well as the thickness of the material.^{82,83} Later, Cody et al.⁸⁴ modified this approach and reduced the uncertainties, however it could not fully resolve the problem.⁸³ Consequently, a rather arbitrary method has become the standard in the photovoltaic a-Si:H community, where the optical band gap is determined by the energy where the absorption coefficient α is equal to 10^4 cm^{-1} , i.e. $\alpha(E_g) = 10^4 \text{ cm}^{-1}$. This value has been shown to be similar to the band gap derived by the Tauc method, but with the advantage of being well-defined.^{85,86}

Organic Solar Cells In organic solar cells there is, in general, more than one material needed in order to generate free charge carriers from an exciton. Therefore the definition of the optical band gap is usually very functional in respect to the absorptance of the bulk material. The band gap is usually determined by a fit to UV-Vis absorptance spectra. This procedure is not well-defined and leaves room for personal interpretation that directly affects the obtained value for $E_g - qV_{oc}$ that is frequently used to judge a certain material combination.^{69,71,72,74,87,88} Here a well-defined standard would ensure data comparability and mitigate the "massaging of data."

Functional Photovoltaic Band Gap - Outlook The band gap definition in its original purpose is an intrinsic material property. However, with the aim of a cross-technology comparison of voltage losses a functional band gap definition with respect to the photovoltaic performance of the device will be introduced in Section 3.2. This concept of a photovoltaic band gap E_g^{PV} is applicable to any solar cell technology and would allow for a reproducible and reliable determination of open-circuit voltage losses. It is worth mentioning that E_g^{PV} is an external parameter of the device and as such depends, for example, on the light-trapping scheme of the cell and not exclusively on the material itself.

Opto-Electronic Reciprocity Validation

The opto-electronic reciprocity is not valid for all types of solar cells. There are a manifold of reasons for the violation, like voltage-dependent collection efficiencies, saturation effects or non-linear recombination rates. All these effects have in common that they are deviations from the linear extrapolation out of thermodynamic equilibrium. However, this linear extrapolation is used to derive the opto-electronic reciprocity relation (2.10).

Depicted in Figure 3.1 is the validation of the opto-electronic relation for ten different materials. Note that on the left side of Equation (2.10),

the electroluminescence spectrum ϕ_{EL} is not measured in absolute values and therefore only the proportionality can be tested experimentally. The shown absolute values for ϕ_{EL} (open red circles) correspond to the equilibrium photon flux that would be exchanged with the environment at $V = 0 \text{ V}$. The external quantum efficiencies $Q_{\text{e}}^{\text{PV}}(E)$ (open black circles) are measured either by FTPS (Fourier Transform Photocurrent Spectroscopy) (b-e), taken from Reference [37] in the case of crystalline silicon (c-Si), or from Reference [66] in the case of PTB7:PC₇₁BM. For each material, the EL is calculated from $Q_{\text{e}}^{\text{PV}}(E)$ and vice versa based on the reciprocity relation shown as solid lines.

In cases (a) to (d), the shape of the curves calculated via the reciprocity relation fit well to the directly measured quantities. For organic semiconductors (f)-(j) the range of overlap is rather limited. However, at the lower energy edge where the reciprocity relation is needed to extend the external quantum efficiency measurements for the open-circuit voltage losses analysis the overlap is present. In contrast, the overlap is not sufficient for a-Si:H, see Figure 3.1e. Since the reciprocity relation is not valid in this case. Moreover, in the case of a-Si:H the radiative ideality factor is greater than one and as a consequence Equation (3.1) is not applicable. Therefore, the voltage loss analysis has to be adjusted as will be described in Section 3.2.3.

3.2 Generalization Across Different Technologies

To overcome the limitations outlined above and reach a meaningful quantification of voltage losses for a wide variety of solar cell technologies, the concept of a band gap distribution is introduced. This concept can be used to define a photovoltaic band-gap energy that is motivated by the SQ theory as shown in Section 3.2.2. Subsequently, the voltage loss theory described in Section 3.1 is extended for materials which exhibit radiative ideality factors greater than one.

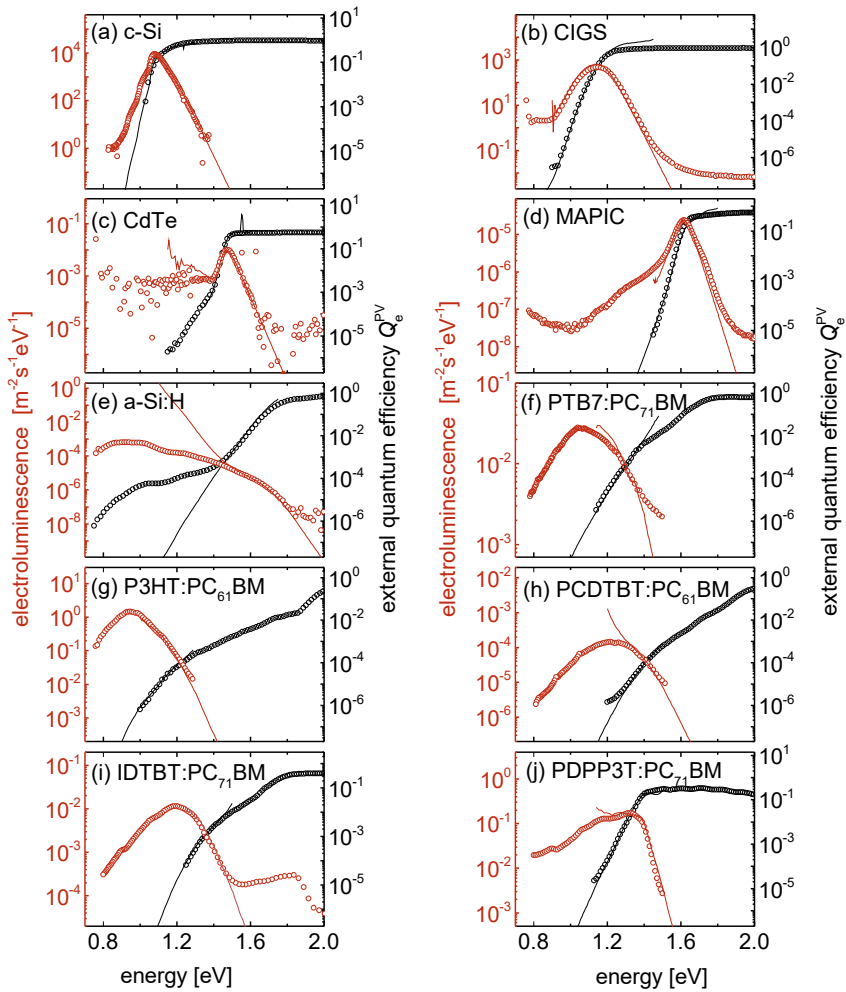


Fig. 3.1 Graphical representation of the reciprocity relation for ten different solar cell technologies. Each graph shows the electroluminescence (EL) spectrum ϕ_{EL} (open red circles) and the external quantum efficiency $Q_e^{\text{PV}}(E)$ (open black circles). Additionally, the EL is calculated from $Q_e^{\text{PV}}(E)$ and vice versa based on the reciprocity relation (2.10). The EL is given in absolute units that correspond to the equilibrium photon flux that would be exchanged with the environment at $V = 0 \text{ V}$.

3.2.1 Distribution of Shockley-Queisser Band Gap Energies

In line with an approach by Rau et al.⁸⁹, that generalizes the original SQ-theory by allowing for non-step function absorptances, the concept of a distribution $P(E_g^{\text{SQ}})$ of SQ-type band-gap energies is used to determine the voltage losses of a wide range of technologies. The original idea of the approach by Rau et al. was to investigate the influence of variations of band-gap energies, e.g. in a semiconductor alloy, on the radiative efficiency limit. Specifically, a Gaussian distribution $P_G(E_g^{\text{SQ}}, \sigma_{E_g})$ was assumed and the standard deviation σ_{E_g} was taken as a measure of the fluctuations. However, the approach can also be applied to general distributions $P(E_g^{\text{SQ}})$. Instead of Equations (2.3) and (2.2) one can write for the saturation and short-circuit current densities

$$\begin{aligned} J_{0/\text{sc}}^{\text{rad}/-} &= q \int_{-\infty}^{\infty} P(E_g) \int_{E_g}^{\infty} \phi_{\text{bb}/\text{sun}}(E) dE dE_g \\ &= q \int_{-\infty}^{\infty} P(E_g) \int_{-\infty}^{\infty} \phi_{\text{bb}/\text{sun}}(E) H(E - E_g) dE dE_g. \end{aligned} \quad (3.5)$$

Because the functions are well-behaved (or can sufficiently be approximated by well-behaved functions) the order of integration is interchangeable and therefore

$$J_{0/\text{sc}}^{\text{rad}/-} = q \int_{-\infty}^{\infty} \phi_{\text{bb}/\text{sun}}(E) \int_{-\infty}^{\infty} P(E_g) H(E - E_g) dE_g dE. \quad (3.6)$$

Comparing Equation (3.6) with Equation (2.2) and (2.3) allows us to connect the external quantum efficiency Q_e^{PV} with the band gap distribution $P(E_g)$ via

$$Q_e^{\text{PV}}(E) = \int_{-\infty}^{\infty} P(E_g) H(E - E_g) dE_g. \quad (3.7)$$

Equation (3.7) thus suggests interpreting the external quantum efficiency $Q_e^{\text{PV}}(E)$ as the result of a distribution of SQ-type band-gap

energies. Finally, taking the derivative of Equation (3.7) with respect to photon energy E leads to

$$\begin{aligned} \frac{d}{dE} Q_e^{\text{PV}}(E) &= \int_{-\infty}^{\infty} P(E_g) \frac{d}{dE} H(E - E_g) dE_g \\ &= \int_{-\infty}^{\infty} P(E_g) \delta(E - E_g) dE_g \\ &= P(E). \end{aligned} \quad (3.8)$$

In Equation (3.8) the derivative theorem for convolutions as been used and the fact that the derivative of the Heaviside function $H(E - E_g)$ is the delta function $\delta(E - E_g)$. Thus, the derivative of the external quantum efficiency $Q_e^{\text{PV}}(E)$ with respect to the photon energy is equal to the band gap distribution of band-gap energies, i.e. $P(E_g) = P(E)$. Because the measurement of $Q_e^{\text{PV}}(E)$ is a standard measurement technique of solar cells, Relation (3.8) makes the distribution of band-gap energies easily experimentally accessible. Figure 3.2 shows schematically the original definition of the band gap of an ideal solar cell in the Shockley and Queisser Model (red) with the continuous and experimentally accessible quantum efficiency $Q_e^{\text{PV}}(E)$ of a real solar cell (blue). The respective distribution of band gap energies is drawn in Figure 3.2b. The distribution of band gap energies is the result of the approximation of $Q_e^{\text{PV}}(E)$ by "Shockley-Queisser"-like step functions.

3.2.2 Photovoltaic Band Gap Definition

In the next step, the photovoltaic band-gap energy E_g^{PV} is defined as the mean peak energy at the absorption edge of the distribution $P(E_g)$,

$$E_g^{\text{PV}} = \frac{\int_a^b E_g P(E_g) dE_g}{\int_a^b P(E_g) dE_g}, \quad (3.9)$$

where the integration limits a and b are chosen as the energy where $P(E_g)$ is equal to 50 % of its maximum, $P(a) = P(b) = \max[P(E_g)]/2$ as exemplarily depicted in Figure 3.2e. This restriction of the integration limits is not motivated physically, but rather by practical reasons as

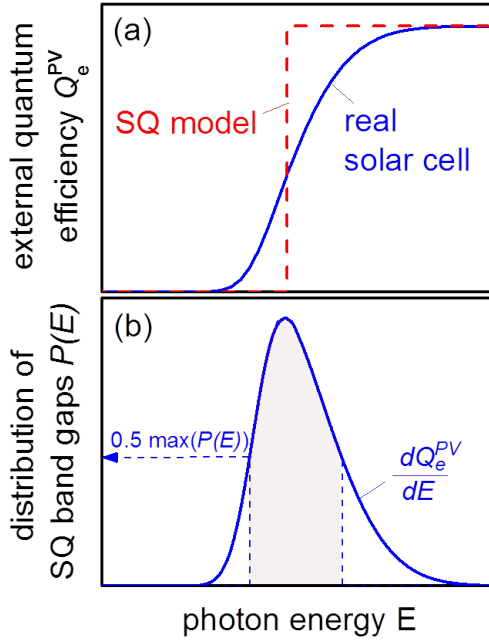


Fig. 3.2 The proposed analysis of practical devices uses the measured external quantum efficiency $Q_e^{\text{PV}}(E)$ (blue curve in a) and interprets its derivative (blue curve in b) as a distribution of SQ-type band gaps. From the distribution $P(E)$ the photovoltaic gap E_g^{PV} is determined. The step-like quantum efficiency (red curve in a) then defines the reference values J_0^{SQ} and $J_{\text{sc}}^{\text{SQ}}$ for SQ-type open-circuit voltage $V_{\text{oc}}^{\text{SQ}}$.

it avoids the influence of noisy data at low energies as well as negative values for $P(E_g)$ in case of $dQ_e^{\text{PV}}/dE < 0$ at high energies. (For a more detailed discussion of the choice of integration limits see the next subsection.) Thus, the present definition of the integration limits should be understood as a convention to determine the band-gap energy E_g^{PV} that is applicable to any solar cell. Furthermore, E_g^{PV} represents an external property of a photovoltaic device and not an (internal) property of a photovoltaic material as is the case for, e.g. the Tauc-gap.⁸¹

The obtained effective band-gap energy E_g^{PV} can then consistently be used to define SQ-type reference values for the saturation current densities $J_0^{\text{SQ}}(E_g^{\text{PV}})$ and $J_{\text{sc}}^{\text{SQ}}(E_g^{\text{PV}})$. Both quantities are determined in the classical way by substituting $Q_e^{\text{PV}}(E)$ by the unit step function

$H(E - E_g^{\text{SQ}})$ in Equations (2.2) and (2.3). Finally, the open-circuit voltage

$$V_{\text{oc}}^{\text{SQ}}(E_g^{\text{PV}}) = \frac{kT_c}{q} \ln \left[\frac{J_{\text{sc}}^{\text{SQ}}(E_g^{\text{PV}})}{J_0^{\text{SQ}}(E_g^{\text{PV}})} \right] \quad (3.10)$$

is established as a reference value in accordance to Equation 3.1.

It should be noted that a definition of the band gap similar to the current proposition was given earlier by Aiken and co-workers.⁹⁰ Helmers et al.⁹¹ criticized this definition as "unphysical" and introduced their own procedure for the analysis of the temperature dependence of band-gap energies in multi-junction solar cells. This approach might better serve the purpose of analyzing the temperature dependence of the direct band gaps because it is concerned with internal semiconductor properties. However, the external definition via a distribution of SQ-type band-gap energies as proposed here addresses a consistent analysis of losses for a solar cell entirely from its external properties. A comparison of different methods for determining the band-gap energy for various solar cell technologies is given in the following subsection.

Comparison of Band Gap Definitions Derived from External Quantum Efficiency Measurements

The distribution of SQ band-gap energies $P(E_g)$ is used to determine the photovoltaic band gap via Equation (3.9), shown in Figure 3.3 as blue half-filled circles for ten different solar cell devices. The photovoltaic band gap is defined via an integral over the distribution with integration limits being 50 % of the maximum. The integral is more robust and reproducible than the maximum of the distribution (red diamonds), which is also shown in Figure 3.3. Low quality data more likely influences the maximum than the integral. Moreover, changing the integration limits of the integral from 50 % to 60 % of the distribution from c-Si, one of the most asymmetric distributions, only leads to a difference in the calculated photovoltaic band-gap energy of 6 meV. This shows the robustness of the integral, as the uncertainty of the

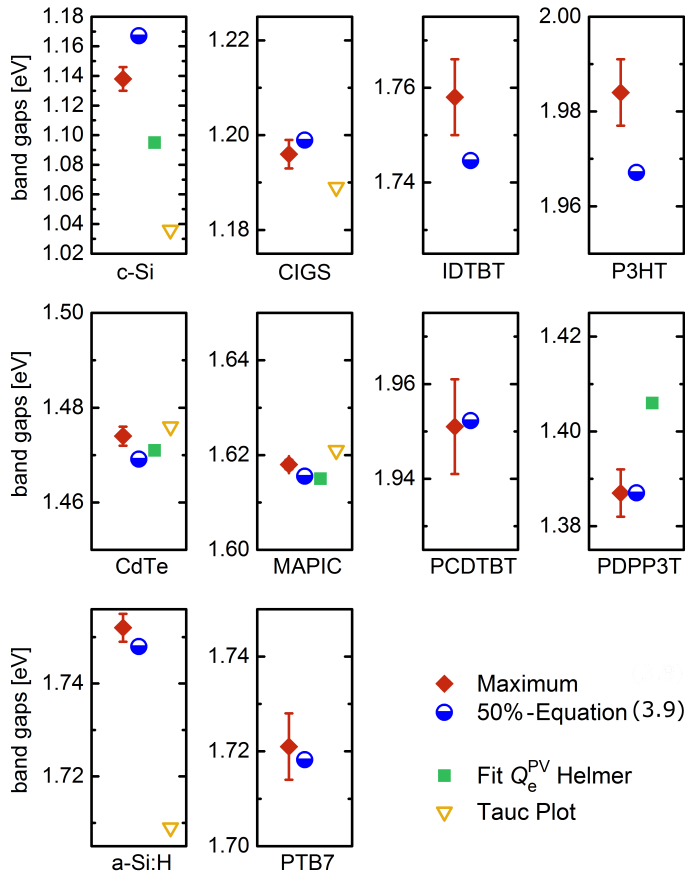


Fig. 3.3 (Photovoltaic) band gaps of ten organic and inorganic, direct and indirect semiconductors as defined by Equation (3.9) (blue half-filled circles), the maximum of the derivative of the Q_e^{PV} (red diamonds), a fit to the Q_e^{PV91} (green squares) and the Tauc plot⁸¹ (yellow triangles).

maximum is in most cases higher. Furthermore, there are a number of different techniques to determine the maximum of a distribution of unknown shape. By using Equation (3.9) this ambiguity is avoided.

In the following, the values of the photovoltaic band gap as previously defined are compared with two other approaches that determine the band gap from external quantum efficiency (EQE) measurements.

Tauc plot For the well-known Tauc⁸¹ plot the approximation $Q_e^{\text{PV}} \propto A \propto \alpha$ for small αd is used, where A denotes the absorptance, α the absorption coefficient and d the thickness of the absorber layer. Then the quantity $(\alpha E_\gamma)^k$ over the photon energy E_γ is plotted. For indirect semiconductors the exponent is $k = 1/2$, whereas for direct semiconductors $k = 2$. The band-gap energies are determined by extrapolating the linear region of this plot to the abscissa. The band-gap energies derived from this method are shown for all inorganic semiconductors in Figure 3.3 (yellow triangles). As it is widely applied for inorganic devices, its applicability to organic devices is questionable and rarely done.

Helmers et al. An alternative approach was suggested by Helmers et al. in 2013.⁹¹ On a logarithmic plot of the EQE a linear function is fitted both to the low energy edge of the EQE as well as to the saturation plateau for higher energies. The intercept of the two functions determines the band-gap energy. For all devices where this method was applicable because the data showed this linear behavior on a logarithmic scale (see Figure 3.1), the values determined by Helmers' method are also shown in Figure 3.3 (green squares).

This comparison shows once more the strength of the present method to determine the photovoltaic band gap, as it is applicable to all technologies and therefore enables establishing an overarching, technology-independent standard of voltage losses in photovoltaic devices.

3.2.3 Radiative Ideality Factors $n_{\text{rad}} > 1$

If band-to-band recombination is not the dominant radiative recombination path in the device, luminescence does not scale with $\exp(qV/kT)$ and Relation (3.1) linking V_{oc} , $V_{\text{oc}}^{\text{rad}}$ and Q_e^{LED} is no longer valid. Therefore, a general expression for $V_{\text{oc}}^{\text{rad}}$ for solar cell technologies with non-ideal luminescence via band-to-dangling bond or tail-to-tail recombination is needed, e.g. for a-Si:H solar cells.⁴¹ In the case of non-ideal

luminescent emission, we may still describe the dependence of the EL intensity Φ_{EL} on voltage with $\Phi_{\text{EL}} \propto \exp(qV/n_{\text{rad}}kT_c)$.

In the radiative limit, the only loss current is via radiative recombination which scales directly with the electroluminescence Φ_{EL} . Therefore, the JV characteristic of a solar cell in the radiative limit can be expressed as $J = J_{\text{sc}} - J_0^{\text{rad}} \exp(qV/n_{\text{rad}}kT_c)$. The open-circuit voltage $V_{\text{oc}}^{\text{rad}}$ can then be consistently described via⁹²

$$V_{\text{oc}}^{\text{rad}} = \frac{n_{\text{rad}}kT_c}{q} \ln \left(\frac{J_{\text{sc}}}{J_0^{\text{rad}}} \right). \quad (3.11)$$

Note that the non-ideality of the radiative recombination has no effect on the idealized voltage limits set by Shockley-Queisser.²² The difference between the SQ-case and the non-ideal radiative limit then reads

$$\begin{aligned} V_{\text{oc}}^{\text{SQ}} - V_{\text{oc}}^{\text{rad}} &= \frac{kT_c}{q} \left[\ln \left(\frac{J_{\text{sc}}^{\text{SQ}}}{J_{\text{sc}}} \right) + \ln \left(\frac{J_0^{\text{rad}}}{J_0^{\text{SQ}}} \right) (n_{\text{rad}} - 1) \ln \left(\frac{J_{\text{sc}}}{J_0^{\text{rad}}} \right) \right] \\ &= \Delta V_{\text{oc}}^{\text{sc}} + \Delta V_{\text{oc}}^{\text{rad,id}} - \Delta V_{\text{oc}}^{\text{rad,corr}}. \end{aligned} \quad (3.12)$$

Thus, the radiative loss term $\Delta V_{\text{oc}}^{\text{rad}} = \Delta V_{\text{oc}}^{\text{rad,id}} - \Delta V_{\text{oc}}^{\text{rad,corr}}$ is obtained from the ideal value $\Delta V_{\text{oc}}^{\text{rad,id}}$ by correcting $\Delta V_{\text{oc}}^{\text{rad,corr}}$ for the non-ideality of radiative recombination.

To calculate the non-radiative voltage loss $\Delta V_{\text{oc}}^{\text{nrad}} = V_{\text{oc}}^{\text{rad}} - V_{\text{oc}}$ we have to take the ideality factor $n_{\text{id}} > 1$ into account because the open-circuit voltage is given by $V_{\text{oc}} = n_{\text{id}}kT_c/q \ln(J_{\text{sc}}/J_0)$. Consequently, we obtain

$$\begin{aligned} \Delta V_{\text{oc}}^{\text{nrad}} &= V_{\text{oc}}^{\text{rad}} - V_{\text{oc}} \\ &= -\frac{n_{\text{rad}}kT_c}{q} \left[-\ln \left(\frac{J_{\text{sc}}}{J_0^{\text{rad}}} \right) + \frac{n_{\text{id}}}{n_{\text{rad}}} \ln \left(\frac{J_{\text{sc}}}{J_0} \right) \right]. \end{aligned} \quad (3.13)$$

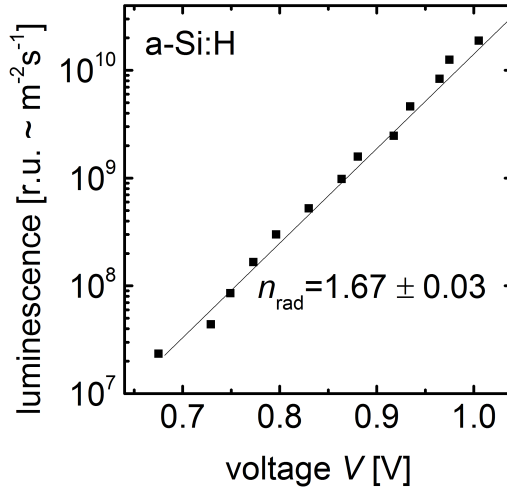


Fig. 3.4 Determination of the radiative ideality factor n_{rad} of a-Si:H by voltage-dependent electroluminescence.

Using $J_{\text{sc}} = J_0 \exp(qV_{\text{oc}}/n_{\text{id}}kT_c)$, we can simplify the term and find for the non-ideal case ($n_{\text{id}} \neq 1$ and $n_{\text{rad}} \neq 1$)

$$\begin{aligned} \Delta V_{\text{oc}}^{\text{nrad}} &= -\frac{n_{\text{rad}}kT_c}{q} \ln \left[\frac{J_0^{\text{rad}} \exp(qV_{\text{oc}}/n_{\text{rad}}kT_c)}{J_0 \exp(qV_{\text{oc}}/n_{\text{id}}kT_c)} \right] \\ &= -\frac{n_{\text{rad}}kT_c}{q} \ln(Q_e^{\text{LED}}). \end{aligned} \quad (3.14)$$

The radiative ideality factor for the examined a-Si:H solar cell is $n_{\text{rad}} = 1.67 \pm 0.3$, see Figure 3.4. The voltage losses for a-Si:H in Figure 3.6 have accordingly been calculated using Equation (3.12).

3.3 Application to Various Photovoltaic Technologies

After the introduction to an overarching, technology-independent standard of voltage losses in photovoltaic devices, this concept will now be applied to various devices including cells with inorganic direct and indirect, crystalline and amorphous absorbers as well as a perovskite

cell and different organic polymer:fullerene bulk-heterojunction solar cells.

Figure 3.5 shows external quantum efficiencies Q_e^{PV} in black, the normalized distribution of SQ band gaps obtained from dQ_e^{PV}/dE in blue, and the measured electroluminescence (EL) spectra ϕ_{EL} in red for solar cells with different absorber materials: crystalline silicon (c-Si), Cu(In,Ga)Se₂ (CIGS), CdTe, CH₃NH₃PbI_{3-x}Cl_x (MAPIC), hydrogenated amorphous silicon (a-Si:H), and the organic polymer-fullerene PTB7:PC₇₁BM. The Q_e^{PV} was either determined via FTSP (Fourier Transform Photocurrent Spectroscopy) measurements (b-e) or taken from Reference [37] in the case of c-Si, and Reference [66] in the case of PTB7:PC₇₁BM.

The c-Si and CIGS samples display a broader distribution $P(E_g)$ of band gaps compared to those of CdTe and MAPIC, which display the sharpest SQ-gap distribution and the sharpest EL emission spectra. The widening of the CIGS distribution results from band gap grading of the direct band gap³⁸, whereas the widening of the c-Si distribution results from the indirect nature of the c-Si band gap and the consequent phononic distributions of the radiative transitions,⁹³ as well as the influence of light trapping in the long wavelength range.⁷⁶ The photovoltaic band-gap energy E_g^{PV} for the c-Si cell (1.17 eV) obtained from $P(E_g)$ is slightly larger than the band-gap energy E_g (1.12 eV) defined by the density of states of an ideal silicon crystal. This difference results from the fact that the definition of E_g^{PV} is functional with respect to the photovoltaic action of the device. Such functional definitions of band-gap energies are especially used for disordered materials where different analysis methods lead to different gaps for different functional purposes.

Unsurprisingly, for the case of the a-Si:H device $E_g^{\text{PV}} = 1.75$ eV is closer to the optical band gap than to the mobility gap. The mobility band gap is typically about 1.7 eV as determined via the activation energy of the conductivity of intrinsic material.⁹⁴ The a-Si:H and PTB7:PC₇₁BM

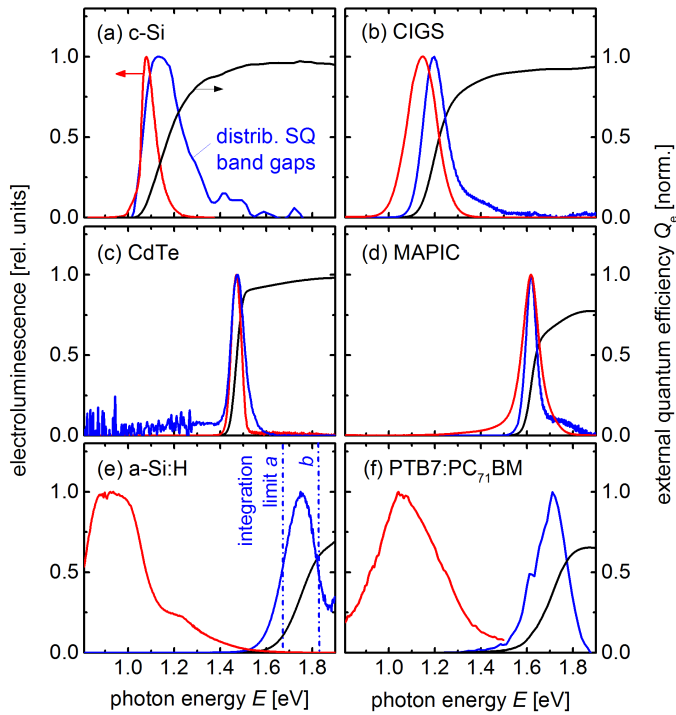


Fig. 3.5 External quantum efficiency Q_e^{PV} (black) and the respective distribution of SQ band gaps (blue) and EL emission ϕ_{em} (red) of six different technologies. The distribution of the SQ band gaps as well as the EL emission is broader for c-Si and CIGS than for CdTe and MAPIC. The broadest distributions are found for a-Si:H and PTB7:PC₇₁BM with a significant peak shift between SQ band gap distribution and EL emission.

cells show the broadest EL spectra and SQ-gap distributions as well as the largest shift between the peak energies. In a-Si:H, this energy shift between absorption and emission is due to the prevailing emission by radiative band-to-dangling bond recombination.^{41,95–97} In PTB7:PC₇₁BM this is attributed to radiative emission involving the charge transfer state between the two organic components which is energetically lower than the dominant absorption contribution of the pure polymer or fullerene.^{66,98}

To obtain $V_{\text{oc}}^{\text{SQ}}$ for all cells in Figure 3.5, the photovoltaic gap E_{g}^{PV} is determined with Equation (3.9) and the quantities $J_{\text{sc}}^{\text{SQ}}$ and J_0^{SQ}

according to Equations (2.2) and (2.3) (for a single band gap distribution $P(E_g) = \delta(E - E_g^{\text{PV}})$) with the help of tabulated values for the solar spectrum AM1.5g³¹ and from Planck's equation for temperature $T = 300$ K. Analogously, J_{sc} and J_0^{rad} is calculated with the help of Equation (2.10) from the measured quantum efficiencies. Note that for the latter step the validity of Equation (2.10) is required and should be checked experimentally by comparing the measured Q_e^{PV} values with those calculated from the EL emission.^{37,38,99} However, some solar cells do not fulfill Equation (2.10).^{41,100,101} This is the case for the a-Si:H cell in the present work where radiative recombination rates change non-linearly with increasing voltage bias.⁴¹ Here, the concept of a radiative ideality factor n_{rad} ^{41,92} provides the possibility to calculate $V_{\text{oc}}^{\text{SQ}}$ in spite of this complication, as shown in Section 3.2.3.

Figure 3.6 summarizes the open-circuit voltage losses $\Delta V_{\text{oc}}^{\text{rad}}$, $\Delta V_{\text{oc}}^{\text{sc}}$, and $\Delta V_{\text{oc}}^{\text{nrad}}$ for different solar cells. The largest radiative losses $\Delta V_{\text{oc}}^{\text{rad}}$ are present in P3HT:PC₆₁BM as expected because of the observed large shift between absorption and emission (see Figure 3.1g). For c-Si and CIGS, these losses are moderate for reasons discussed above. The virtual absence of $\Delta V_{\text{oc}}^{\text{rad}}$ in Figure 3.6 because of its extremely sharp optical absorption edge is considered a primary quality of MAPIC as a photovoltaic material.^{66,102} GaAs with data taken from Reference [65] exhibits the smallest overall losses in voltage of only $V_{\text{oc}}^{\text{rad}} - V_{\text{oc}} \approx 47$ mV.

The short-circuit loss term $\Delta V_{\text{oc}}^{\text{sc}}$ is small for all devices, though one should keep in mind that carrier collection losses showing up in J_{sc} become significant when considering the device efficiency. Finally, the non-radiative losses $\Delta V_{\text{oc}}^{\text{nrad}}$ depend to a great extent on the optimization of the materials and the devices. Except for the c-Si sample, these losses are relatively large in all devices presented here, but are substantially reduced when considering champion efficiency devices.⁶⁵

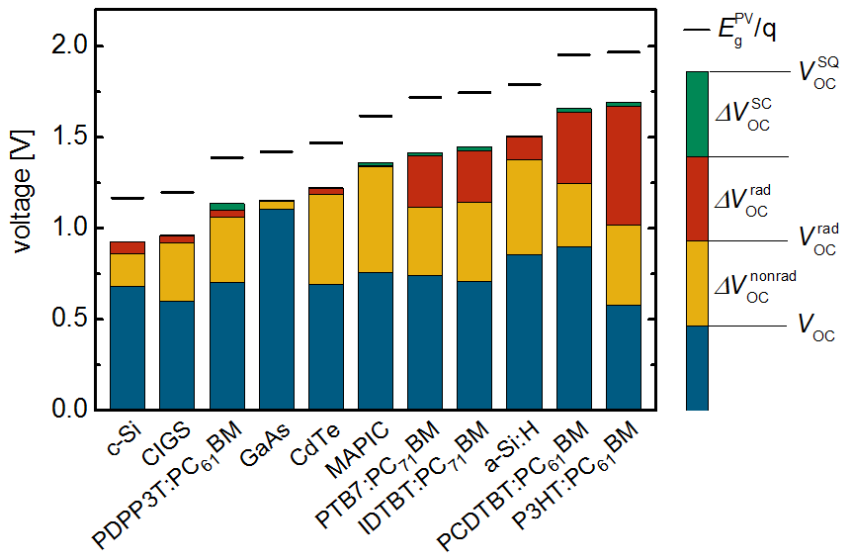


Fig. 3.6 Open-circuit voltage losses ΔV_{oc}^{sc} due to a non-ideal short-circuit current density (green), ΔV_{oc}^{rad} due to radiative recombination (red), and ΔV_{oc}^{nonrad} due to non-radiative recombination for a variety of different solar cell technologies. The SQ band gap is indicated by a black line and the measured V_{oc} as a blue bar.

3.4 Voltage vs. Efficiency Losses

To determine the loss mechanisms in solar cells the quantification of voltage losses as shown in the previous sections have been a very powerful characterization tool. However, optimizing the voltage alone does not make a good solar cell. In truth, the power output and therefore the current multiplied by the voltage is the figure of merit that needs to be optimized. However, the efficiency η normalized by the Shockley-Queisser limit η^{SQ} is strongly correlated to the non-ideal voltage losses $\Delta V_{oc}^{sc} + \Delta V_{oc}^{rad} + \Delta V_{oc}^{nonrad}$.

This correlation is shown in Figure 3.7. It shows the normalized efficiency η/η^{SQ} versus the non-ideal voltage losses for 13 solar cell devices of different technologies. The organic solar cells (black) show the weakest correlation because low performance devices usually have

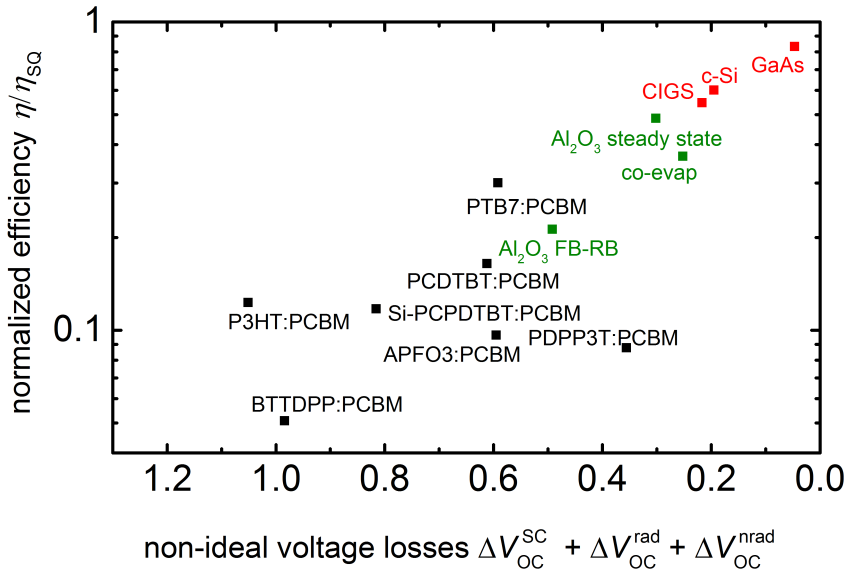


Fig. 3.7 Correlation of the non-ideal voltage losses $\Delta V_{oc}^{sc} + \Delta V_{oc}^{rad} + \Delta V_{oc}^{nrاد}$ with the normalized efficiency η/η^{SQ} . The broadest scattering is shown for low performance organic solar cells with $\eta/\eta^{SQ} < 11\%$ whereas high performance cells exhibit a strong correlation between normalized efficiency and voltage loss.

additional performance losses due to insufficient collection efficiency. Perovskite solar cells are shown in green, solar cells based on inorganic absorber materials in red. The correlation between efficiency and voltage is especially strong for high performing devices, where they usually exhibit charge carrier collection efficiencies close to unity.

3.5 Summary and Outlook

In summary, the concept of a distribution of SQ-gaps bridges the gap between the idealization underlying the SQ-theory and the physical properties of any real world photovoltaic device. Moreover, the voltage loss analysis can be extended to materials with non-unity radiative ideality factors, given a high sensitivity of the absorptance measurement setup. The concept is the basis for a quantitative and intuitive detailed

balance analysis of thermodynamic losses that can be readily applied to any solar cell. The extension of this concept to the analysis of photovoltaic absorber materials without the need for preparing complete devices is straightforward. Additionally to the analysis of the difference between the voltage losses, a similar metric for the comparison of the other solar cell parameters are needed for a complete picture of the cell's performance. For a complete analysis of the solar cell performance in respect to the ideal case in the SQ-theory, the respective difference in the short-circuit current and the fill factor is needed.

Efficiency Limits of New Absorber Materials

“*Life is the continuous adjustment of internal relations to external relations.*”

— **Herbert Spencer**
(Polymath)

This chapter is motivated by the rapidly evolving field of computational and experimental high-throughput materials screening for photovoltaics. In this research field new absorber materials are rated for their potential use in photovoltaic applications by calculating their efficiency limits. In contrast to the extended Shockley-Queisser limit that uses exclusively one external parameter to describe a solar cell, namely the absorptance, the efficiency limit in materials screening has to be calculated starting from internal material properties such as the absorption coefficient. Consequently there is a need to connect internal and external parameters consistently and this is what will be described in this chapter. Results of this chapter have partially been published before in *Physical Review Applied*, see *List of Publications*.

Initially, an explanation will be given as to what exactly is referred to as external and internal parameters and how these are connected by the principle of detailed balance and the fundamental laws of optics. It follows a detailed comparison of the model developed in the current thesis to the state-of-the-art selection metric introduced by Yu and Zunger in 2012, thereby pointing out the major drawback of their

model. Finally, an alternative and physically sound selection metric is introduced that is specifically designed to fulfill the needs of PV absorber materials screening. Results of this chapter have partially been published before in *Physical Review Applied*, see *List of Publications*.

4.1 From Internal to External Parameters

The original SQ-theory is in general straightforward to generalize because Equations (2.3) and (2.2) are also valid for non-step-function-like absorptances, thereby allowing for the calculation of the radiative efficiency limit of real materials, see Equation (2.8).^{67,77,89,103–106} For computational materials screening, however, one has to go one step further and connect the internal material properties with external device properties. This is frequently not implemented correctly and has led to confusion and mistakes in the past.^{24,107–118}

Internal parameters describe material properties that are independent of any solar cell geometry. Here, the path of the photons inside the volume or bulk and their interaction with electron-hole pairs are considered as depicted on the bottom left of Figure 4.1. Such material properties are volume or bulk properties like the absorption coefficient α , the refractive index n , the radiative recombination rate R^{rad} , the non-radiative recombination rate R^{nrad} , and the internal luminescence quantum efficiency Q_i .

In contrast, external parameters are described as a property per surface area and serve as input and output parameters to describe the solar cell. Such cell properties are, for example, the short-circuit current density J_{sc} , the radiative saturation current density J_0^{rad} , the non-radiative saturation current density J_0^{nrad} , and the external luminescence quantum efficiency Q_e^{LED} . One commonly committed mistake, for instance, is the assumption that the internal and external luminescence quantum

Tab. 4.1 Internal vs. external parameter. The radiative and non-radiative recombination rates as defined here are the recombination rates in thermodynamic equilibrium.

INTERNAL PARAMETER		EXTERNAL PARAMETER	
absorption coefficient	α	$1 - \exp(\alpha d) = A(E)$	absorptance
non-radiative recombination rate	R_0^{nrad}	$q \int R_0^{\text{nrad}} dx = J_0^{\text{nrad}}$	non-radiative saturation current
radiative recombination rate	R_0^{rad}	$p_e q \int R_0^{\text{rad}} dx = J_0^{\text{rad}}$	radiative saturation current
internal (luminescence) quantum efficiency	Q_i	$\frac{p_e Q_i}{1 + (p_e - 1) Q_i} = Q_e^{\text{LED}}$	external luminescence quantum efficiency

efficiency is equal, however, the Q_i is a material property while Q_e^{LED} is a property of the cell and as such depends on things like the texturing of the surface, i.e. light trapping in the cell. Those two quantities are therefore only equal for $Q_i = 1$ because if all electron-whole pairs recombine exclusively radiatively any generated photon will eventually escape out of the cell and therefore the emission probability is $p_e = 1$.

The internal and external parameters used within the scope of this work as well as the equations that connect the internal parameter with its external counterpart are listed in Table 4.1. These equations are explained and discussed in the following section.

4.1.1 Model - Consistent with Detailed Balance

It is obvious that materials screening will provide internal parameters while efficiency estimates require external properties. Any sensible selection metric, therefore, has to provide a way to self-consistently and correctly calculate external parameters from internal parameters.

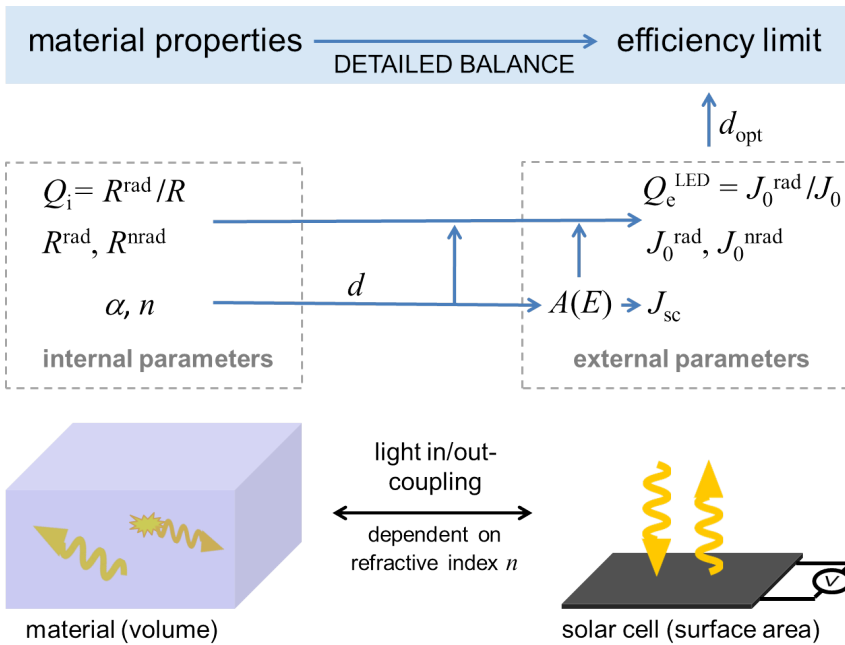


Fig. 4.1 Illustration of the internal material description and the external device description of a solar cell. On the left the path of the photons inside the volume of the cell and their interaction with electron-hole pairs are considered, on the right side light and current are described as input and output parameters of a photovoltaic device. For the calculation of the efficiency limit of a device from material properties (absorption coefficient α , refractive index n , (non-)radiative recombination rate $R^{(n)rad}$, and internal luminescence quantum efficiency Q_i) towards external variables (short-circuit current density J_{sc} , (non-)radiative saturation current density $J_0^{(n)rad}$, and external luminescence quantum efficiency Q_e^{LED}) these two descriptions have to be carefully connected. The maximum device efficiency is obtained by assuming a specific light-trapping scheme and optimizing the cell thickness d .

Figure 4.1 illustrates the “internal material world” and the “external device world” where the solar cell is treated as a black box with optical and electrical inputs and outputs. The connection between the internal and the external picture is light incoupling and outcoupling, i.e. optics, and will henceforth be described consistently with the principle of detailed balance.

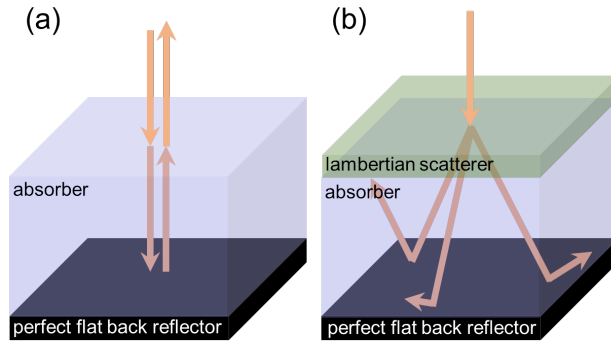


Fig. 4.2 The two light-trapping concepts used in this work. (a) Flat front surface and back reflector. (b) A Lambertian scatterer as front surface combined with a flat back reflector.

Absorption Coefficient and Absorptance

To begin with, the absorptance $A(E)$ is an external property that needs to be computed from the absorption coefficient $\alpha(E)$, a volume related internal property of the photovoltaic absorber material. This requires assumptions on both the thickness d and on the applied light-trapping scheme.¹⁰³ As discussed below, two different light-trapping schemes are considered in this chapter.

Flat Solar Cell This first model represents the case of a solar cell with flat front and back surfaces as depicted in Figure 4.2a. For simplicity, the reflectance at the front surface is set to zero and the reflectance at the back is assumed to be unity. The absorptance can then be written as

$$A(E) = 1 - \frac{\int_0^{\theta_c} \exp\left(\frac{-2\alpha d}{\cos\theta}\right) \sin\theta \cos\theta \, d\theta}{\int_0^{\theta_c} \sin\theta \cos\theta \, d\theta}, \quad (4.1)$$

where $\theta_c = \arcsin(n^{-1})$ is the critical angle of total internal reflection.¹¹⁹ In contrast to the widely applied Lambert-Beer approximation $A \approx 1 - \exp(-2\alpha d)$, this equation takes into account that the solar cell emits light into the solid angle 2π of a hemisphere. One might argue that the absorptance used to calculate the short-circuit current

$J_{sc} = q \int A(E) \phi_{sun} dE$ for a flat cell is best given by the Lambert-Beer approximation, to better resemble the normal incidence used for standard testing conditions, whereas the radiative saturation current $J_0^{rad} = q \int A(E) \phi_{bb} dE$ needs to be calculated with the help of Equation (4.1). In practice, however, the difference between these two equations is rather small and one can argue that the angle of incidence varies throughout the day and year. Therefore J_{sc} as well as J_0^{rad} is calculated with the absorptance given by Equation (4.1).

Lambertian Scatterer The second model is identical with respect to the assumption of zero front and unity back reflectance but it assumes a Lambertian scatterer at the front surface (see Figure 4.2b). In this case, the difference between emission and absorptance is not relevant, as the angle of light is randomized at the front surface. To calculate the absorptance the analytical solution published by Green¹²⁰ is used where he calculates the absorptance via the exponential integral function. Combining Equation 3, 9 and 13 in Reference [120] leads to the absorptance

$$A = (1 - T_r) / [1 - (1 - 1/n^2)T_r], \quad (4.2)$$

where T_r is the fraction of light that is transmitted from the front to the rear surface, reflected there and transmitted back to the front surface. Green calculates the transmittance via

$$T_r = \exp(-2\alpha d) - 2\alpha d \exp(-2\alpha d) - (2\alpha d)^2 Ei(-2\alpha d), \quad (4.3)$$

with $Ei(x)$ being the exponential integral function given by $Ei(x) = \int_{-\infty}^x \exp(y)/y dy$.

Recombination Rates and Currents

A similar step from volume to surface properties with careful distinction between internal and external parameters is required for the description of recombination. Here the internal volume parameters are the

radiative and non-radiative recombination rates R^{rad} and R^{nrad} defining the internal luminescence quantum efficiency Q_i as follows

$$Q_i = \frac{R^{\text{rad}}}{R^{\text{rad}} + R^{\text{nrad}}}. \quad (4.4)$$

For the calculations in the following sections it is assumed that the radiative and non-radiative recombination rates show the same voltage dependence, i.e. $R^{\text{rad}}/R^{\text{nrad}} = R_0^{\text{rad}}/R_0^{\text{nrad}}$.

The external surface property, i.e. the saturation-current densities, are related to the recombination rates as follows

$$J_0 = J_0^{\text{nrad}} + J_0^{\text{rad}} = q \int R_0^{\text{nrad}} dx + p_e q \int R_0^{\text{rad}} dx. \quad (4.5)$$

It is worth mentioning, that the integral $\int dx$ over the depth of the absorber material connects the non-radiative recombination rate R_0^{nrad} in thermodynamic equilibrium directly with the non-radiative saturation current J_0^{nrad} , whereas the emission probability p_e of a generated photon has to be considered in the case of radiative recombination. Using the van Roosbroeck-Shockley¹²¹ equation to describe the radiative recombination rate R^{rad} as a function of n , α , and ϕ_{bb} and combining it with Equation (2.2), the quantity p_e is given by

$$p_e = \frac{J_0^{\text{rad}}/q}{\int R_0^{\text{rad}} dx} = \frac{\int A(E)\phi_{\text{bb}}(E) dE}{4d \int n^2(E)\alpha(E)\phi_{\text{bb}}(E) dE} \quad (4.6)$$

for non-concentrating solar cells.⁷⁶ The emission probability p_e is the factor that connects the internal description of a recombination rate R^{rad} to the external description of a current density J_0^{rad} . This factor depends on the refractive index, i.e. $p_e(n)$.

Therefore, it is evident that the refractive index $n(E)$ must be considered in addition to the absorption coefficient $\alpha(E)$ for a consistent description of the solar cell behavior from internal to external properties. This holds even if the Lambert-Beer approximation $A \approx 1 - \exp(-2\alpha d)$ is used where $n(E)$ is not needed to calculate the absorbance A . The influence of total internal reflection and subsequent reabsorp-

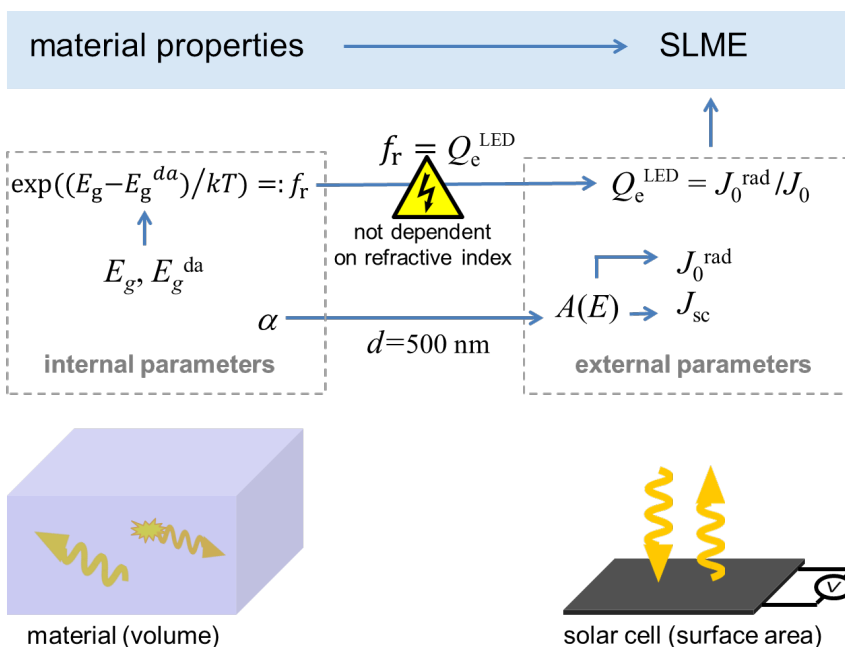


Fig. 4.3 Illustration of the calculation of SLME from internal material properties. The external luminescence yield Q_e^{LED} is set equal to the internal parameter f_r without the necessary consideration of the light outcoupling probability p_e . For comparison see Figure 4.1.

tion $p_e \leq 1/n^2$ in the absorber material can intuitively explain the dependence on the refractive index. Note, however, that in the widely applied selection metric proposed by Yu and Zunger (spectroscopic limited maximum efficiency – SLME)²⁴ the refractive index is neglected, as shown in the following section.

4.1.2 State-of-the-Art Model by Yu and Zunger

In 2012, Yu and Zunger²⁴ introduced their spectroscopic limited maximum efficiency (SLME), which has now become the state-of-the-art selection metric for absorber materials screening. The authors modified the SQ approach to calculate efficiency limits in two ways:

They included non-step function absorptance and non-radiative recombination losses. The absorptance A is calculated from the absorption coefficient α using the Lambert-Beer approximation $A(E) = 1 - \exp(-2\alpha(E)d)$. Here, thickness is set to a rather arbitrary constant value of $d = 0.5\mu\text{m}$. From the calculated absorptance the radiative saturation current J_0^{rad} and the short-circuit current J_{sc} is determined analogously to Shockley and Queisser via Equations (2.2) and (2.3). Consequently, the radiative efficiency η^{rad} follows directly from Equation (2.8).

To calculate efficiency limits beyond the radiative limit, Yu and Zunger introduce the fraction of the radiative recombination current $f_r = J_0^{\text{rad}}/J_0$. This fraction is approximated by $f_r = \exp(E_g - E_g^{\text{da}}/kT)$, where E_g^{da} is the dipole-allowed transition energy that is given by electronic structure simulations. This is motivated by the assumption that the electron densities are governed by Boltzmann statistics and that the ratio of electron concentrations at the different energy levels determines the ratio of radiative to non-radiative recombination. This implies $f_r = 1$ for all direct semiconductors where $E_g = E_g^{\text{da}}$, and $f_r < 1$ for all indirect semiconductors with $E_g < E_g^{\text{da}}$. In their model $\alpha(E)$ and f_r fully determine the non-radiative efficiency limit η .

Discussion

Despite the convincing simplicity of estimating the fraction of the radiative recombination current f_r with the band gap energy difference $E_g - E_g^{\text{da}}$, the physical meaningfulness of this approximation is questionable. For crystalline silicon ($E_g = 1.2\text{eV}$ and $E_g^{\text{da}} = 3.3\text{eV}$), for example, the fraction of the radiative electron-hole recombination current is estimated to be $f_r = 10^{-39}$, a value more than 30 orders of magnitude off from state-of-the-art devices. In addition, the simplified approach to calculate the potential for one thickness only might be misleading. For a differently chosen standard thickness the materials would also be ranked in a different order. Choosing, for example,

smaller thicknesses would favor higher absorption coefficients with low f_r over materials with lower absorption coefficient but high f_r .

More importantly, the selection metric has a major flaw in that it does not distinguish between internal material properties and external device properties in a thermodynamically correct way. The authors derive an external parameter (the ratio of current densities f_r) directly from an internal parameter (the band gap energy difference $E_g - E_g^{\text{da}}$) without taking the refractive index into account, see Figure 4.3 for an illustration. This directly contradicts the fundamental laws of physics, given that $Q_i \neq 1$, as revealed in the previous Section.

To show the implications of ignoring the refractive index the present model will be systematically compared to SLME in the following section. For this purpose, SLME is not considered to be a method that determines the efficiency limit for a fixed thickness and a fixed f_r given by the band gap differences, but rather as a model that describes a way to calculate the efficiency limit of a device starting from internal material properties. Note that SLME does not introduce the internal luminescence quantum efficiency Q_i in a strict sense. Nonetheless, given the explanation in Reference [24] f_r is interpreted as Q_i for the comparison of the here introduced model to the SLME. Due to the unsatisfactory approximations of this parameter in the current state of theoretical solid state physics the internal (luminescence) quantum efficiency Q_i will be treated as an adjustable parameter in the following comparison.

4.2 Model Comparison

The influence of the internal luminescence quantum efficiency Q_i , the refractive index n , and the thickness d on the efficiency limit is discussed for both models in this section in order to understand the dependencies on these parameters and their resulting difference in the calculated efficiency limit. This systematic study on two exemplarily

designed model absorption coefficients in combination with three freely adjustable parameters, e.g. d , Q_i and n , lead to the selection metric that will be introduced in Section 4.3.

Up to this point, we have learned that the absorption coefficient and refractive index of a photovoltaic absorber material are mandatory inputs for a consistent evaluation of the material's prospective photovoltaic efficiency limit. Moreover, the step from treating a solar cell in terms of a mere surface with the property of an absorptance towards a bulk material, volume-related model requires taking the thickness into account. In the first part of this section, the influence of the cell's thickness on the predicted efficiency potential is systematically investigated with the help of model absorption coefficients defined by

$$\alpha = \left\{ \begin{array}{ll} 0 & \text{for } E < E_0 \\ \alpha_0 \exp\left(\frac{E-E_g}{E_{ch}}\right) \sqrt{\frac{E_{ch}}{2 \exp(1)kT}} & \text{for } E_0 \leq E < E_g + E_{ch}/2 \\ \alpha_0 \sqrt{\frac{E-E_g}{kT}} & \text{for } E_g + E_{ch}/2 \leq E \end{array} \right\}. \quad (4.7)$$

For photon energies $E \geq E_g + E_{ch}/2$ the absorption coefficient follows the square root law of a direct semiconductor,²⁶ for $E < E_g + E_{ch}/2$ the absorption is described by an exponential band tail with Urbach¹²² energy E_{ch} , and for all energies below the cut-off energy E_0 the absorption is set to zero. The cut-off energy is motivated by the unavoidable experimental and computational limitations in the determination of α in practice.

Figure 4.4 depicts the two model absorption coefficients that are used in this work as well as the well-known curve of the SQ efficiency limit over band gap energy E_g (black dashed line). One model absorption coefficient has a band gap energy of $E_g = 1.0$ eV and a cut-off energy of $E_0 = 0.9$ eV (red) and for the other one $E_g = 1.5$ eV and $E_0 = 1.4$ eV (blue). The band gap energies as well as the cut-off energies have been selected in a way that they are either both below or both above the two local maxima of the SQ limit. The motivation for this specific choice of energy values becomes clearer in the ensuing discussion of

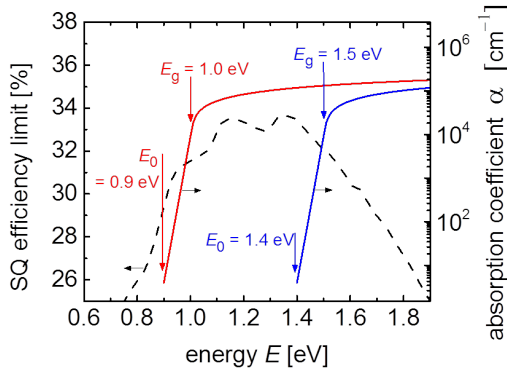


Fig. 4.4 Two model absorption coefficients versus energy. One absorption coefficient curve (red) is chosen so that both the band gap energy $E_g = 1.0$ eV and the cut-off energy $E_0 = 0.9$ eV are below the two maxima of the SQ efficiency limit (black-dashed). The other one (blue) with $E_g = 1.5$ eV and $E_0 = 1.4$ eV is only non-zero for energies above 1.35 eV (second maximum of SQ). In both cases the characteristic energy of the tail is set to $E_{ch} = 1/2kT$.

the optimal absorber thickness. The tail slope is in both cases equal to $E_{ch} = 0.5kT$, a reasonable value for common solar cell materials.¹⁰² The scaling factor α_0 can vary strongly for different materials, but the absolute value is of no importance in the following discussion, as all functions that are going to be referred to are functions of the normalized thicknesses $\alpha_0 d$. For the sake of simplicity, the absorption coefficients in Figure 4.4 are exemplarily shown for $\alpha_0 = 1 \times 10^5 \text{ cm}^{-1}$.

4.2.1 Impact of Thickness on Conversion Efficiency

In the Radiative Limit Figure 4.5a shows the efficiency as a function of normalized thickness $\alpha_0 d$ for these two exemplary materials in the radiative limit ($Q_i = 1$) for flat devices. For devices with a Lambertian scatterer as front surface see Figure 6.1 in the appendix. In the case of $E_g = 1.0$ eV (red), the maximum efficiency is reached at a finite normalized thickness of $\alpha_0 d_{opt} = 0.7$. In contrast, in the case of $E_g = 1.5$ eV (blue) the efficiency approaches its maximum at infi-

nite thickness. The monotonic increase in efficiency with thickness for the latter case can be explained by the fact that both E_g and E_0 are above the energy of the maxima of the SQ limit. Making the absorber thicker and thicker leads to an absorption that is closer and closer to a step-like absorption at E_0 . As the SQ limit monotonously decreases from 1.4 eV to 1.5 eV, the maximum efficiency for the exemplary system with $E_g = 1.5$ eV and $E_0 = 1.4$ eV increases with increasing thickness. The efficiency asymptotically reaches the efficiency of the SQ limit at 1.4 eV, $\eta^{\text{SQ}}(E_g = 1.4 \text{ eV}) = \eta^{\text{rad}}(d = \infty)|_{E_0=1.4 \text{ eV}} \approx 33\%$. Following this reasoning, all absorption coefficients with a cut-off energy higher than 1.33 eV, the energy of the second maximum of the SQ limit, reach their radiative maximum efficiency at infinite thickness. The gain in short-circuit current with increasing thickness in those cases is higher than the loss in open-circuit voltage.

The situation is different for band gap energies below the energy of the SQ maxima. For the absorption coefficient with $E_g = 1.0$ eV (red line) the efficiency for infinite thickness is still equal to the SQ limit of the respective cut-off energy: $\eta^{\text{SQ}}(0.9 \text{ eV}) = \eta^{\text{rad}}(d = \infty)|_{E_0=0.9 \text{ eV}}$. However, this limit $\eta^{\text{SQ}}(0.9 \text{ eV})$ is lower than the SQ limit of its corresponding band gap energy $\eta^{\text{SQ}}(1.0 \text{ eV})$. Therefore the $n_{\text{rad}}(d)$ -curve increases until it reaches its maximum of $n_{\text{rad}} = 31.17\%$, and finally decreases asymptotically towards $\eta^{\text{SQ}}(0.9 \text{ eV})$ for infinite thickness.

These simulations shows that apparent subtleties of the optical data (namely the cut-off energy E_0 , the photon energy of the first data point with $\alpha > 0$) become increasingly important when looking for the optimum thickness in the radiative limit. Note that in the radiative limit there are no differences in the calculated efficiency limits between the newly developed model and SLME.

For Low Internal Luminescence Quantum Efficiencies As evident from Figure 4.5b, the behavior drastically changes when an internal luminescence quantum efficiency of $Q_i = 10^{-4}$ is assumed. For $Q_i < 1$, the efficiencies calculated from the new model (solid lines) and the SLMEs

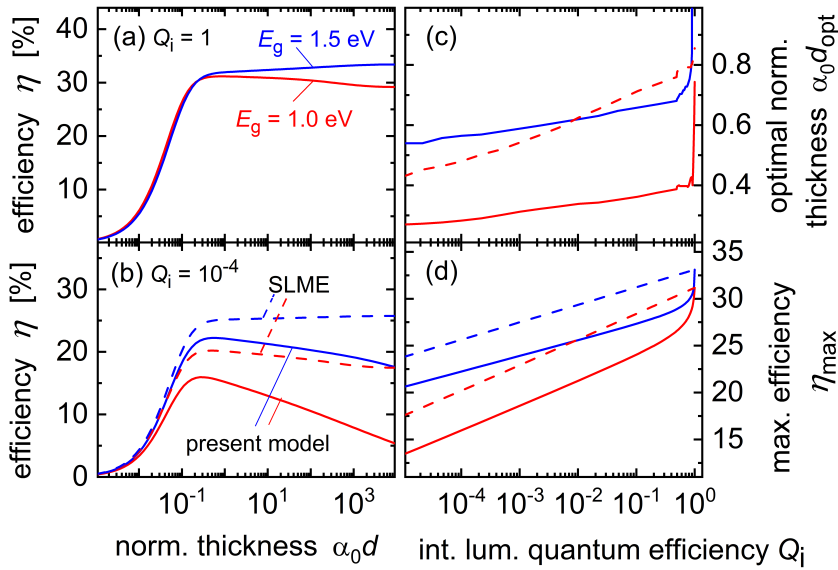


Fig. 4.5 Efficiency as a function of normalized thickness $\alpha_0 d$ for the model systems $E_g = 1.0$ eV (red) and $E_g = 1.5$ eV (blue). The corresponding absorption coefficients are as presented in Figure 4.4, the refractive index is set to 3.5. (a) In the radiative limit, $E_g = 1.0$ eV reaches maximum efficiency at an optimal normalized thickness of $\alpha_0 d_{\text{opt}} \approx 0.7$. In contrast, in the case of $E_g = 1.5$ eV the efficiency approaches its maximum at infinite thickness. (b) For $Q_i = 10^{-4}$, the efficiencies as calculated with SLME (dashed lines) and the present model (solid lines), which takes the refractive index into account, are seen to deviate from one another. The difference in the two models leads to differences in (c) the optimal thickness, for all $Q_i \neq 1$, as well as (d) the absolute maximal achievable efficiencies η_{max} , which are significantly overestimated by SLME. Note that in the case of $E_g = 1.0$ eV, the SLME does not predict an optimal thickness, whereas the present model always leads to an optimal efficiency for $d \neq \infty$ (given that $Q_i \neq 1$).

(dashed lines) deviate from one another. In the case of $E_g = 1.0$ eV (red), both models predict similar optimal thicknesses. The absolute maximum efficiency of about 20 % is, however, highly overestimated by SLME in comparison to the present model, which predicts an efficiency limit of about 16 %.

Note that when $E_g = 1.5 \text{ eV}$ (blue) not only the maximum efficiencies deviate strongly, but the curves also show a qualitatively different behavior. If one neglects the refractive index (SLME, dashed blue line), the efficiency over thickness curve no longer exhibits a global maximum. To explain the observed differences between the two approaches the equations introduced in Section 4.1 will now be analyzed more thoroughly.

The short-circuit currents in both models follow directly from $J_{sc} = q \int A \phi_{\text{sun}} dE$ and are therefore independent of Q_i . The saturation current J_0 scales with $1/Q_i$ in the SLME model, which leads to the same normalized $J_0(d)$ -curves for $Q_i = 1$ and $Q_i = 10^{-4}$. Therefore, J_0 saturates for large thicknesses for all $Q_i \neq 1$, just like it saturates in the radiative limit. This leads to efficiencies greater than 0% for infinite thickness for all $Q_i \neq 1$, which is physically unreasonable. In the suggested model on the other hand, the outcoupling efficiency p_e decreases with thickness, which leads to a linear increase in J_0 for sufficiently large thicknesses due to the non-radiative term. Consequently, J_0 does not saturate for $Q_i < 1$ and the present model predicts an efficiency of 0% for infinite thickness, as one would expect.

Optimal Thickness as a Function of Internal Luminescence Quantum Efficiency Figure 4.5c shows the effect of the internal luminescence quantum efficiency on the optimal normalized thickness. The optimal thicknesses for $E_g = 1.0 \text{ eV}$ (red) and $E_g = 1.5 \text{ eV}$ (blue) are of the same order of magnitude. The same holds for the SLME in the case of $E_g = 1.0 \text{ eV}$ (dashed line). Nevertheless, it should be pointed out that the SLME does not predict this strong increase in optimal thickness for the last 10% gain of internal luminescence quantum efficiency ($Q_i = 0.9$ to 1) that is visible in the present model (solid lines). As stated above, for the SLME metric the maximum efficiency for $E_g = 1.5 \text{ eV}$ is reached at infinite thickness, and is therefore not included in this graph.

4.2.2 Impact of the Internal Luminescence Quantum Efficiency on the Maximum Conversion Efficiency

In the following, the impact of the internal luminescence quantum efficiency on the efficiency at optimal thickness is analyzed. The maximum efficiency at optimal thickness versus the internal luminescence quantum efficiency is plotted in Figure 4.5d. The SLME exhibits a linear decrease in efficiency with decreasing $\ln(Q_i)$ for the entire range of Q_i shown in this graph. The proposed model shows the same linear decrease solely for $Q_i \ll 1$, in contrast, however, a dramatic drop in maximum efficiency with decreasing Q_i close to the radiative limit of $Q_i = 1$ is seen.

As the underlying equations for the maximum efficiency calculation cannot be solved analytically, a different approach is needed to make the observed dependency of the maximum efficiency on Q_i plausible. For this purpose the efficiency is written as $\eta = J_{sc} V_{oc} FF / P_{sun}$, where P_{sun} is the power density of the incident sunlight. According to Equation (2.3), J_{sc} is independent of the internal luminescence quantum efficiency Q_i . The fill factor FF can also be considered to be almost independent of the internal luminescence quantum efficiency. Therefore, the derivative of η can be approximately calculated via

$$\frac{d\eta}{d\ln(Q_i)} = \frac{J_{sc} FF}{P_{sun}} \times \frac{dV_{oc}}{d\ln(Q_i)}. \quad (4.8)$$

For the SLME metric, J_0 scales with $1/Q_i$ and consequently the open-circuit voltage can be written as $V_{oc} = V_{oc}^{rad} + kT/q \ln(Q_i)$, where V_{oc}^{rad} is the open-circuit voltage in the radiative limit. These considerations explain the linear increase in efficiency with $\ln(Q_i)$ for the SLMEs (dashed lines) depicted in Figure 4.5d.

For $Q_i = 1$, the SLME limit reaches a value that is between the SQ limit of the band gap energy E_g and the cut-off energy E_0 , and is identical

to that predicted by the present model (solid lines). However, even small deviations in Q_i away from the radiative limit lead to significant differences in the predicted efficiencies. Following Equation (24) in Reference [76], the open-circuit voltage can be written as

$$V_{oc} = V_{oc}^{rad} + \frac{kT}{q} \ln \left(\frac{p_e Q_i}{1 + (p_e - 1) Q_i} \right), \quad (4.9)$$

where p_e denotes the emission probability of a photon that has been generated by radiative recombination. Note here that the influence of parasitic absorption is neglected in the calculation of efficiency limits.

For $Q_i \ll 1$, the denominator in the logarithmic argument is close to 1 and Equation (4.9) simplifies to $V_{oc} = V_{oc}^{rad} + kT/q \ln(p_e Q_i)$ implying the same linear increase in efficiency with $\ln(Q_i)$ as in the SLME, whereas the absolute efficiency is overestimated in the SLME by approximately $\Delta\eta = J_{sc}^{FF}/P_{sun} \times kT/q \ln(p_e)$.

For $Q_i \approx 1$, the denominator in Equation (4.9) cannot be neglected anymore. Now, the open-circuit voltage, and as a result the efficiency, increases rapidly as Q_i approaches the radiative limit. In the radiative limit V_{oc} reaches the same value as predicted by the SLME. Note that the slope in the linear range ($Q_i \ll 1$) is the same for the proposed model and the SLME. The absolute gradient depends on the band gap energy E_g as will be discussed in the following paragraphs.

Figure 4.6a shows the maximum efficiency versus internal luminescence quantum efficiency (as in Figure 4.5d) but for various band gap energies and shown for the proposed model only. Here, flat surfaces are one again assumed. (For the case of a Lambertian scatterer as front surface see Figure 6.2 in the Appendix) All absorption coefficients used are defined by Equation (4.7) with $E_g = 0.7$ to 1.9 eV in steps of 0.2 eV (red to blue, (i) to (viii)), the characteristic energy is set to $E_{ch} = 0.5kT$ and the cut-off energies are 0.1 eV below the respective band gap energies, i.e. $E_0 = E_g - 0.1$ eV. The maximum efficiency in the radiative limit is reached for band gaps of 1.3 eV and 1.5 eV with cut-off energies of 1.2 eV

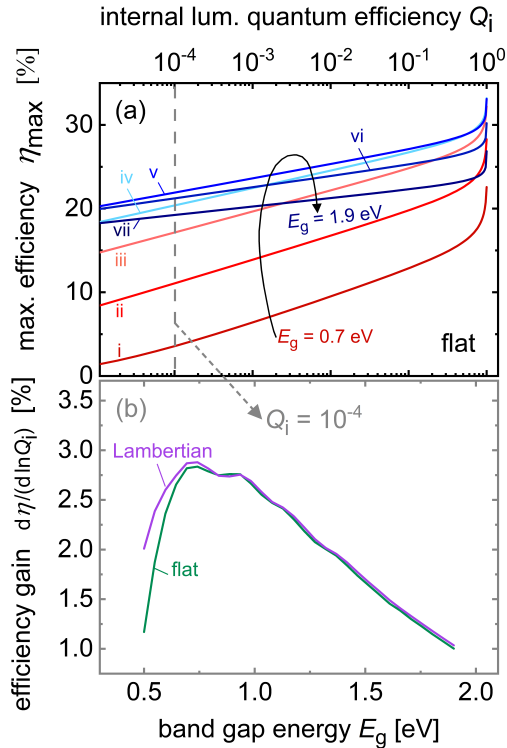


Fig. 4.6 (a) Maximum efficiency versus internal luminescence quantum efficiency Q_i for band gaps $E_g = 0.7$ to 1.9 eV in steps of 0.2 eV (red to blue, (i) to (vii)) assuming flat devices. Note how both the absolute efficiency for $Q_i = 1$ and the slope of the efficiency depend on E_g . (b) The derivative $d\eta/d\ln(Q_i)$ plotted as a function of E_g for flat surfaces (green) and Lambertian scatterers (purple) at $Q_i = 10^{-4}$.

and 1.4 eV respectively. This is expected given that the SQ efficiency maxima are reached in the range of these band gap energies. All curves show the already discussed significant drop in efficiency as Q_i decreases from 100% to 60% . For all $Q_i < 60\%$, the efficiency decreases linearly with decreasing $\ln(Q_i)$ until it asymptotically approaches 0% , as can be surmised for very low Q_i in the case of $E_g = 0.7$ eV (red line).

Let us concentrate now on the range where $\eta(\ln(Q_i))$ increases linearly. Figure 4.6b presents the derivative $d\eta/d\ln(Q_i)$ as a function of the band gap energy for $Q_i = 10^{-4}$. The plotted function in the case of the Lambertian light scatterer (purple) only slightly de-

viates from the curve corresponding to a flat front surface (green) for very low band gaps $E_g < 0.7$ eV. For band gap energies above 0.7 eV, the gain in efficiency $d\eta/d\ln(Q_i)$ monotonically decreases from 3% to 1% in absolute efficiency per decade of internal luminescence quantum efficiency. As the gain in efficiency can be expressed by $d\eta(E_g)/d\ln(Q_i) \approx J_{sc}(E_g)FF(E_g)kT/q/P_{sun}$, the shape of the curve $d\eta/d\ln(Q_i)$ plotted in Figure 4.6b can be explained by the dependency of the product FFJ_{sc} on the band gap energy E_g . Whereas J_{sc} decreases monotonously with band gap energy, the fill factor FF increases strongly for small band gaps and saturates for higher band gap energies. The product of J_{sc} and FF explains the behavior of the efficiency gain $d\eta/d\ln(Q_i)$. The efficiency gain is illustrated in Figure 4.6b.

4.2.3 Impact of the Refractive Index on the Maximum Conversion Efficiency

After discussing the impact of the internal luminescence quantum efficiency and the thickness on the maximum efficiency, this section will close with an analysis on how the refractive index affects the maximal achievable efficiency. For simplicity only the case $E_g = 1.5$ eV will be discussed as there are no qualitatively different effects in the case of $E_g = 1.0$ eV.

Figure 4.7 illustrates the dependency of the efficiency limit on the refractive index calculated by the newly developed model and the SLME model. For $Q_i = 1$ (solid line), there is no difference between the new model and the SLME as has been pointed out before. The maximum efficiency in the radiative limit is approximately 33.4% independent of the light-trapping scheme (see Figure 4.7a for a flat front surface and Figure 4.7b for a Lambertian scatterer as front surface). The value reached is equal to the SQ limit for $E_g = 1.4$ eV which corresponds to the cut-off energy $E_0 = 1.4$ eV of the examined absorption coefficient. In the SLME model the achievable efficiency is independent of the refractive index and the texture of the front for all Q_i . In contrast,

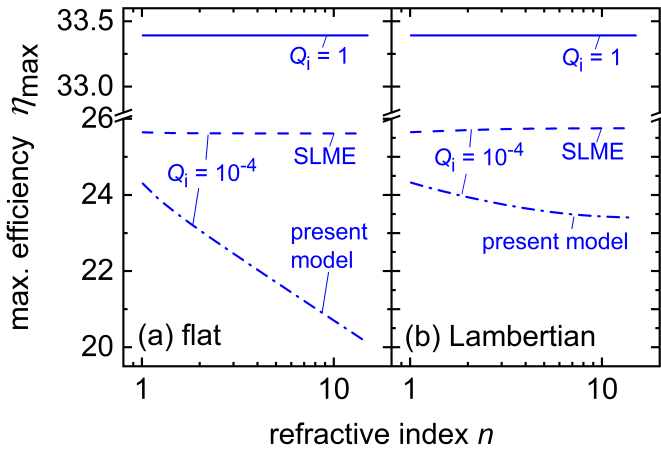


Fig. 4.7 Dependence of the maximum efficiency η_{\max} on the refractive index n for $E_g = 1.5$ eV. In both the radiative limit ($Q_i = 1$, solid lines) and the SLME for $Q_i = 10^{-4}$ (dashed lines) the efficiencies are independent of n . (a) The new model presented here (dashed-dotted line) shows a significant efficiency drop of almost 20% as the refractive index n varies from 1 to 10 for flat devices. (b) Assuming a Lambertian scatterer, the refractive index has a much weaker influence on η_{\max} of a mere 4%.

the present model (dash-dotted line) shows a relative decrease in efficiency of 20% as the refractive index varies from 1 to 10 for flat surfaces. Therefore the overestimation of the maximum efficiency by SLME increases with increasing refractive index.

The decrease in efficiency with refractive index in the new model is a direct consequence of Equation (4.6). The radiative recombination rate R^{rad} is proportional to n^2 , and because $Q_i = 10^{-4}$ is held constant, the non-radiative recombination rate R^{nrad} and R^{rad} have the same dependence on n . The same dependence follows directly from Equation 4.4. Note that $Q_i = 10^{-4}$ implies $R^{\text{rad}} \ll R^{\text{nrad}}$. Consequently, the saturation current J_0 increases with n^2 and the efficiency η decreases linearly with $\ln(n)$, as seen in Figure 4.7a in the case of flat devices. For devices with a Lambertian scatterer as front surface the absorption $A(E)$ and therefore the short-circuit current J_{sc} increase with n . This increase in J_{sc} compensates the increase of J_0 to some extent and the loss in

efficiency with n for fixed $Q_i = 10^{-4}$ is smaller, as can be seen from the dashed-dotted line in Figure 4.7b.

4.2.4 Towards a Meaningful Selection Metric

The detailed examination of different models and their behavior under certain circumstances deepened the understanding of how to calculate a reasonable and also practical efficiency limit from available optical data, either gathered experimentally or from electronic structure calculations. Given the strong dependence of the maximum efficiency on the refractive index it cannot be neglected. Moreover, the calculated efficiency is also very sensitive to the internal luminescence quantum efficiency.

The internal luminescence quantum efficiency Q_i arises from a complex interplay between energy levels in the material, defects, and kinetics in the device. It is therefore very challenging to determine Q_i computationally though it might be possible to determine it experimentally without having to fabricate devices.¹²³ Approaches based on first-principles calculations of non-radiative recombination rates due to point defects are emerging^{124–126} and could provide in the future at the very least an estimate of the upper limit of Q_i under idealized situations.

In practice, it is useful to treat the internal luminescence quantum efficiency as an independent parameter, in particular at an early stage of material investigation when layer growth and device fabrication have not yet been optimized. A third point that needs to be stressed is the thickness dependency of the efficiency. The results presented in this section show that a comparison of different materials at a fixed thickness favor certain materials over others without proper justification. Therefore, the optimal thickness should be considered in the figure of merit for all cases for which $Q_i < 1$.

4.3 Selection Metric for Photovoltaic Absorber Materials Screening

After the detailed discussion of the present model and the state-of-the-art selection for absorber materials screening, finally a recipe for calculating efficiency limits will be introduced in this section. By applying this recipe to computationally determined material properties an physically sound selection metric is developed.

4.3.1 Recipe for Calculating Efficiency Limits

To make full use of the available optical data from electronic structure theory the potential of a new material should be estimated as follows:

1. Decide on a light-trapping scheme ($\alpha \rightarrow A$), e.g. for a flat device use Equation (4.1) and for a Lambertian scatterer as front surface use Equations (4.2) and (4.3).
2. Calculate the short-circuit current J_{sc} and the radiative saturation current J_0^{rad} from the absorptance A according to Equations (2.3) and (2.2), respectively. This calculation yields the radiative efficiency limit via Equation (2.8).
3. Calculate the efficiency for numerous thicknesses to end up with an efficiency-over-thickness curve $\eta(d)$.
4. Find the maximum η_{max} of this curve, i.e. $\eta_{max} := \max_d(\eta(d))$, and determine the corresponding optimal thickness d_{opt} for which $\eta(d_{opt}) = \eta_{max}$.
5. For reasons stated above it is advisable to repeat steps 2-4 for a number of reasonable internal luminescence quantum efficiencies.

To determine the efficiency limit for $Q_i \neq 1$ Equations (4.4) to (4.6) are needed in addition to Equations (2.3), (2.2) and (2.8). Additionally, it is worth mentioning that this selection metric just like the selection metric from Yu and Zunger can only be applied to materials with a tail

slope E_{ch} smaller than kT , for more details see Section 4.3.3 "Outlook and Limitations".

4.3.2 Application to Calculated Material Properties

The suggested method is exemplarily applied to a few complex refractive indices that have been determined via first principles calculations. These calculations were performed within the GW approximation,¹²⁷ as implemented in the VASP code,^{128,129} and are part of a larger database. A more detailed description of the approach is given in Reference [130, 131]. For this dataset the dielectric function is calculated in the independent particle approximation. Figure 4.8 presents the input data in the form of absorption coefficients α and the refractive index n as a function of photon energy E .

The described method is applied to eight selected materials, namely CuInSe₂ (grey), Cu₂ZnSnSe₄ (CZTSe - red), CuSbSe₂ (orange), Sb₂Se₃ (green), CZTS (turquoise), CuGaSe₂ (blue), CuSbS₂ (purple), Sb₂S₃ (pink). All these materials have sharp absorption edges with $E_{\text{ch}} < kT$, a reasonable absorption coefficient for high energies between 10^5 cm^{-1} to 10^6 cm^{-1} , and band gap energies between 1 eV and 2 eV. At first sight they all appear as promising photovoltaic absorber materials.

Figure 4.9 illustrates the maximum efficiencies calculated for internal luminescence quantum efficiencies $\log(Q_i) = 0$ to -7 in steps of -1 (dark to light) sorted according to the energy of the direct band gap. In the radiative limit ($Q_i = 1$) the highest efficiencies are reached for CZTSe (red), CuSbSe₂ (orange), and Sb₂Se₃ (green). This corresponds well with the maxima of the SQ limit (see Figure 4.4 at the beginning of Section 4.2), which predicts the highest efficiencies for materials with band gap energies of 1.1 eV to 1.3 eV. Assuming more realistic quantum efficiencies of $Q_i < 10^{-2}$, the highest efficiency is reached for CZTS with a band gap energy of approximately 1.56 eV. This is a

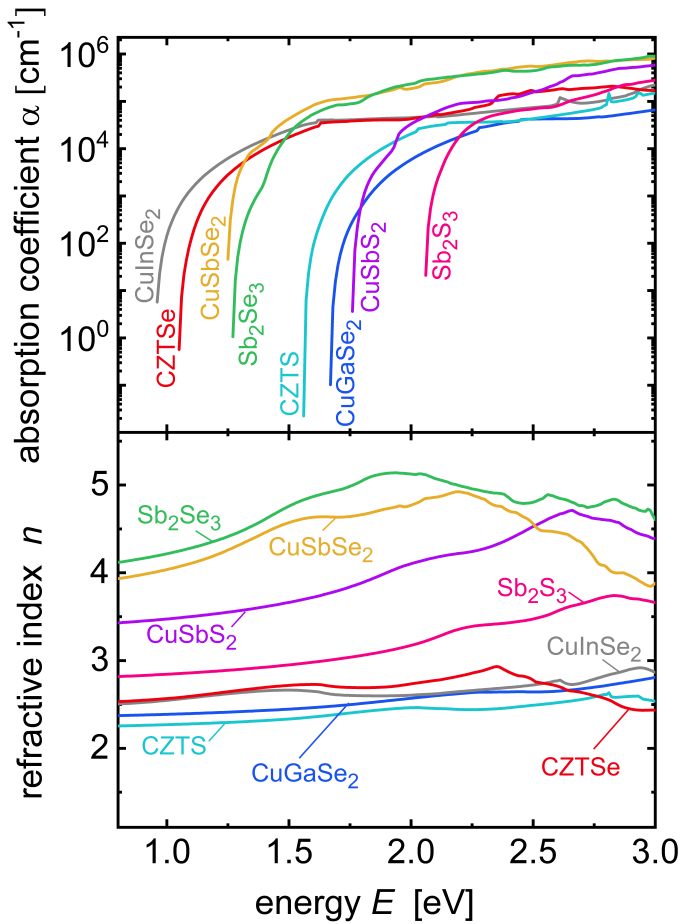


Fig. 4.8 Absorption coefficient α and refractive index n of CuInSe₂ (grey), CZTSe (red), CuSbSe₂ (orange), Sb₂Se₃ (green), CZTS (turquoise), CuGaSe₂ (blue), CuSbS₂ (purple), and Sb₂S₃ (pink) as a function of energy as simulated via electronic structure theory.

direct consequence of the band gap dependent loss in efficiency due to the internal luminescence quantum efficiency. This effect has been addressed in detail in Section 4.2.2. Note that all these efficiencies have been calculated assuming flat devices, with a perfect back reflector and no reflectivity at the front surface.

However, these results are not yet very conclusive: For instance, in the radiative limit a very weakly absorbing material could outperform

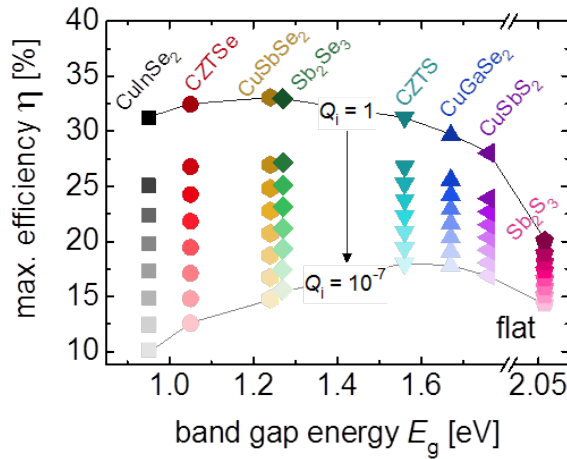


Fig. 4.9 Maximal efficiencies of 8 materials (sorted by direct band gap, see Figure 4.8) for different internal luminescence quantum efficiencies $\log(Q_i) = 0$ to -7 in steps of -1 (dark to light colors). For $Q_i = 1$, CuSbSe_2 achieves the highest efficiency, whereas for $Q_i < 10^{-2}$ CZTS takes the lead.

other materials with higher absorption if one does not consider the thickness of the device. As the non-radiative recombination in the bulk can normally not be neglected, the carrier collection efficiency decreases significantly with thickness. Additionally, very thick devices will exhibit very low efficiencies in real life due to the finite mobility of the investigated materials. Therefore, in a realistic scenario the aim is to identify materials that can reach as high efficiencies as possible at as small a thickness as possible.

Figure 4.10 shows the maximum efficiency over the optimal thickness d_{opt} for the same eight materials (colors and symbols allocated analogously to Figure 4.9) to address the importance of thickness on a selection metric. Here, the case of Q_i equals unity is not shown as some of the samples then reach their efficiency maximum at infinite thickness, which is unreasonable for a realistic estimation of the photovoltaic potential of a certain material. For flat surfaces as shown in Figure 4.10a, CuSbSe_2 (orange) exhibits the smallest optimal thicknesses between $6 \mu\text{m}$ for $Q_i = 10^{-7}$ and $1 \mu\text{m}$ for $Q_i = 0.1$. In Fig-

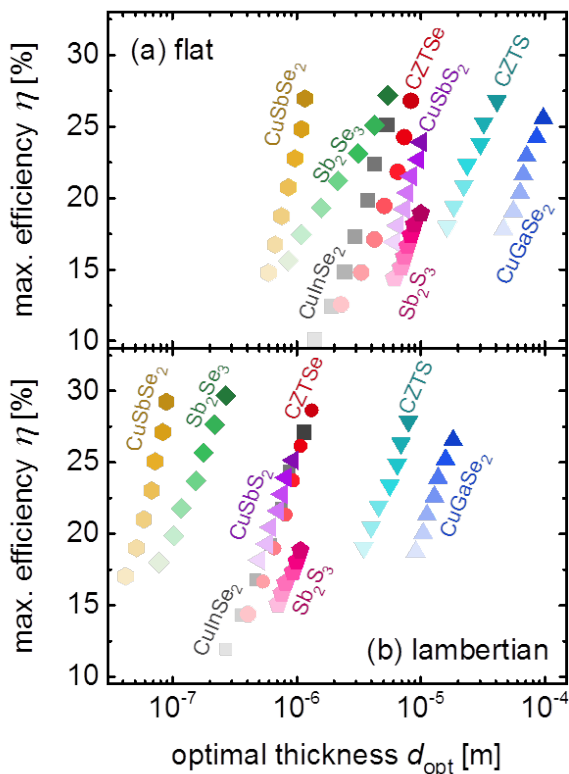


Fig. 4.10 Efficiency at the optimal thickness for the same materials (see Fig. 4.8) for internal luminescence quantum efficiencies $\log(Q_i) = -1, -2, -3, -4, -5, -6, -7$ (colors and symbols same as in Figure 4.9) with (a) a flat front surface and (b) a Lambertian scatterer as front surface. For both systems a flat perfect back reflector is assumed.

ure 4.10b a Lambertian scatterer as front surface and a perfect flat back reflector is assumed. This light-trapping scheme leads to considerably smaller optimal thicknesses and higher efficiencies for all materials. The quantitative gain in efficiency and loss in optimal thickness is, however, distinct for each material. This becomes especially apparent when looking at the difference in optimal thickness between CuInSe_2 (grey), and CuSbS_2 (purple). For flat devices the optimal thicknesses for CuInSe_2 are on average $5 \mu\text{m}$ smaller than for CuSbS_2 . In contrast,

assuming a Lambertian light scatterer this difference in optimal thickness diminishes, e.g. $d_{\text{opt}}(\text{CuSbS}_2) < d_{\text{opt}}(\text{CuInSe}_2)$ for high Q_i and $d_{\text{opt}}(\text{CuSbS}_2) > d_{\text{opt}}(\text{CuInSe}_2)$ for low Q_i .

From Figure 4.10 it can finally be concluded that CuSbSe_2 reaches the highest efficiencies for the smallest thicknesses and therefore is an excellent candidate for a high performance photovoltaic absorber material based on its complex refractive index. Given that the materials presented in Figures 4.8 to 4.10 are all materials that have already been used for photovoltaics, it is worth briefly comparing the results of the assessment based on the complex refractive index and internal luminescence quantum efficiency with the empirical results for these technologies. A technology like $\text{Cu}(\text{In,Ga})\text{Se}_2$ is based closely on CuInSe_2 and it is capable of achieving efficiencies higher than 22 %, ¹³² the analysis at constant Q_i does not suggest that this material is superior to the others based just on its complex refractive index. This is not particularly surprising given that the here exemplarily chosen materials generally exhibit quite good optical properties for photovoltaic applications. The current lack of success of materials such as CZTSe, ¹³³ CuSbS_2 ^{134,135} or CuSbSe_2 ¹³⁶ is a matter of Q_i being lower than that of $\text{Cu}(\text{In,Ga})\text{Se}_2$. Thus, there is a need for computational materials screening to focus on parameters that are related to the presence of defects, such as those based on the search for defect-tolerant materials.

4.3.3 Limitations and Outlook

Requirement on the Tail Slope The introduced selection metric can only be applied to materials that fulfill the requirement $E_{\text{ch}} < kT$. This is also a requirement for the selection metric of Yu and Zunger. This restriction can readily be understood by taking a closer look at Equation (2.2), $J_0^{\text{rad}} = q \int_0^\infty A(E) \phi_{\text{bb}}(E, T = 300\text{K}) dE$. The black-body radiation $\phi_{\text{bb}}(E, T = 300\text{K})$ decreases approximately with $\exp(-E/kT)$ close to energies relevant for photovoltaic applications, $E_g = 0.8\text{ eV}$ to 2.0 eV . As a consequence, the radiative saturation current can only be determined via Equation (2.2) if the absorption $A(E)$ increases stronger

than $\exp(E/kT)$. In other words, the integral has to be well-defined and not defined by the cut-off energy E_0 that is not an intrinsic property of the material. For both light-trapping concepts used here, $E_{\text{ch}} < kT$ is a sufficient condition to fulfill this requirement. This limitation on the applicability is, however, not of major importance for materials screening for photovoltaic absorbers, as all known high performing solar cell absorbers fulfill this requirement.

Infinite Mobility and Contacts For the proposed selection metric, perfect carrier collection is assumed. Therefore any limitations due to finite mobility of the absorber have not been taken into account at this stage. Furthermore, device specific challenges like contacts have not been considered but are known to considerably influence device performance.

Internal Luminescence Quantum Efficiency Besides these simplifications, Figures 4.9 and 4.10 show that the calculated efficiency is enormously influenced by the internal luminescence quantum efficiency Q_i . Up to this point Q_i is an independent and unknown parameter in the present model that is not given by the difference between direct and indirect band gap as suggested in the concept of SLME as it oversimplifies the complex kinetic interplay of material properties and Q_i . So far, computational materials screening for the discovery of new absorbers for PV applications has focused on the band gap and absorption coefficients. However, material properties such defect formation, grain boundaries and many more have been shown to significantly affect Q_i . Therefore, extending the scope of high-throughput computations to more of these properties will have a high impact on successful selection and implementation of novel PV materials.

4.4 Summary

The Shockley-Queisser theory describes a solar cell device solely by a single external surface property, a step-like absorption. However,

for computational materials screening there is a need for a theory to calculate efficiency limits from internal volume material properties such as the absorption coefficient. It was shown in this chapter that the refractive index of photovoltaic absorber materials is a necessary input parameter for a consistent evaluation of their prospective photovoltaic potential which has often been neglected in the past. A generalized Shockley-Queisser theory has been introduced that describes solar cells by their internal properties. In addition, the effect of the internal luminescence quantum efficiency, the thickness and the refractive index on the predicted efficiency limit have been comprehensively analyzed. Based on this detailed examination it was concluded that all of these parameters have to be fully considered in a selection metric for photovoltaic absorber materials. Consequently, a selection metric was suggested to rate a material's potential for PV applications that on the one hand is easy to apply to a large amount of data and on the other hand does not neglect important readily available information. Note that the rating of the material depends on the assumed light-trapping scheme which has to be decided on beforehand. The selection metric is applicable to either simulated or experimentally determined complex refractive indices.

The Organic Solar Cell Described by Internal Parameters

” *The real Jihad is an internal process,
not an external one.*

— **Abhijit Naskar**
(Neuroscientist)

In this chapter a rate model is developed to describe the kinetics within an organic solar cell. The included states and transfer rates are kept to an absolute minimum, namely, an exciton state, charge transfer states, a ground state as well as a free carrier state. Two different theories for transfer rates are applied and compared: The hopping model by Miller-Abrahams⁴³ which is most often applied to inorganic semiconductors and the Marcus Theory⁵⁷ developed to explain the rates of electron transfer reactions from one chemical species to another. Section 5.1 introduces the rate model, including the mathematical description of the transfer rates. In Section 5.2 the occupation probability of the charge transfer state under steady-state conditions is discussed in detail for electro- and photoluminescence. A proof for the validity of superposition of electro- and photoluminescence as well as the opto-electronic reciprocity for this rate model under non-saturation conditions is provided in Sections 5.3 and 5.4. The chapter closes with an analysis of the collection efficiency for various illumination intensities and parameter variations in Section 5.5.

5.1 Introduction to the Rate Model

The 0-dimensional rate model used in this chapter is designed to be as simple as possible, yet at the same time to include the currently-known most dominant interstate transfer paths of charge carriers in organic photovoltaic devices. The charge carriers can occupy a total of three different states, namely, two bounded states, the exciton/singlet state and the charge transfer (CT) state, and the state of free charges. The energy of the excitons is referred to as E_x , the energy of the CT state E_{ct} and the energy difference of the free electrons and holes E_g .

Figure 5.1 shows schematically the states and the considered transfer, recombination and generation rates. An exciton is generated from a photon flux ϕ_x^{in} with a generation rate given by

$$r_{\text{gr} \rightarrow \text{x}} = R_x^{\text{gr}} \phi_x^{\text{in}} (1 - f_x) N_x,$$

where N_x is the number of exciton states with occupation probability f_x and R_x^{gr} is the respective rate coefficient. The exciton recombination rate can be described analogously by

$$r_{\text{x} \rightarrow \text{gr}} = R_{\text{gr}}^{\text{x}} f_x N_x.$$

The transfer rate of excitons from the polymer into the CT state is given by

$$r_{\text{x} \rightarrow \text{ct}} = R_{\text{ct}}^{\text{x}} f_x N_x (1 - f_{\text{ct}}) N_{\text{ct}},$$

where the occupation probability is f_{ct} , number of CT states is N_{ct} and the respective rate coefficient is R_{ct}^{x} . The inverse process is expressed by

$$r_{\text{ct} \rightarrow \text{x}} = R_{\text{ct}}^{\text{ct}} (1 - f_x) N_x f_{\text{ct}} N_{\text{ct}}.$$

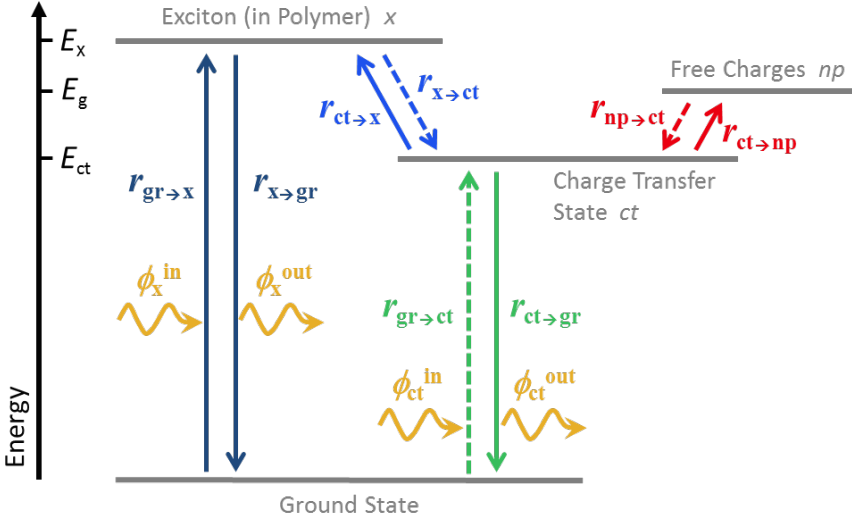


Fig. 5.1 Schematic drawing of the rate model including the considered states along with the associated transfer, generation and recombination rates.

The recombination and generation rate of the CT state can be described analogously to the exciton generation and recombination as

$$r_{\text{gr} \rightarrow \text{ct}} = (1 - f_{\text{ct}}) N_{\text{ct}} \int R_{\text{ct}}^{\text{gr}} \phi_{\text{ct}}^{\text{in}} dE_{\gamma} \quad \text{and}$$

$$r_{\text{ct} \rightarrow \text{gr}} = f_{\text{ct}} N_{\text{ct}} \int R_{\text{gr}}^{\text{ct}} dE_{\gamma},$$

where E_{γ} stands for the photon energy.

The dissociation rate of bounded CT electron-hole pairs into free carriers $r_{\text{ct} \rightarrow \text{np}}$ and its inverse process $r_{\text{np} \rightarrow \text{ct}}$ are given by

$$r_{\text{ct} \rightarrow \text{np}} = R_{\text{np}}^{\text{ct}} f_{\text{ct}} N_{\text{ct}} \quad \text{and}$$

$$r_{\text{np} \rightarrow \text{ct}} = R_{\text{ct}}^{\text{np}} np (1 - f_{\text{ct}}) N_{\text{ct}},$$

where np denotes the number of free charge carriers, $R_{\text{np}}^{\text{ct}}$ and $R_{\text{ct}}^{\text{np}}$ the respective rate coefficients.

Detailed Balance All introduced rates fulfill the principle of detailed balance which states that in thermodynamic equilibrium every rate is counterbalanced by its reverse process, i.e. $r_{ct \rightarrow x} = r_{x \rightarrow ct}$, $r_{ct \rightarrow gr} = r_{np \rightarrow gr}$, $r_{ct \rightarrow np} = r_{np \rightarrow ct}$, and $r_{x \rightarrow gr} = r_{gr \rightarrow x}$. Therefore, each respective pair of coefficient rates bears only one free parameter, which are in the following referred to as the rate constants.

In the following, two different electron transfer theories that provide a mathematical description of the newly introduced rate coefficients are introduced. The two theories will be applied and compared throughout the subsequent sections.

Rate Coefficients by Miller-Abrahams Obeying the principle of detailed balance the rate coefficients according to Miller-Abrahams are given by

$$\begin{aligned}
 R_{np}^{ct} &= \begin{cases} k_{np} N_{np} e^{E_{ct} - E_g/kT} \\ k_{np} N_{np} \end{cases} & R_{ct}^{np} &= \begin{cases} k_{np} \\ k_{np} e^{E_g - E_{ct}/kT} \end{cases} \quad \text{for } \begin{cases} E_{ct} < E_g \\ E_{ct} \geq E_g \end{cases} \\
 R_x^{ct} &= \begin{cases} k_x e^{E_{ct} - E_x/kT} \\ k_x \end{cases} & R_{ct}^x &= \begin{cases} k_x \\ k_x e^{E_x - E_{ct}/kT} \end{cases} \quad \text{for } \begin{cases} E_{ct} < E_x \\ E_{ct} \geq E_x \end{cases} \\
 R_{gr}^{ct} &= k_{gr} \delta(E_{ct} - E_\gamma) & R_{ct}^{gr} &= k_{gr} / \phi_{y,0}^{in} e^{-E_{ct}/kT} \delta(E_{ct} - E_\gamma) \\
 R_{gr}^x &= \tilde{k}_x & R_x^{gr} &= \tilde{k}_x / \phi_{x,0}^{in} e^{-E_x/kT}
 \end{aligned}$$

where k_{np} , k_x , k_{gr} , and \tilde{k}_x denote the respective rate constants, $\phi_{ct,0}^{in}(E_\gamma)$ is the incoming photon flux at photon energy E_γ per unit energy in thermodynamic equilibrium. The photon flux $\phi_{x,0}^{in}$, however, is independent of energy and denotes the flux of all photons in thermodynamic equilibrium with energies high enough to generate excitons.

Rate Coefficients by Marcus According to the Marcus theory the rate coefficients exhibit an inverse regime in which the transfer rate $A \rightarrow B$

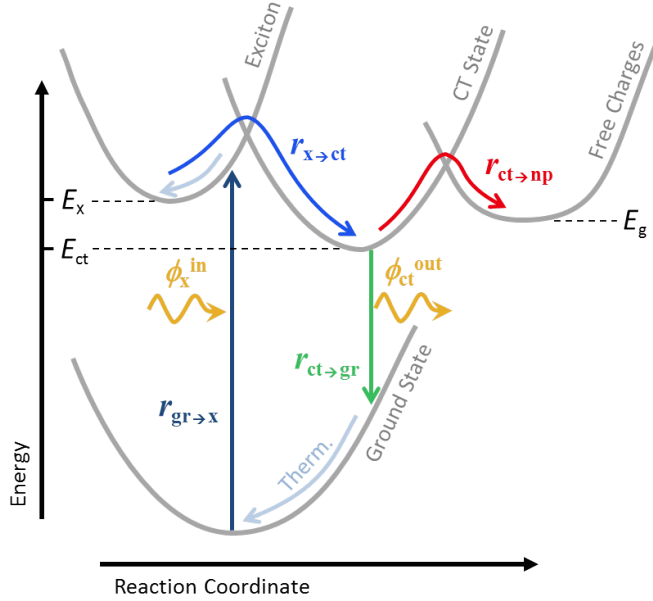


Fig. 5.2 Schematic drawing of the rate model with the reaction coordinate and typical parabolic representation according to Marcus theory. For clarity, only the predominant transfer rates of a solar cell under illumination are shown.

decreases for increasing energy difference $E_A - E_B$. The rate coefficients can be written as

$$R_{np}^{ct} = k_{np} N_{np} e^{-(E_g - E_{ct} + \lambda)^2 / 4\lambda kT} \quad R_{ct}^{np} = k_{np} e^{-(E_g - E_{ct} - \lambda)^2 / 4\lambda kT}$$

$$R_x^{ct} = k_x e^{-(E_x - E_{ct} + \lambda)^2 / 4\lambda kT} \quad R_{ct}^x = k_x e^{-(E_x - E_{ct} - \lambda)^2 / 4\lambda kT}$$

$$R_{gr}^{ct} = k_{gr} e^{-(E_{ct} - E_g + \lambda)^2 / 4\lambda kT} \quad R_{ct}^{gr} = k_{gr} / [\phi_{y,0}^{in} (e^{E_g/kT} - 1)] e^{-(E_{ct} - E_g + \lambda)^2 / 4\lambda kT}$$

Because the Marcus Theory and Miller-Abrahams theories are both compatible with the principle of detailed balance, the parameters for the rate coefficients R_{gr}^x and R_x^{gr} in the Marcus theory can be chosen to be the same as for Miller-Abrahams without changing the kinetics of the model.

Tab. 5.1 Overview of introduced variables and their units.

transfer and generation rates							
$r_{\text{gr} \rightarrow \text{x}}$	s^{-1}	$r_{\text{x} \rightarrow \text{ct}}$	$\text{eV}^{-1} s^{-1}$	$r_{\text{gr} \rightarrow \text{ct}}$	$\text{eV}^{-1} s^{-1}$	$r_{\text{np} \rightarrow \text{ct}}$	$\text{eV}^{-1} s^{-1}$
$r_{\text{x} \rightarrow \text{gr}}$	s^{-1}	$r_{\text{ct} \rightarrow \text{x}}$	$\text{eV}^{-1} s^{-1}$	$r_{\text{ct} \rightarrow \text{gr}}$	$\text{eV}^{-1} s^{-1}$	$r_{\text{ct} \rightarrow \text{np}}$	$\text{eV}^{-1} s^{-1}$
rate coefficients							
R_{x}^{gr}	—	R_{ct}^{x}	s^{-1}	$R_{\text{ct}}^{\text{gr}}$	—	$R_{\text{ct}}^{\text{np}}$	s^{-1}
R_{gr}^{x}	s^{-1}	R_{x}^{ct}	s^{-1}	$R_{\text{gr}}^{\text{ct}}$	$\text{eV}^{-1} s^{-1}$	$R_{\text{np}}^{\text{ct}}$	s^{-1}
rate constants							
\tilde{k}_{x}	s^{-1}	k_{x}	s^{-1}	k_{gr}	$\text{eV}^{-1} s^{-1}$	k_{np}	s^{-1}
weighted rate coefficients (defined in Equation 5.3)							
$W_{\text{x}}^{\text{out}}$	s^{-1}	$W_{\text{gr}}^{\text{out}}$	s^{-1}	$W_{\text{np}}^{\text{out}}$	s^{-1}		
W_{x}^{in}	s^{-1}	$W_{\text{gr}}^{\text{in}}$	s^{-1}	$W_{\text{np}}^{\text{in}}$	s^{-1}		
photon fluxes and number of states							
$\phi_{\text{x}}^{\text{in}}$	s^{-1}	$\phi_{\text{ct}}^{\text{in}}$	$\text{eV}^{-1} s^{-1}$	N_{x}	—	N_{ct}	eV^{-1}

In addition to Figure 5.1, a schematic drawing of the rate model is illustrated in Figure 5.2. This drawing is for the reader that is more familiar with the well-known picture of the transfer rates according to Marcus theory where states are represented as parabolas over the reaction coordinate. In the interest of greater clarity, only the predominant transfer rates of a solar cell under illumination are shown this time.

Units of Introduced Variables For clarity Table 5.1 summarizes the introduced variables and their units. Even though the units are chosen here as 0-dimensional, it is straightforward to interpret these variables also as properties in the 3-dimensional space.

5.2 Occupation Probability of Charge Transfer States

The change of the occupied exciton x and CT states ct over time can be calculated by summing up all incoming rates and subtracting all outgoing rates

$$\begin{aligned}\frac{dx}{dt} &= r_{gr \rightarrow x} - r_{x \rightarrow gr} + \int r_{ct \rightarrow x} dE_{ct} - \int r_{x \rightarrow ct} dE_{ct} \\ \frac{dct}{dt} &= r_{np \rightarrow ct} + r_{x \rightarrow ct} + r_{gr \rightarrow ct} - r_{ct \rightarrow np} - r_{ct \rightarrow x} - r_{ct \rightarrow gr}.\end{aligned}\quad (5.1)$$

Under steady-state conditions the number of occupied CT states is constant, i.e. $\frac{dct}{dt} = 0$, and Equation (5.1) can be solved for f_{ct} as

$$f_{ct} = \frac{(W_{np}^{in} + W_x^{in} + W_{gr}^{in})}{(W_{np}^{in} + W_x^{in} + W_{gr}^{in}) + (W_{np}^{out} + W_x^{out} + W_{gr}^{out})}.\quad (5.2)$$

For simplicity, the weighted rate coefficients for all rates into and out of the CT state are introduced

$$\begin{aligned}W_{gr}^{in} &= \int R_{ct}^{gr} \phi_{ct}^{in} dE_\gamma & W_{gr}^{out} &= \int R_{gr}^{ct} dE_\gamma \\ W_{np}^{in} &= R_{ct}^{np} np & W_{np}^{out} &= R_{np}^{ct} \\ W_x^{in} &= R_{ct}^x f_x N_x & W_x^{out} &= R_x^{ct} (1 - f_x) N_x.\end{aligned}\quad (5.3)$$

Figure 5.3 shows the incoming weighted rate coefficients W_{np}^{in} (red), W_x^{in} (blue), and W_{gr}^{in} (green) as solid lines. The respective outgoing weighted rate coefficients are depicted as dashed lines. The weighted rate coefficients for the electron transfer between the CT and the ground state W_{gr}^{in} and W_{gr}^{out} are in relation to the other coefficients almost constant as a function of energy for Miller-Abrahams (a) and the Marcus Theory (b). In the case of the Miller-Abrahams theory, all other outgoing rates increase exponentially for low CT state energies E_{ct} and then stay constant above a certain energy. In contrast, the incoming

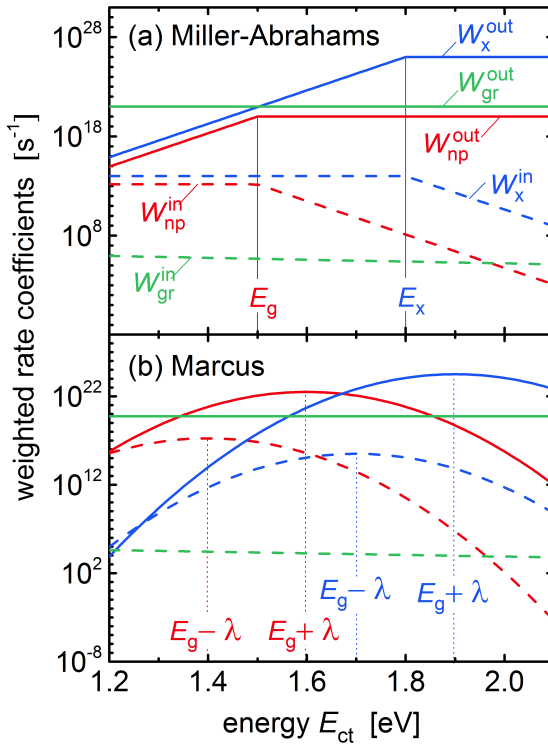


Fig. 5.3 The incoming (dashed) and outgoing (solid) weighted rate coefficients $W_{\text{np}}^{\text{in}}$ (red), $W_{\text{np}}^{\text{out}}$ (red), W_{x}^{in} (blue), $W_{\text{x}}^{\text{out}}$ (blue), $W_{\text{gr}}^{\text{in}}$ (green) and $W_{\text{gr}}^{\text{out}}$ (green) defined by Equation (5.3) according to (a) Miller-Abrahams and (b) the Marcus Theory.

rates are first constant and then decrease exponentially. The turning point for the weighted coefficient describing the transfer between bounded charge carriers in the CT state and free carriers $W_{\text{np}}^{\text{in}}$ and $W_{\text{np}}^{\text{out}}$ is at $E_{\text{ct}} = E_g$, and the turning points for W_{x}^{in} and $W_{\text{x}}^{\text{out}}$ are at $E_{\text{ct}} = E_x$ respectively. For the Marcus theory, the four weighted rates $W_{\text{np}}^{\text{in}}$, $W_{\text{np}}^{\text{out}}$, W_{x}^{in} and $W_{\text{x}}^{\text{out}}$ follow a Gaussian distribution with maxima at $E_g - \lambda$, $E_g + \lambda$, $E_x - \lambda$ and $E_x + \lambda$ and a width of $\sigma = \sqrt{2\lambda kT}$.

5.2.1 Occupation According to Miller-Abrahams Transfer Rates

In this subsection the occupation probability f_{ct} will be analyzed assuming Miller-Abrahams transfer rates for two different excitation paths: electroluminescence and photoluminescence. A solar cell is considered to be under electroluminescence condition if the applied voltage is high enough that the weighted rate coefficient W_{np}^{in} dominates all incoming coefficients, i.e. $W_{np}^{in} \gg W_{gr}^{in} + W_x^{in}$. An illuminated solar cell is under photoluminescence condition if f_{ct} is dominated by W_x^{in} , i.e. $W_x^{in} \gg W_{gr}^{in} + W_{np}^{in}$. Theoretically there is a third option, where the input rates are dominated by a direct excitation of the CT state. However, this case is highly unrealistic for state-of-the-art solar cells and therefore not treated in this thesis.

Electroluminescence

Figure 5.4 depicts the interplay between weighted rate coefficients and occupation probability in the case of electroluminescence. As can be seen in Figure 5.4a, the weighted rate coefficients W_{gr}^{out} (green), W_x^{out} (blue) and W_{np}^{out} (red solid) as well as the incoming coefficient W_{np}^{in} (red dashed) for $V = 0.5-2$ V in steps of 0.25 V are shown. The corresponding occupation probabilities f_{ct} are shown in Figure 5.4b. According to Equation (5.2) the slope of f_{ct} is completely determined by the energy range and the dominant outgoing weighted coefficient.

Non-Saturation Figure 5.4c depicts the dependence of f_{ct} on E_{ct} in the case of non-saturation for all possible dominating outgoing weighted rate coefficients (W_{gr}^{out} , W_{np}^{out} and W_x^{out}) and energy ranges $E_{ct} < E_g$ (left column), $E_g < E_{ct} < E_x$ (middle column) and $E_{ct} < E_g$ (right column). A constant occupation probability (light gray horizontal line) can only be observed in the case of dominating W_{gr}^{out} with $E_{ct} < E_g$. If W_x^{out} dominates in the interval $E_g < E_{ct} < E_x$, it holds

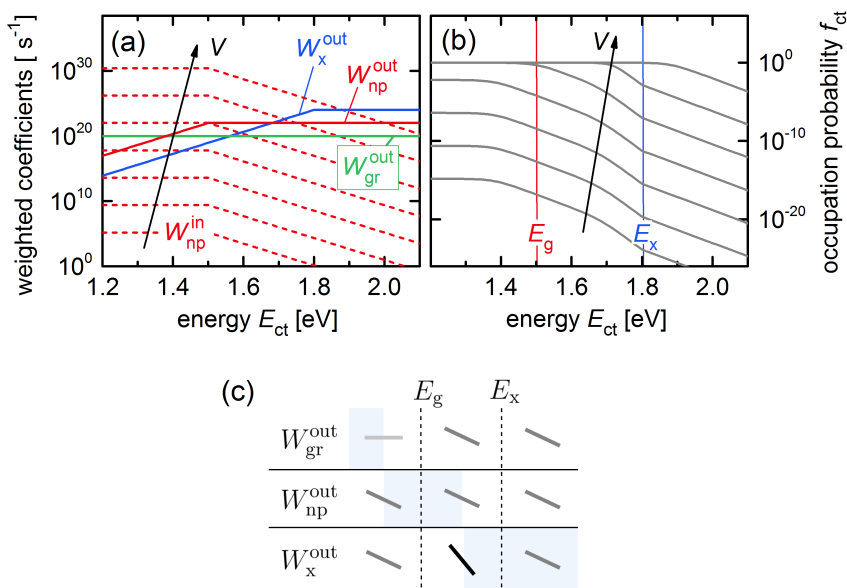


Fig. 5.4 Miller-Abrahams, Electroluminescence (EL): (a) Weighted coefficients $W_{\text{gr}}^{\text{out}}$ (green), $W_{\text{x}}^{\text{out}}$ (blue) and $W_{\text{np}}^{\text{out}}$ (red solid) in the case of EL where $W_{\text{np}}^{\text{in}}$ (red dashed) is the dominating input coefficient shown for voltages from 0.5 V to 2 V in steps of 0.25 V. (b) Corresponding occupation probability f_{ct} of the CT state. (c) Gives a schematic overview on how the weighted rate coefficients determine the slope of f_{ct} assuming non-saturation. The slope of f_{ct} is determined by the energy range and dominant weighted outgoing coefficient. There are three possible dependencies of f_{ct} on energy: it can be constant (light gray), proportional to $\exp(-E/kT)$ (gray), or $\exp(-2E/kT)$ (black). The light blue background indicates the cases displayed in (b).

that $f_{\text{ct}} \propto \exp(-2E_{\text{ct}}/kT)$ (black line). In all other cases f_{ct} decreases with $\exp(-E_{\text{ct}}/kT)$ (gray lines). The light blue rectangles highlight all cases that can be seen in Figure 5.4a and 5.4b.

Saturation With reference to Equation (5.2), it can be shown that the CT state is saturated if $W_{\text{np}}^{\text{in}}$ is much greater than all outgoing coefficients leading to $f_{\text{ct}} \approx 1$. For the chosen parameters saturation occurs for example at 1.5 V for energies lower than 1.5 eV and for 2 V all states with $E_{\text{ct}} < 1.85$ eV are saturated.

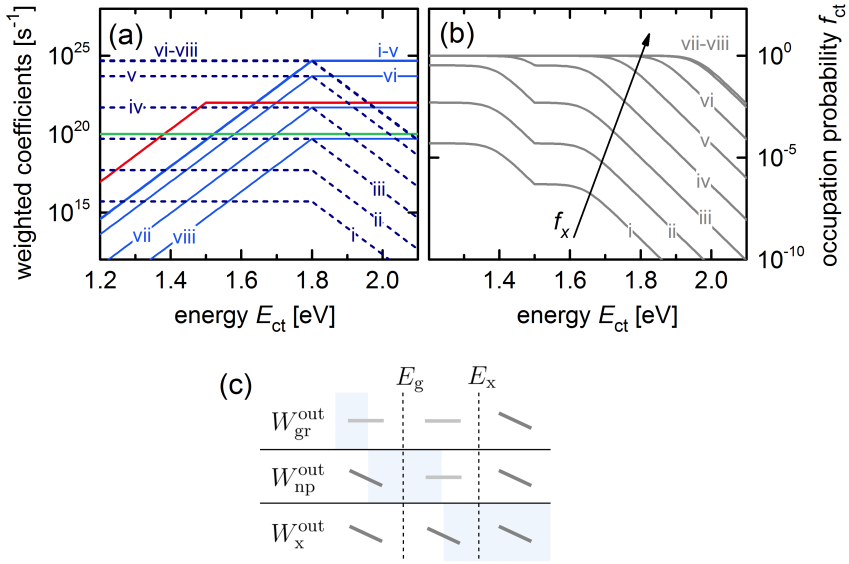


Fig. 5.5 Miller-Abrahams, Photoluminescence (PL): (a) Weighted coefficients W_{gr}^{out} (green), W_{np}^{out} (red) and W_x^{out} (blue solid) under PL conditions where W_x^{in} (blue dashed) is the dominating input coefficient for $\log(f_x) = -9, -7, -5, -3, -1$ (i-v) and $\log(1 - f_x) = -1, -3, -5$ (vi-viii). (b) Corresponding occupation probability f_{ct} of the CT state. (c) Gives a schematic explanation on how the weighted rate coefficients determine the slope of f_{ct} assuming non-saturation. The metric distincts different energy ranges and dominant weighted output coefficients. There are two possible dependencies of f_{ct} on energy: proportional to $\exp(-E/kT)$ (dark gray) or constant (light gray). The light blue background indicates the cases presented in (b).

Photoluminescence

Analogously to Figure 5.4, Figure 5.5 shows the weighted coefficients (a) and the resulting occupation probability f_{ct} (b) under eight exemplarily chosen illumination levels. The variation of illumination is simulated by different occupation probabilities f_x of the exciton states $\log(f_x) = -9, -7, -5, -3, -1$ (i to v) and $\log(1 - f_x) = -1, -3, -5$ (vi to viii). The values for f_x have been chosen to logarithmically approach 0 and 1 to clearly visualize the effects of the full range of illumination intensity. The weighted coefficients W_{gr}^{out} (green) and W_{np}^{out} (red) are

chosen to be the same as in Figure 5.4 and independent on f_x . However, W_{np}^{out} (blue solid) is proportional to $1 - f_x$ and therefore decreases with increasing f_x . For cases (i) to (v) the effect is too small to be visible, in contrast to cases (vi) to (viii) where the decrease becomes significant. The ingoing coefficient W_x^{in} (blue dashed) is proportional to f_x and an increase of W_x^{in} with f_x is evident for (i) to (vi) in Figure 5.5a.

Saturation Under saturation, the occupation f_{ct} is close to unity which holds if $W_x^{in} \gg \sum_{j=\{gr,np,x\}} W_j^{out}$. The saturation of f_{ct} can, for example, be seen in the energy range 1.2 eV to 1.7 eV for $f_x = 0.1$ (v). For $f_x > 0.1$ (vi-viii), the outgoing rate W_x^{out} decreases such that W_{np}^{out} is dominant even for higher energies and $f_{ct} \approx 1$ is valid for energies up to 1.9 eV. Saturation of f_{ct} for $E_{ct} < 1.9$ eV is prevented by the then dominating W_{np}^{out} .

Non-Saturation The CT state is non-saturated for cases (i) to (iii), i.e. $W_x^{in} \ll \sum_{j=\{gr,np,x\}} W_j^{out}$. Figure 5.5c shows the dependence of f_{ct} on E_{ct} for the case of non-saturation for all possible dominating outgoing weighted rate coefficients (W_{gr}^{out} , W_{np}^{out} and W_x^{out}) and energy ranges $E_{ct} < E_g$ (left column), $E_g < E_{ct} < E_x$ (middle column) and $E_{ct} < E_g$ (right column). The occupation probability f_{ct} is constant for energies where the dominating ingoing and outgoing rate coefficients are constant, i.e. from approximately 1.2 eV to 1.4 eV where W_{gr}^{out} dominates and from 1.5 eV to 1.6 eV with dominating W_{np}^{out} . Under non-saturation, f_{ct} decreases with $\exp(-E_{ct}/kT)$ for $1.4 \text{ eV} < E_{ct} < 1.5 \text{ eV}$ and approximately $E_{ct} > 1.6 \text{ eV}$. The cases that are shown in Figure 5.5a and 5.5b are highlighted in the overview table shown in Figure 5.5c.

5.2.2 Occupation According to Marcus Transfer Rates

Analogously to the previous analysis of f_{ct} for Miller-Abrahams, the occupation probability f_{ct} will now be discussed for transfer rates

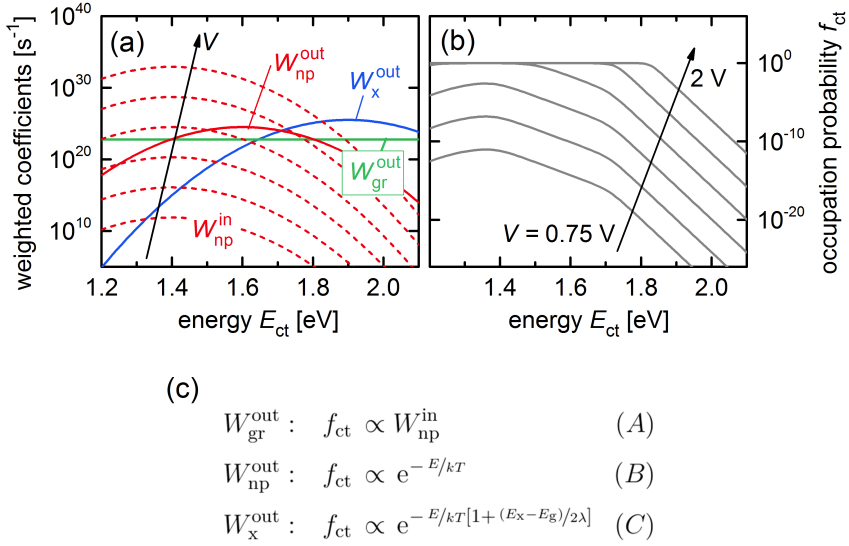


Fig. 5.6 Marcus, Electroluminescence (EL): (a) Weighted coefficients $W_{\text{gr}}^{\text{out}}$ (green), $W_{\text{x}}^{\text{out}}$ (blue) and $W_{\text{np}}^{\text{out}}$ (red solid) in the case of EL where $W_{\text{np}}^{\text{in}}$ (red dashed) is the dominating input coefficient for voltages $V = 0.75\text{--}2\text{ V}$ in steps of 0.25 V . (b) Corresponding occupation probability f_{ct} of the CT state. (c) Gives an overview on how the dominating weighted outgoing coefficients determine the slope of f_{ct} under non-saturation.

according to Marcus theory. Again, two different excitation paths are distinguished: electro- and photoluminescence.

Electroluminescence

In Figure 5.6a the outgoing weighted coefficients $W_{\text{gr}}^{\text{out}}$ (green), $W_{\text{x}}^{\text{out}}$ (blue) and $W_{\text{np}}^{\text{out}}$ (red solid) are depicted. As noted previously, under electroluminescence the incoming weighted coefficient $W_{\text{np}}^{\text{in}}$ (red dashed) dominates the incoming fluxes and is shown here for voltages of 0.75 V to 2.0 V in steps of 0.25 V . The occupation probabilities f_{ct} resulting from the applied voltages are shown in Figure 5.6b.

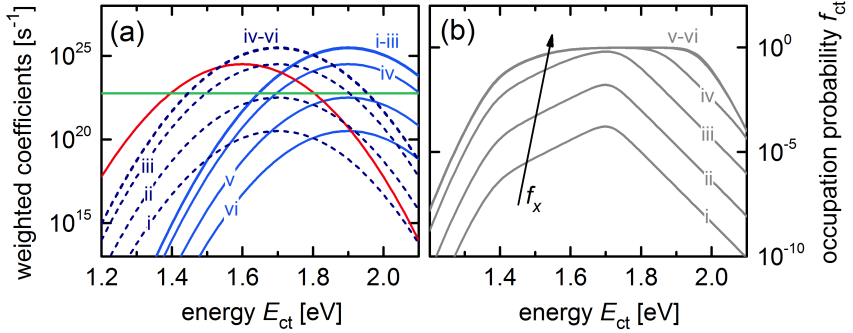
Saturation The CT state is saturated for $W_{np}^{in} \gg \sum_{j=\{gr,np,x\}} W_j^{out}$ as can be seen for example for the highest applied voltage $V = 2$ V for all energies below 1.8 eV.

Non-Saturation One can distinguish between three cases under non-saturation, where $W_{np}^{in} \ll \sum_{j=\{gr,np,x\}} W_j^{out}$, as noted in Figure 5.6c. (A) denotes the case for which W_{gr}^{out} is the dominant output channel. In this case the occupation f_{ct} is proportional to W_{np}^{in} , thus, follows a Gaussian shape with maximum at $E_g + \lambda$. For the chosen parameters, (A) holds for energies $E_{ct} < 1.4$ eV. For 1.4 eV $< E_{ct} < 1.7$ eV, the outgoing coefficients are dominated by W_{np}^{out} . This is referred to as case (B) where the occupation f_{ct} decreases exponentially. Finally, case (C) denotes the steepest decrease exhibited for $E_{ct} > 1.7$ eV. In this case the weighted coefficient W_x^{out} is higher than all other outgoing coefficients. It follows that the peak occupation in the CT state can be reached at any energy with $E_{ct} \leq E_g - \lambda$.

Photoluminescence

Depicted in Figure 5.7, are the weighted rate coefficients and resulting occupation for an exemplarily chosen case of photoluminescence. The outgoing weighted rate coefficients W_{gr}^{out} (green), W_{np}^{out} (red) and W_x^{out} (blue solid) are chosen to be the same as in the case of electroluminescence in Figure 5.6. The input coefficient W_x^{in} (blue dashed), the dominant channel under photoluminescence, is shown for $\log(f_x) = -5, -3, -1$ (i-iii) and $\log(1 - f_x) = -1, -3, -5$ (iv-vi). Note that the inverse channel W_x^{out} is also dependent on the occupation probability f_x of the exciton state which becomes visible for high excitation levels $f_x \approx 1$ (iv-vi). The resulting occupation probabilities f_{ct} of the chosen excitation levels are shown in Figure 5.7b.

Saturation For $W_x^{in} \gg \sum_{j=\{gr,np,x\}} W_j^{out}$, the CT state is saturated ($f_{ct} \approx 1$). The saturation can readily be seen in Figure 5.7b for the



(c)

$$W_{\text{gr}}^{\text{out}} : f_{\text{ct}} \propto W_x^{\text{in}} \quad (A)$$

$$W_{\text{np}}^{\text{out}} : f_{\text{ct}} \propto e^{-E/kT[1-(E_x-E_g)/2\lambda]} \quad (B)$$

$$W_x^{\text{out}} : f_{\text{ct}} \propto e^{-E/kT} \quad (C)$$

Fig. 5.7 Marcus, Photoluminescence (PL): (a) Weighted coefficients $W_{\text{gr}}^{\text{out}}$ (green), $W_{\text{np}}^{\text{out}}$ (red) and W_x^{out} (blue solid) in the case of PL where W_x^{in} (blue dashed) is the dominating input coefficient for $\log(f_x) = -5, -3, -1$ (i-iii) and $\log(1 - f_x) = -1, -3, -5$ (iv-vi). (b) Corresponding occupation probability f_{ct} of the CT state. (c) Gives an overview on how the weighted rate coefficients determine the slope of f_{ct} under non-saturation conditions.

highest excitation levels (v) and (vi) at CT state energies between 1.53 eV and 1.96 eV.

Non-Saturation In the non-saturated case three cases are once again differentiated. An overview of the different cases with their respective f_{ct} functional proportionalities is provided in Figure 5.7c. Case (A) denotes the case for which $W_{\text{gr}}^{\text{out}}$ is the dominating output channel. In this case the occupation f_{ct} is proportional to W_{x}^{in} following a Gaussian shape with maximum at $E_{\text{x}} - \lambda$. For the chosen parameters (A) holds for energies $E_{\text{ct}} < 1.4 \text{ eV}$. For $1.4 \text{ eV} < E_{\text{ct}} < 1.7 \text{ eV}$, the outgoing coefficients are dominated by $W_{\text{np}}^{\text{out}}$ and the occupation f_{ct} decreases exponentially which is referred to as case (B). Note that in contrast to the occupation under electroluminescence, f_{ct} can also increase in case (B) under photoluminescence. The occupation f_{ct} decreases in case (B) only if $E_{\text{x}} - E_{\text{g}} < 2\lambda$. The weighted coefficient $W_{\text{x}}^{\text{out}}$ dominates all other outgoing coefficients in case (C). For case (C), the occupation f_{ct} is always exponentially decreasing and can be seen in Figure 5.7b for $E_{\text{ct}} > 1.7 \text{ eV}$. In summary, under photoluminescence, in contrast to electroluminescence, the peak occupation of the CT state can be reached at any energy E_{ct} .

5.3 Superposition of Electro- and Photoluminescence

The luminescence $\phi_{\text{ct}}^{\text{out}}$ of the CT state is given by

$$\phi_{\text{ct}}^{\text{out}}(E_\gamma) = \int f_{\text{ct}} N_{\text{ct}} R_{\text{gr}}^{\text{ct}} dE. \quad (5.4)$$

The superposition of electroluminescence EL, the photoluminescence via CT state excitation PL_{ct} and the photoluminescence via exciton excitation PL_{x} can therefore be proven by showing that the overall occupation probability f_{ct} is the sum of the occupation probabilities of each individual input channel. As can be seen from Equation (5.2), the occupation probability f_{ct} can directly be expressed by the weighted coefficients.

It follows that the superposition is only valid in the non-saturated case, i.e. for $1 - f_{\text{ct}} \approx 1 - f_{\text{x}} \approx 1$. Under non-saturation conditions, the denominator is determined by the sum of the outgoing weighted coefficients $\sum W^{\text{out}} = W_{\text{gr}}^{\text{out}} + W_{\text{np}}^{\text{out}} + W_{\text{x}}^{\text{out}}$. Moreover, as $1 - f_{\text{x}} \approx 1$, the sum $\sum W^{\text{out}}$ is independent of the different injection/excitation rates np , $\phi_{\text{ct}}^{\text{in}}$, and f_{x} . Equation (5.2) can thus be written as

$$f_{\text{ct}} \stackrel{\text{non. sat.}}{=} \underbrace{\frac{W_{\text{np}}^{\text{in}}}{\sum W^{\text{out}}}}_{\text{EL}} + \underbrace{\frac{W_{\text{x}}^{\text{in}}}{\sum W^{\text{out}}}}_{\text{PL}_{\text{x}}} + \underbrace{\frac{W_{\text{gr}}^{\text{in}}}{\sum W^{\text{out}}}}_{\text{PL}_{\text{ct}}} \quad (5.5)$$

in the non-saturation case. Hence, the occupation of the CT state f_{ct} is the sum of the occupation probabilities for each individual excitation path. Consequently, Equation (5.5) in combination with Equation (5.4) proves, due to the linearity of integration, that the superposition of electro- and photoluminescence is valid if and only if the exciton and CT states are not saturated.

5.4 Opto-Electronic Reciprocity

The opto-electronic reciprocity relation, Equation (2.10), also holds for the introduced model for organic solar cells if no saturation effects occur. A proof will be presented by discretization of the charge transfer energy ($E_{ct}^1, \dots, E_{ct}^n$) and the photon energy ($E_\gamma^1, \dots, E_\gamma^m$). This approach is legitimate because only continuous functions are involved. In the case of non-saturation ($1 - f_{ct} \approx 1 - f_x \approx 1$), Equation (5.1) can be written as

$$\begin{aligned} \frac{dx}{dt} &= N_x \left[R_x^{gr} \phi_x^{in} - R_{gr}^x f_x + \sum_{E_{ct}} R_x^{ct} f_{ct} N_{ct} - f_x \sum_{E_{ct}} R_{ct}^x N_{ct} \right] = 0 \\ \frac{dct}{dt} &= N_{ct} \left[\sum_{E_\gamma} R_{ct}^{gr} \phi_{ct}^{in} - f_{ct} \sum_{E_\gamma} R_{gr}^{ct} + R_{ct}^x f_x N_x - R_x^{ct} N_x f_{ct} \right. \\ &\quad \left. + R_{ct}^{np} np - R_{np}^{ct} f_{ct} \right] = 0. \end{aligned}$$

Note that the photon fluxes ϕ and the number of states N are dimensionless, i.e. number of photons/states per chosen discretization interval. Moreover, the later equation represents a set of equations as it holds for each charge transfer energy.

Motivated by the principle of detailed balance that connects each electron transfer with its inverse process, the normalized rate constants

$$\begin{aligned} \rho_{x/ct}^{gr} &:= R_{x/ct}^{gr} \phi_{x/ct,0}^{in} = R_{gr}^{x/ct} f_{x/ct,0} \\ \rho_{ct}^x &:= R_{ct}^x f_{x,0} = R_x^{ct} f_{ct,0} \quad \text{and} \quad (5.6) \\ \rho_{ct}^{np} &:= R_{ct}^{np} n_0 p_0 = R_{np}^{ct} f_{ct,0} \end{aligned}$$

are introduced.

With the normalized excess occupation probabilities $\chi = (f_x - f_{x,0})/f_{x,0}$ and $\xi = (f_{ct} - f_{ct,0})/f_{ct,0}$, as well as the normalized parameters of the optical input $\varphi_{x/ct} = (\phi_{x/ct}^{in} - \phi_{x/ct,0}^{in})/\phi_{x/ct,0}^{in}$ and of the electrical

input $\nu = (np - n_0p_0)/n_0p_0$, the above equation system can be written in matrix notation as

$$\begin{aligned}
 A \cdot \begin{bmatrix} \chi \\ \vec{\xi} \end{bmatrix} &= \begin{bmatrix} \rho_x^{\text{gr}} + \sum_i \rho_{\text{ct}}^x(E_{\text{ct}}^i) & -\rho_{\text{ct}}^x(E_{\text{ct}}^1) & \dots & -\rho_{\text{ct}}^x(E_{\text{ct}}^n) \\ -\rho_{\text{ct}}^x(E_{\text{ct}}^1) & & & \\ \vdots & & D & \\ -\rho_{\text{ct}}^x(E_{\text{ct}}^n) & & & \end{bmatrix} \cdot \begin{bmatrix} \chi \\ \xi(E_{\text{ct}}^1) \\ \vdots \\ \xi(E_{\text{ct}}^n) \end{bmatrix} \\
 = B \begin{bmatrix} \varphi_x \\ \vec{\varphi}_{\text{ct}} \\ \nu \end{bmatrix} &= \begin{bmatrix} \rho_x^{\text{gr}} & 0 & \dots & 0 & 0 \\ 0 & \rho_{\text{ct}}^{\text{gr}}(E_{\text{ct}}^1, E_{\gamma}^1) & \dots & \rho_{\text{ct}}^{\text{gr}}(E_{\text{ct}}^1, E_{\gamma}^m) & \rho_{\text{ct}}^{\text{np}}(E_{\text{ct}}^1) \\ \vdots & \vdots & \ddots & \vdots & \vdots \\ 0 & \rho_{\text{ct}}^{\text{gr}}(E_{\text{ct}}^n, E_{\gamma}^1) & \dots & \rho_{\text{ct}}^{\text{gr}}(E_{\text{ct}}^n, E_{\gamma}^m) & \rho_{\text{ct}}^{\text{np}}(E_{\text{ct}}^n) \end{bmatrix} \cdot \begin{bmatrix} \varphi_x \\ \varphi_{\text{ct}}(E_{\gamma}^1) \\ \vdots \\ \varphi_{\text{ct}}(E_{\gamma}^m) \\ \nu \end{bmatrix}
 \end{aligned}$$

where the diagonal matrix D is given by

$$D_{mn} = \rho_{\text{ct}}^x(E_{\text{ct}}^n) + \rho_{\text{ct}}^{\text{np}}(E_{\text{ct}}^n) + \sum_i \rho_{\text{ct}}^{\text{gr}}(E_{\text{ct}}^n, E_{\gamma}^i). \quad (5.7)$$

This matrix equation links the normalized optical and electrical input potentials of an organic solar cell with the normalized occupation probabilities of its exciton and charge transfer states. Analogously,

$$\begin{bmatrix} \delta\phi_x^{\text{out}} \\ \delta\phi_{\text{ct}}^{\text{out}}(E_{\gamma}^1) \\ \vdots \\ \delta\phi_{\text{ct}}^{\text{out}}(E_{\gamma}^m) \\ \delta j_{\text{np}}^{\text{out}} \end{bmatrix} = B^{\text{tr}} \begin{bmatrix} \chi \\ \xi(E_{\text{ct}}^1) \\ \vdots \\ \xi(E_{\text{ct}}^n) \end{bmatrix} \quad (5.8)$$

describes the influence of the occupation probabilities χ and ξ on the optical and electrical output terminals of the solar cell, namely, the excess output photon fluxes $\delta\phi_{\text{x/ct}}^{\text{out}} := \phi_{\text{x/ct}}^{\text{out}} - \phi_{\text{x/ct},0}^{\text{out}}$ and the excess current $\delta j_{\text{np}}^{\text{out}}$ resulting from electron-hole pairs in the charge transfer state dissociating into free carriers. The matrix B^{tr} denotes the transposed matrix of B .

Therefore the electrical and optical input potentials φ and ν and output fluxes are directly connected via matrix S

$$\begin{bmatrix} \delta\phi_x^{\text{out}} \\ \delta\phi_{\text{ct}}^{\text{out}}(E_\gamma^1) \\ \vdots \\ \delta\phi_{\text{ct}}^{\text{out}}(E_\gamma^m) \\ \delta j_{\text{np}}^{\text{out}} \end{bmatrix} = \underbrace{B^{\text{tr}}A^{-1}B}_{=: S \text{ is symmetric}} \cdot \begin{bmatrix} \varphi_x \\ \varphi_{\text{ct}}(E_\gamma^1) \\ \vdots \\ \varphi_{\text{ct}}(E_\gamma^m) \\ \nu \end{bmatrix}. \quad (5.9)$$

Note, that S is symmetric because A is symmetric, see definition of matrices A and D .

The opto-electronic reciprocity relation connects the experimentally accessible electroluminescence ϕ_{em} of a solar cell with the external quantum efficiency Q_e^{PV} . In the present model the electroluminescence is equal to the outgoing excess photon flux $\delta\phi_{\text{ct}}^{\text{out}}$ that is caused exclusively by the electrical potential ν .

The external quantum efficiency Q_e^{PV} is determined by the quotient of the outgoing excess current $\delta j_{\text{np}}^{\text{out}}$ generated by the incoming excess photon flux $\delta\phi_{\text{ct}}^{\text{in}}(E_\gamma)$, $Q_e^{\text{PV}}(E_\gamma) = \delta j_{\text{np}}^{\text{out}} / \delta\phi_{\text{ct}}^{\text{in}}(E_\gamma)$. Under the conditions of electroluminescence or external quantum efficiency measurements, Equation (5.9) states

$$\begin{aligned} \delta j_{\text{np}}^{\text{out}} &= S_{m+2,k+1} \cdot \varphi_{\text{ct}}(E_\gamma^k) & \text{and} \\ \delta\phi_{\text{ct}}^{\text{out}}(E_\gamma^k) &= S_{k+1,m+2} \cdot \nu. \end{aligned} \quad (5.10)$$

By using the symmetry of S we finally attain the opto-electronic reciprocity relation

$$\begin{aligned} \phi_{\text{em}}(E_\gamma) &= \delta\phi_{\text{ct}}^{\text{out}}(E_\gamma) = \frac{\delta j_{\text{np}}^{\text{out}}}{\varphi_{\text{ct}}(E_\gamma)} \nu \\ &= Q_e^{\text{PV}}(E_\gamma) \phi_{\text{bb}}(E_\gamma, T_c) \left[\exp\left(\frac{qV}{kT}\right) - 1 \right], \end{aligned} \quad (5.11)$$

where ϕ_{bb} denotes the black body radiation and T_c temperature of the cell, i.e. $\phi_{\text{bb}}(E_\gamma, T_c) = \phi_{\text{ct},0}^{\text{in}}(E_\gamma)$.

This proof shows that the opto-electronic reciprocity relation that was originally derived for inorganic pn-junction solar cells²³ also holds for the rate model for organic solar cells introduced in this chapter under the assumption of linear recombination and generation rates as well as non-saturation. This model includes CT states and is valid for the Miller-Abrahams as well as the Marcus transfer rates. It is in fact valid for any recombination rate that fulfills the principle of detailed balance.

5.5 Collection Efficiency

For high power conversion efficiency it is crucial to optimize the overall collection efficiency of a cell defined by the fraction of generated excitons that dissociate into free charge carriers. For an exciton to dissociate in the present model, and therefore contribute to the current of the cell, it has to be captured by the CT state and then transferred into the state of free charges. Those two processes scale with the rate constants k_x and k_{np} . Intuitively, one would guess that collection becomes more efficient the faster the capture and transfer occurs, thus, that the collection efficiency increases with increasing k_x and/or k_{np} .

However, Figure 5.8 shows that the collection efficiency $\bar{\eta}_{\text{coll}}$ decreases for increasing k_x . The contour map visualizes $\bar{\eta}_{\text{coll}}$ as a function of k_x and k_{np} for (a) Miller-Abrahams and (b) Marcus theory. This counter-intuitive effect can be seen for both theories and is emphasized by the cross-sections in red at (a) $k_{np} = 10^4 \text{ s}^{-1}$ and (b) $k_{np} = 10^5 \text{ s}^{-1}$. The decrease in collection efficiency with increasing k_x cannot be explained by saturation effects since the occupation of the CT state is lower than 10^{-3} for the chosen parameters.

In order to more deeply understand the underlying mechanisms, it is necessary to take a closer look into the energy-dependent efficiencies. The following subsection defines the energy-dependent capture, transfer and collection efficiency as well as the respective overall efficiencies.

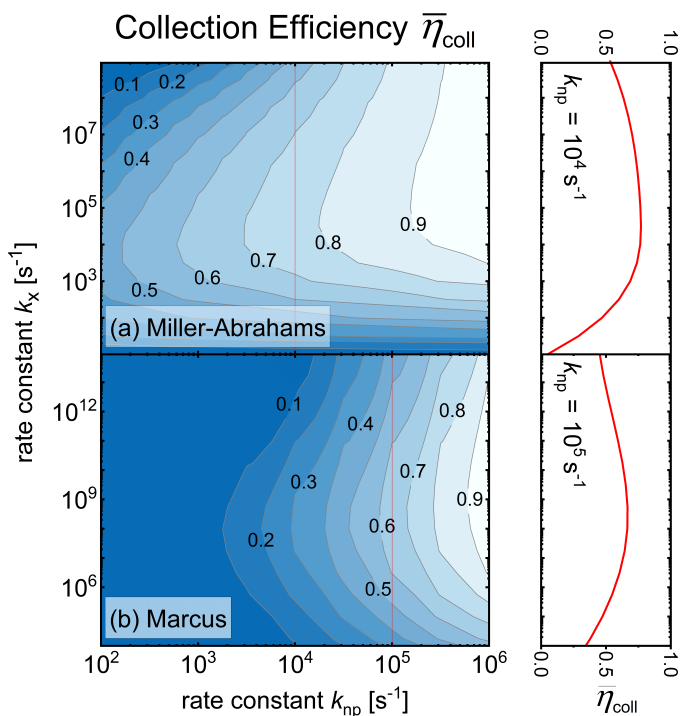


Fig. 5.8 Contour map of the overall collection efficiency $\bar{\eta}_{\text{coll}}$ as a function of rate constants for capture and transfer k_x and k_{np} for (a) Miller-Abrahams model and (b) Marcus theory. Counter-intuitively $\bar{\eta}_{\text{coll}}$ decreases for increasing k_x as illustrated exemplarily by the cross-sections (red) through the contour plots.

The effect of different parameters on the transfer efficiency will be analyzed in Section 5.5.2 and on the capture efficiency and its influence on the average efficiencies in Section 5.5.3.

5.5.1 Definition of the Capture, Transfer and Collection Efficiency

The overall collection efficiency $\bar{\eta}_{\text{coll}}$ is defined by the total current J of the cell divided by the generated current J_{gen} in the polymer. From there the energy-dependent collection, capture and transfer efficiencies, η_{coll} , η_{capt} , and η_{trans} are derived as follows

$$\begin{aligned}\bar{\eta}_{\text{coll}} &= \frac{J}{J_{\text{gen}}} = \int \frac{r_{\text{ct} \rightarrow \text{np}} - r_{\text{np} \rightarrow \text{ct}}}{r_{\text{gr} \rightarrow \text{x}}} dE_{\text{ct}} = \int \eta_{\text{coll}}(E_{\text{ct}}) dE_{\text{ct}} \\ &= \int \underbrace{\frac{r_{\text{ct} \rightarrow \text{np}} - r_{\text{np} \rightarrow \text{ct}}}{r_{\text{x} \rightarrow \text{ct}} - r_{\text{ct} \rightarrow \text{x}}}}_{\eta_{\text{trans}}(E_{\text{ct}})} \cdot \underbrace{\frac{r_{\text{x} \rightarrow \text{ct}} - r_{\text{ct} \rightarrow \text{x}}}{r_{\text{gr} \rightarrow \text{x}}}}_{\eta_{\text{capt}}(E_{\text{ct}})} dE_{\text{ct}} \\ &= \int \eta_{\text{trans}}(E_{\text{ct}}) \cdot \eta_{\text{capt}}(E_{\text{ct}}) dE_{\text{ct}}.\end{aligned}\quad (5.12)$$

The transfer efficiency η_{trans} is a measure of how efficiently bound charge carriers in a CT state, originating from the exciton state X , are transferred into a free charge carrier state np . The average transfer efficiency $\bar{\eta}_{\text{trans}}$ is defined as

$$\bar{\eta}_{\text{trans}} = \frac{\int r_{\text{ct} \rightarrow \text{np}} - r_{\text{np} \rightarrow \text{ct}} dE_{\text{ct}}}{\int r_{\text{x} \rightarrow \text{ct}} - r_{\text{ct} \rightarrow \text{x}} dE_{\text{ct}}}.\quad (5.13)$$

The capture efficiency η_{capt} states how efficiently generated excitons in the polymer are captured into a CT state before they would otherwise annihilate without getting the chance to be transferred into the state of free charges. The average capture efficiency can be calculated via

$$\bar{\eta}_{\text{capt}} = \int \eta_{\text{capt}}(E_{\text{ct}}) dE_{\text{ct}} = \frac{\int r_{\text{x} \rightarrow \text{ct}} - r_{\text{ct} \rightarrow \text{x}} dE_{\text{ct}}}{r_{\text{gr} \rightarrow \text{x}}}.\quad (5.14)$$

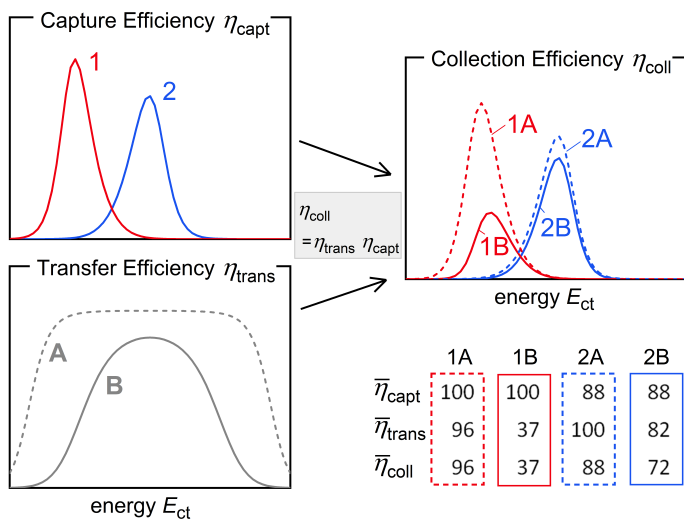


Fig. 5.9 Illustration of the interplay of the energy-dependent collection, capture and transfer efficiencies, η_{coll} , η_{capt} , and η_{trans} . Exemplarily two possibilities of η_{capt} with different peak positions and heights but similar shapes (1-red and 2-blue) are shown and two possible η_{trans} with same peak position but different shapes (A-dashed and B-solid). All cases are simulated cases according to the Marcus model. This leads to four cases for η_{coll} . The corresponding average efficiencies $\bar{\eta}_{\text{capt}}$, $\bar{\eta}_{\text{trans}}$, and $\bar{\eta}_{\text{coll}}$ are listed in the overview table.

Note that $r_{\text{gr} \rightarrow \text{x}}$ is independent of energy E_{ct} and therefore

$$\bar{\eta}_{\text{coll}} = \bar{\eta}_{\text{trans}} \cdot \bar{\eta}_{\text{capt}}.$$

Figure 5.9 illustrates the interplay of the introduced efficiencies and respective average efficiencies. Two different energy-dependent capture efficiencies η_{capt} labeled η_{capt}^1 (red) and η_{capt}^2 (blue) as well as two transfer efficiencies η_{trans} designated as $\eta_{\text{trans}}^{\text{A}}$ (dashed) and $\eta_{\text{trans}}^{\text{B}}$ (solid line) are exemplarily shown. These capture and transfer efficiencies are then combined to four different cases 1A, 1B, 2A and 2B indicating the respective capture and transfer efficiencies used to calculate the energy-dependent collection efficiency η_{coll} . For these four cases the

values of the corresponding average efficiencies $\bar{\eta}_{\text{capt}}$, $\bar{\eta}_{\text{trans}}$ and $\bar{\eta}_{\text{coll}}$ are listed in the overview table.

Capture efficiency η_{capt}^1 has a lower peak energy than η_{capt}^2 and a higher average efficiency $\bar{\eta}_{\text{capt}}^1 = 100\% > 88\% = \bar{\eta}_{\text{capt}}^2$. Note, that the average capture efficiency $\bar{\eta}_{\text{capt}}$ is according to Definition (5.14) equal to the area underneath η_{capt} . The two exemplarily shown transfer efficiencies have the same peak energy, however, the distribution of η_{trans}^A is much wider than η_{trans}^B . Additionally, the maximum of η_{trans}^A is higher and is almost the same value for the peak energies of η_{capt}^1 and η_{capt}^2 . The corresponding collection efficiencies η_{coll}^{1A} and η_{coll}^{2B} therefore resemble the functions of η_{capt}^1 and η_{capt}^2 . In contrast, η_{trans}^B is much lower at peak energy of η_{capt}^1 than of η_{capt}^2 and the collection efficiency is scaled accordingly. Leading to a smaller overall collection efficiency $\bar{\eta}_{\text{coll}}$ in case 1B than in case 2B even though $\bar{\eta}_{\text{capt}}^1 > \bar{\eta}_{\text{capt}}^2$.

It is important to point out that the average transfer efficiency $\bar{\eta}_{\text{trans}}$ is not the integral over η_{trans} . The transfer efficiency $\eta_{\text{trans}}(E_{\text{ct}})$ states how efficiently each CT state with energy E_{ct} dissociates charge carriers into free carrier. On the other hand $\bar{\eta}_{\text{trans}}$ is a measure of how efficiently the cell dissociates charge carriers meaning that only the CT states that capture efficiently excitons are important for the overall transfer efficiency of the CT state and hence $\bar{\eta}_{\text{trans}}^{1B} \neq \bar{\eta}_{\text{trans}}^{2B}$. In case 2B the state that most efficiently capture excitons are at the same time the one that most efficiently transfer them to the free charge carrier state whereas in case 1B most carriers that are captured by the CT states recombine in the CT state. Accordingly, only 37% are transferred to the free charge carrier state.

In the following, the focus will first be on the analysis of the energy-dependent transfer efficiency and its dependency on the relevant rate constants because this analysis is independent of saturation effects. In a second step, the dependency of the capture efficiency on the rate constant k_x under non-saturation are discussed for one exemplarily chosen η_{trans} . Last, the effect of saturation on the capture efficiency

as well as the consequences for the overall collection efficiency are presented.

5.5.2 Analysis of the Transfer Efficiency

If the solar cell is under collection condition, meaning that photons are converted into free charge carriers, we can assume that the overall rates from the exciton state to the CT state is much higher than its reverse process $\int r_{x \rightarrow ct} \gg \int r_{ct \rightarrow x}$. Moreover, under collection conditions more free charge carriers are generated from bounded charges in the CT state than vice versa $\int r_{ct \rightarrow np} \gg \int r_{np \rightarrow ct}$. Furthermore, it is assumed that the main generation path is via an exciton and not directly via excitation of the CT state and consequently $\int r_{ct \rightarrow gr} \gg \int r_{gr \rightarrow ct}$.

These assumptions hold under a wide and reasonable parameter range at each CT state energy, i.e. $r_{x \rightarrow ct} \gg r_{ct \rightarrow x}$, $r_{ct \rightarrow np} \gg r_{np \rightarrow ct}$ and $r_{ct \rightarrow gr} \gg r_{gr \rightarrow ct}$. The transfer efficiency can then be simplified under steady-state conditions, see Equation (5.1), to

$$\eta_{\text{trans}} \approx \frac{r_{ct \rightarrow np}}{r_{ct \rightarrow np} + r_{ct \rightarrow gr}} = \frac{R_{np}^{\text{ct}}}{R_{np}^{\text{ct}} + \int R_{gr}^{\text{ct}} dE_{\gamma}} = \frac{W_{np}^{\text{out}}}{W_{np}^{\text{out}} + W_{gr}^{\text{out}}}. \quad (5.15)$$

Figure 5.10 shows the transfer efficiency η_{trans} as a function of E_{ct} for different dissociation-to-recombination quotients $\beta := k_{np}N_{np}/k_{gr} = 0.1, 1, 10, 10^2, 10^3$, and 10^4 . (a) In the case of Miller-Abrahams, η_{trans} follows a mirrored Fermi-Dirac function $1/[\exp -(E_{ct} - \mu)/kT + 1]$ with $\mu = E_g - kT \log(\beta)$ for $E_{ct} < E_g$. Like any Fermi-Dirac distribution it reaches 50% at $E_{ct} = \mu$. For $E_{ct} > E_g$, the transfer efficiency η_{trans} is constant and equal to $1/(1 + \beta^{-1})$. (b) For Marcus Theory W_{gr}^{out} is constant whereas W_{np}^{out} is proportional to a Gaussian distribution with peak energy at $E_g + \lambda$ and width of $\sqrt{2\lambda kT}$. Therefore η_{trans} exhibits the Gaussian shape scaled by β with attenuation if the efficiency approaches 100%. Note, that the transfer efficiency only shows a

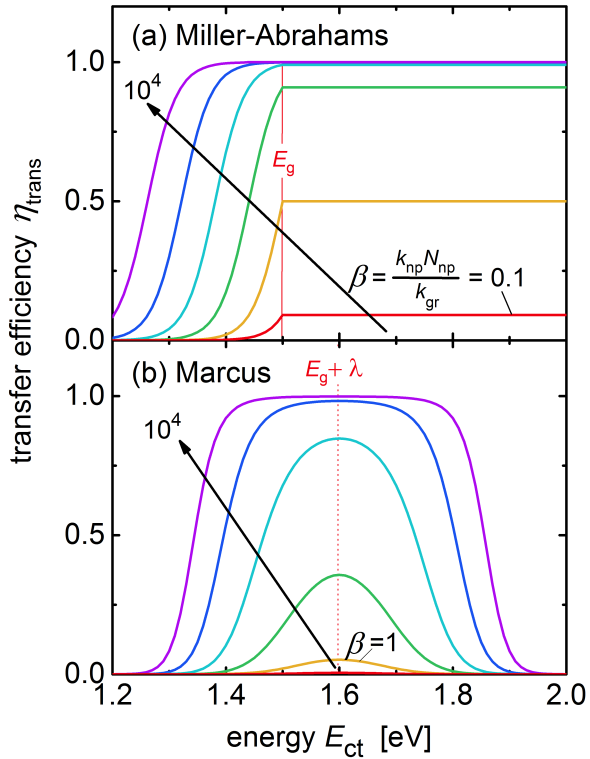


Fig. 5.10 The transfer efficiency η_{trans} is shown for the rate coefficient ratio $k_{\text{np}} N_{\text{np}} / k_{\text{gr}} = 0.1, 1, 10, 10^2, 10^3$ and 10^4 . (a) The transfer efficiency increases monotonously with energy for Miller-Abrahams whereas (b) the Marcus Theory shows its typical inverse regime with decreasing η_{trans} .

significant dependency on E_g and β , and in case of Marcus Theory additionally on λ .

5.5.3 Analysis of the Capture Efficiency

Because charge conservation holds in every CT state its capture efficiency can be written as

$$\eta_{\text{capt}} = \frac{[R_{\text{ct}}^{\text{x}} f_{\text{x}}(1 - f_{\text{ct}}) - R_{\text{x}}^{\text{ct}}(1 - f_{\text{x}})f] N_{\text{CT}}}{\int [R_{\text{ct}}^{\text{x}} f_{\text{x}}(1 - f_{\text{ct}}) - R_{\text{x}}^{\text{ct}}(1 - f_{\text{x}})f] N_{\text{CT}} dE + f_{\text{x}} R_{\text{gr}}^{\text{x}}}. \quad (5.16)$$

In the following the effect of different parameters on the capture efficiency under non-saturation and saturation will be discussed. Note that the recombination rate R_{gr}^{x} is independent of the CT state energy E_{ct} and therefore is not varied in the following analysis.

For all graphs in this section the energy-dependent transfer efficiency is chosen to be the one that corresponds to $\beta = 10^2$, shown as light blue curves in Figure 5.10.

Non-Saturation

In the case of non-saturation, $1 - f_{\text{x}} \approx 1 \approx 1 - f_{\text{ct}}$, the capture efficiency simplifies to

$$\eta_{\text{capt}} \stackrel{\text{non. sat.}}{=} \frac{[R_{\text{ct}}^{\text{x}} - R_{\text{x}}^{\text{ct}}(f_{\text{ct}}/f_{\text{x}})] N_{\text{CT}}}{\int [R_{\text{ct}}^{\text{x}} - R_{\text{x}}^{\text{ct}}(f_{\text{ct}}/f_{\text{x}})] N_{\text{CT}} dE + R_{\text{gr}}^{\text{x}}}. \quad (5.17)$$

Under collection conditions the CT states incoming fluxes are dominated by W_{x}^{in} . Therefore it follows directly from Equation (5.2) and (5.3) that under the assumption of non-saturation $f_{\text{ct}}/f_{\text{x}}$ is constant and consequently the capture efficiency is independent of f_{x} . Hence, the following discussion and conclusion on the capture effi-

ciency is generally valid in the case of non-saturation independent of the absolute occupation.

Figure 5.11a displays the effect of the rate constant k_x , the scaling factor of R_{ct}^x and R_x^{ct} , on the energy-dependent capture efficiency η_{capt} of the CT state assuming Miller-Abrahams kinetics. The rate constant k_x is varied from $10^2 s^{-1}$ (rot) to $10^{10} s^{-1}$ (blue). The efficiency η_{capt} decreases at high energies with increasing k_x . However, the tremendous increase for low energy states outweighs this loss at higher energies leading to an increase in the overall capture efficiency $\bar{\eta}_{capt}$, see Figure 5.11b colored triangles. Note, however, that the transfer efficiency is much smaller below the band gap energy E_g than above, see Figure 5.10a, which leads to an monotonously decreasing overall transfer efficiency $\bar{\eta}_{trans}$ (grey diamonds). The overall collection efficiency $\bar{\eta}_{coll}$ (black circles) exhibits consequently a maximum between $k_x = 10^4 s^{-1}$ and $10^6 s^{-1}$.

Figure 5.11c shows the capture efficiency η_{capt} over energy assuming Marcus theory. The rate constant k_x is varied from $10^4 s^{-1}$ (yellow) to $10^{12} s^{-1}$ (purple). The efficiency η_{capt} follows the for Marcus typical Gaussian shape. For $k_x = 10^4 s^{-1}$ the position of the maximum is at CT state energy $E_{ct} = E_g - \lambda$ and shifts toward lower energies with increasing k_x . The height of the maximum increases with k_x whereas the width narrows. The overall capture efficiency $\bar{\eta}_{capt}$ increases with k_x , see Figure 5.11c colored triangles. Because the transfer efficiency η_{trans} reaches its maximum at $E_g + \lambda = 1.6 eV$ the overall transfer $\bar{\eta}_{trans}$ increases as long as the capturing becomes more efficient in this energy range, i.e. for $k_x \leq 10^8$ but drops for even higher k_x . Like in the case of Miller-Abrahams, the average collection efficiency $\bar{\eta}_{coll}$ as a function of k_x exhibits therefore a maximum which might be contra intuitive at first sight.

Under non-saturation and assuming Miller-Abrahams kinetics, the analysis shows that the overall collection efficiency can be improved by increasing the energy difference of the exciton states and the band gap $E_x - E_g$. A reduction of E_g improves the transfer efficiency η_{trans} for

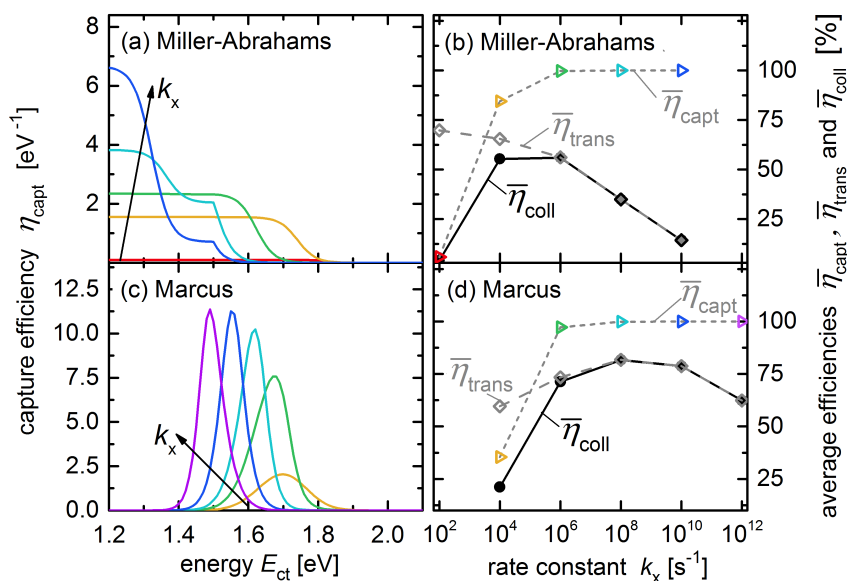


Fig. 5.11 The energy-dependent capture efficiency η_{capt} for (a) Miller-Abrahams and (c) Marcus theory for varied rate coefficients $k_x = 10^2, 10^4, 10^6, 10^8, 10^{10}$ and 10^{12} s⁻¹. The resulting average efficiencies $\bar{\eta}_{\text{coll}}$ (black circles), $\bar{\eta}_{\text{trans}}$ (grey diamonds) and $\bar{\eta}_{\text{capt}}$ (colored triangles) are shown exemplarily for $k_{\text{np}}N_{\text{np}}/k_{\text{gr}} = 10^2$. Both models, (b) Miller-Abrahams and (d) Marcus, show an initial rise in overall collection efficiency $\bar{\eta}_{\text{coll}}$ with increasing k_x . However, towards high k_x the efficiency $\bar{\eta}_{\text{coll}}$ decreases, due to the favored capture of excitons into low energy CT states, see (a) and (b), that are less likely to dissociate, see Fig. 5.10.

low energy states whereas an increment in E_x improves the capture efficiency of high energy CT states leading to an overall improved $\bar{\eta}_{\text{coll}}$. In contrast, for Marcus theory this simple rule-of-thumb to enhance η_{coll} does not hold. Here, the product of the energy-dependent efficiencies η_{trans} and η_{capt} has to be optimized. The transfer efficiency η_{trans} is maximal at $E_g + \lambda$, see Figure 5.10b, the maximum of η_{capt} is sensible to k_x , making it impossible to come up with a simple rule of parameter variation to improve the average collection efficiency. For both models, however, the collection efficiency can be improved by increasing the number of CT states N_{ct} at energies that maximize $\eta_{\text{capt}}(E_{\text{ct}}) \cdot \eta_{\text{trans}}(E_{\text{ct}})$.

After discussing the effect of k_x , E_g , E_x and λ and therefore R_{ct}^x and R_x^{ct} as well as the density of CT states N_{ct} on the capture efficiency η_{capt} and the consequences for the overall collection efficiency $\bar{\eta}_{\text{coll}}$, the last missing parameter in Equation (5.16) the occupation f_x of the exciton states and its effect on collection is analyzed in the following.

Saturation

The effect of saturation on the collection efficiency is analyzed by varying the occupation probability of the exciton states f_x . The rate coefficient k_x is hold constant at 10^6 s^{-1} . In order to visualize saturation effects the values of f_x are chosen to approach 0 and 1 logarithmically, i.e. $\log(f_x) = -9, -7, -5, -3, -1$ and $\log(1 - f_x) = -1, -3, -5$. Accordingly, the occupation metric $\zeta := \log(1/f_x - 1)$ is introduced to facilitate the graphical representation in Figure 5.13.

Figure 5.12 displays the occupation probability of the CT states over energy E_{ct} for (a) Miller-Abrahams and (c) Marcus theory and its resulting capture efficiencies $\eta_{\text{capt}}(E_{\text{ct}})$ in (b) and (d). The occupation probability f_{ct} is exemplarily displayed for $f_x = 10^{-9}, 10^{-7}, 10^{-5}, 10^{-3}, 0.1$ and 0.9 for Miller-Abrahams and $f_x = 10^{-5}, 10^{-3}, 0.1, 0.9, 0.999, 0.99999$ in the case of Marcus theory. Note, that the lowest two occupation probabil-

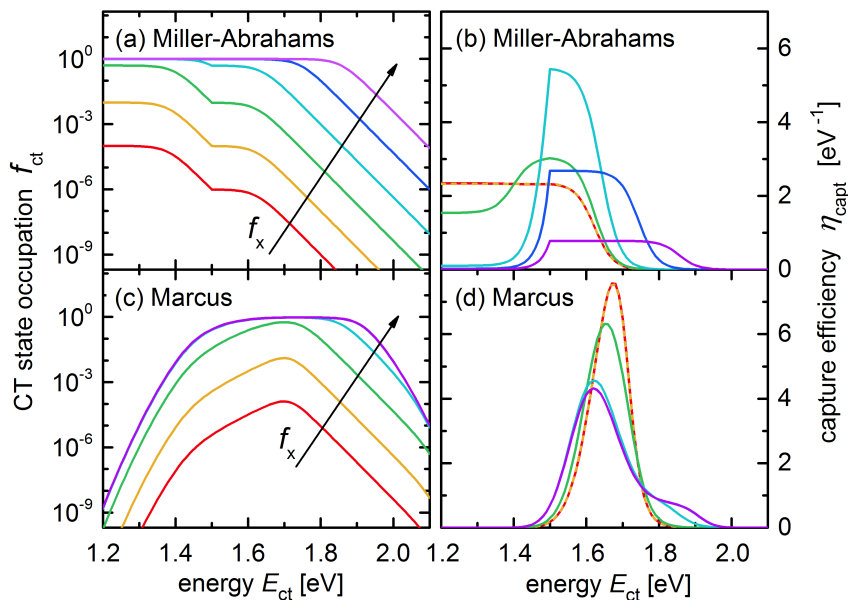


Fig. 5.12 The impact of saturation on the energy-dependent capture efficiency η_{capt} . (a) The CT state occupation probability f_{ct} is varied by changing the occupation of the exciton states $f_x = 10^{-9}, 10^{-7}, 10^{-5}, 10^{-3}, 0.1, 0.9$ in the case of Miller-Abrahams, and (b) for Marcus theory $f_x = 10^{-5}, 10^{-3}, 0.1, 0.9, 0.999, 0.99999$. Note that the first two occupation levels are chosen to be in the non-saturation case (red and yellow) and the respective capture efficiencies are indistinguishable (b) and (d). (b) For Miller-Abrahams, the lower energy CT states saturate first, see (a), and therefore the capture efficiency decreases for lower energies whereas the capture of excitons into higher CT states become more likely. For Marcus theory, the CT states with energies $E_{ct} \approx 1.7$ eV saturate first which leads to a loss of η_{capt} into these states and gain of η_{capt} for lower and higher energy states.

ities f_x (red and yellow) represent the non-saturation case and lead to the same capture efficiency (dashed red and yellow in (b) and (d)). Moreover, the highest two chosen occupation levels for Marcus theory $f_x = 0.999$ and 0.99999 , cannot be distinguished in the graph. For Miller-Abrahams, the lowest CT states saturate first and therefore become less efficient in capturing excitons, leading to a higher η_{capt} for energetically higher CT states. Assuming Marcus kinetics, however, the CT states at $E_x - \lambda = 1.7$ eV saturate first for the chosen parameters. The capture efficiency is suppressed for these energies and slightly improves for lower and higher energies. The consequence for the average efficiencies are discussed with the help of Figure 5.13.

Figure 5.13 shows the average efficiencies over the occupation metric $\zeta := \log(1/f_x - 1)$ that is introduced to facilitate the graphical representation. With rising occupation, the overall capture efficiency $\bar{\eta}_{\text{capt}}$ (colored triangles) decreases as intuitively expected for both models. For Miller-Abrahams, the overall transfer efficiency $\bar{\eta}_{\text{trans}}$ (grey diamonds) increases with ζ which can be explained by the more efficient capturing into high energy states resulting in a maximum of average collection efficiency $\bar{\eta}_{\text{coll}}$ (black circles) at $\zeta = -3$. For Marcus, $\bar{\eta}_{\text{trans}}$ falls monotonously for higher occupation and therefore leads to an overall loss of collection efficiency $\bar{\eta}_{\text{coll}}$.

5.6 Summary and Outlook

The 0-dimensional rate model was introduced that was designed to be as simple as possible but at the same time to include the most current and widely used dominant interstate transfer paths of charge carriers in organic photovoltaic devices. It was proven that the optoelectronic reciprocity relation and the superposition of electro- and photoluminescence are valid for this rate model if no saturation effects are considered. Moreover, the occupation probability of the CT state under photo- and electroluminescence was analyzed for two different transfer rate theories: Miller-Abrahams and Marcus. The two theories

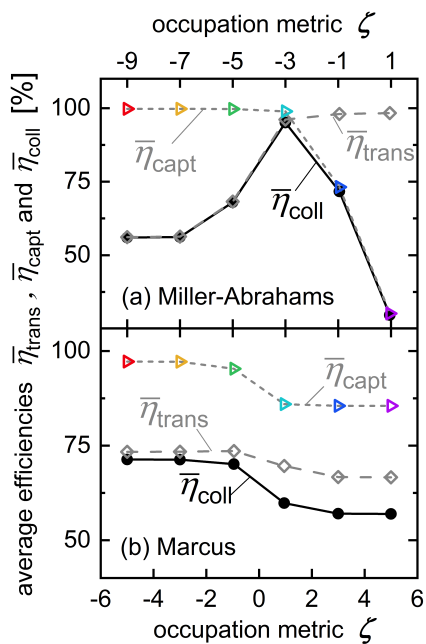


Fig. 5.13 The impact of saturation on the average CT state capture, transfer and collection efficiencies $\bar{\eta}_{\text{capt}}$ (grey diamonds), $\bar{\eta}_{\text{trans}}$ (colored triangles) and $\bar{\eta}_{\text{coll}}$ (black circles). As x-axis the occupation metric ζ is chosen for improved visibility, the shown data points correspond to the exciton occupation probabilities f_x presented in Fig. 5.12. (a) For Miller-Abrahams, $\bar{\eta}_{\text{capt}}$ is relatively constant for low occupation whereas $\bar{\eta}_{\text{capt}}$ rises explained by the more effective capturing of higher CT states, see Fig. 5.12. However, for $\zeta > -3$ capture becomes inefficient and limits $\bar{\eta}_{\text{coll}}$. (b) For Marcus theory $\bar{\eta}_{\text{coll}}$ falls monotonously with occupation as well as $\bar{\eta}_{\text{capt}}$ and $\bar{\eta}_{\text{trans}}$.

lead to qualitatively different occupation probabilities and possible peak positions. In the last section the collection efficiency was examined with the counter-intuitive outcome that the overall collection efficiency can increase with decreasing transfer rate from the exciton state into the CT state. Further investigations have to show if this effect can explain the efficient charge collection of polymer/non-fullerene acceptor organic cells despite the small energy difference between the CT state and the exciton state.

Conclusion and Outlook

“*Next to love, balance is the most important thing.*”

— **John Wooden**
(Basketball Coach)

The foundation of the current thesis is the approach by Shockley and Queisser who determined a theoretical efficiency limit by applying the laws of thermodynamics on an idealized solar cells. The underlying concept is the principle of detailed balance and its extrapolation to steady-state conditions, which are the operating conditions for conventional solar cell technologies.

The developed concept of a distribution of Shockley-Queisser band gaps allows for a meaningful comparison of voltage and efficiency losses across different solar cell technologies. It leads to a functional definition of the band gap that is by definition an external parameter of the device and not an internal parameter of the absorber material and thereby dependent on the solar cell device structure. The voltage loss analysis could self-consistently be extended to materials with non-unity radiative ideality factors, as shown for a thin film amorphous silicon solar cell. A prerequisite for this analysis, however, is a high sensitivity of the absorptance measurement setup. The concept allows for a quantitative and intuitive detailed balance analysis of thermodynamic losses that can be readily applied to any solar cell. The extension of this concept to the analysis of photovoltaic absorber materials without the need for preparing complete devices is straightforward. For the

quantitative analysis of losses of the solar cell performance in respect to the ideal case in the SQ-theory, the respective losses in the short-circuit current and the fill factor would complete the picture.

A generalized Shockley-Queisser theory has been introduced that describes solar cells by their internal properties. This inside view is needed, for example, in the field of high-throughput materials screening for photovoltaic absorber. The presented theory allows for the calculation of an efficiency limit from material properties derived from first-principle calculations or calculations based on electronic structure theory. It was demonstrated that the refractive index is a mandatory input parameter for a consistent evaluation of the potential of any material as a photovoltaic absorber, a fact that has often been neglected in the past.

The method takes as input parameter the complex refractive index and its calculated efficiency limit is dependent on the assumed light-trapping scheme, the thickness of the absorber layer and the internal luminescence quantum efficiency. Based on this theory, a selection metric was suggested to rate a material's potential for photovoltaic applications that on the one hand is computationally not demanding and on the other hand does not neglect important readily available information. In addition, this selection metric is applicable to either simulated or experimentally determined complex refractive indices. Further improvement of high-throughput materials screening for absorber materials must be driven by the improvement of the first-principles calculations to reliably calculate transport properties, defect formation and the internal quantum efficiency of potential materials.

Moreover, a 0-dimensional rate model was introduced that was designed to be as simple as possible, but at the same time to include the most current and widely used dominant interstate transfer paths of charge carriers in organic photovoltaic devices. Two different transfer rate theories, namely the Miller-Abrahams and the Marcus theory, were applied and the occupation probability of the charge-transfer state

under electro- and photoluminescence conditions was analyzed. The occupation is strongly dependent on the assumed electron transfer theory leading to quantitatively different behavior, ranging from different possible peak positions in the non-saturated case to different peak shifts under saturation. Therefore, further experimental investigation might be able to show which theory can more reliably describe the experimental data.

It was proven that under non-saturation, the superposition of electro- and photoluminescence and the opto-electronic reciprocity relation are valid independently of the electron transfer theory, as long as the theory fulfills the principle of detailed balance. The validity of both concepts is in good agreement with experiments. The detailed analysis of the collection efficiency had the counter-intuitive outcome that the collection efficiency can increase with decreasing exciton to charge-transfer state electron-transfer rate. Further theoretical and experimental investigations will have to show if this counter-intuitive effect could explain the surprisingly efficient charge collection of polymer/non-fullerene acceptor organic cells. These solar cells exhibit a much higher collection efficiency than expected by the small energy offset between the exciton state and the charge-transfer state.

Bibliography

- [1]E. Zermelo. “Über einen Satz der Dynamik und die mechanische Wärmetheorie”, *Annalen der Physik und Chemie*, **293**:3 (1896) 485–494 (cit. on p. 7).
- [2]Ludwig Boltzmann. “Entgegnung auf die wärmetheoretischen Betrachtungen des Hrn. E. Zermelo”, *Annalen der Physik und Chemie*, **293**:4 (1896) 773–784 (cit. on p. 7).
- [3]H.S. Leff and A.F. Rex. *Maxwell’s Demon: Entropy, Information, Computing*. Adam Hilger, 1990 (cit. on p. 7).
- [4]H. A. Posch, C. Dellago, W. G. Hoover, and O. Kumm. “Microscopic Time-Reversibility and Macroscopic Irreversibility - Still a Paradox?”, *Pioneering Ideas for the Physical and Chemical Sciences*. 1997 (cit. on p. 7).
- [5]P. J. Zwart. *About time: A philosophical inquiry into the origin and nature of time*. 1976 (cit. on pp. 7, 8).
- [6]Claire Elizabeth Smith and Joseph Wayne Smith. “Economics, Ecology and Entropy: The Second Law of Thermodynamics and the Limits to Growth”, *Population and Environment*, **17**:4 (1996) 309–321 (cit. on p. 7).
- [7]N. Georgescu-Roegen. *The Entropy Law and the Economic Process*. 1971 (cit. on pp. 7, 8).
- [8]Reiner Kümmel. *The Second Law of Economics*. Springer New York, 2011 (cit. on p. 7).
- [9]Robert U Ayres. “Eco-thermodynamics: economics and the second law”, *Ecological Economics*, **26**:2 (1998) 189–209 (cit. on p. 7).

- [10]Elias L. Khalil. “The Three Laws of Thermodynamics and the Theory of Production”, *Journal of Economic Issues*, **38**:1 (2004) 201–226 (cit. on p. 7).
- [11]F. Söllner. *Thermodynamik und Umweltökonomie*. 1996 (cit. on p. 7).
- [12]Ludwig Boltzmann. *Über die Beziehung zwischen dem zweiten Hauptsatze der mechanischen Wärmetheorie und der Wahrscheinlichkeitsrechnung, respective den Sätzen über das Wärmegleichgewicht*. Kk Hof- und Staatsdruckerei, 1877 (cit. on p. 7).
- [13]E. Schrödinger. *What is Life?: The Physical Aspect of the Living Cell*. The University Press, 1962 (cit. on p. 8).
- [14]I. Prigogine. *Introduction to Thermodynamics of Irreversible Processes*. Wiley, 1968 (cit. on p. 8).
- [15]Nicholas Georgescu-Roegen. “The Entropy Law and the Economic Process in Retrospect”, *Eastern Economic Journal*, **12**:1 (1986) 3–25 (cit. on p. 8).
- [16]Jeremy Rifkin and Ted Howard. *Entropy: A New World View*. Viking Adult, 1980 (cit. on p. 8).
- [17]Herman E. Daly. *Steady-State Economics*. Island Press, 1991. 318 pp. (cit. on p. 8).
- [18]Robert U Ayres. “The second law, the fourth law, recycling and limits to growth”, *Ecological Economics*, **29**:3 (1999) 473–483 (cit. on p. 8).
- [19]Jeffrey T Young. “Is the entropy law relevant to the economics of natural resource scarcity?”, *Journal of Environmental Economics and Management*, **21**:2 (1991) 169–179 (cit. on p. 8).
- [20]Jeroen C.J.M. van den Bergh. “Robert Ayres, Ecological Economics and Industrial Ecology”, *Environmental Innovation and Societal Transitions*, **9** (2013) 1–7 (cit. on p. 8).
- [21]Reiner Kümmel. “Why energy’s economic weight is much larger than its cost share”, *Environmental Innovation and Societal Transitions*, **9** (2013) 33–37 (cit. on p. 8).
- [22]W. Shockley and H. J. Queisser. “Detailed Balance Limit of Efficiency of P-N Junction Solar Cells”, *Journal of Applied Physics*, **32**:3 (1961) 510–519 (cit. on pp. 8, 18, 39).

- [23]U. Rau. “Reciprocity relation between photovoltaic quantum efficiency and electroluminescent emission of solar cells”, *Physical Review B*, **76**:8 (2007) 085303 (cit. on pp. 9, 19, 20, 26, 28, 97).
- [24]L. P. Yu and A. Zunger. “Identification of Potential Photovoltaic Absorbers Based on First-Principles Spectroscopic Screening of Materials”, *Physical Review Letters*, **108**:6 (2012) 068701 (cit. on pp. 10, 48, 54, 56).
- [25]N. W. Ashcroft and N. Mermin. *Solid State Physics*. Cengage Learning, Inc, 1976. 848 pp. (cit. on p. 13).
- [26]S. M. Sze. *Physics of Semiconductor Devices*. 2nd. New York: John Wiley & Sons, 1936, 641 ff (cit. on pp. 13, 57).
- [27]J. Nelson. *The Physics of Solar Cells*. ICP, 2003. 384 pp. (cit. on p. 13).
- [28]M. Planck. “Entropie und Temperatur strahlender Wärme”, *Annalen der Physik*, **306**:4 (1900) 719–737 (cit. on p. 16).
- [29]M. Planck. “Über das Gesetz der Energieverteilung im Normalspectrum”, *Annalen der Physik*, **309**:3 (1901) 553–563 (cit. on p. 16).
- [30]G. Kirchhoff. “Über das Verhältniss zwischen dem Emissionsvermögen und dem Absorptionsvermögen der Körper für Wärme und Licht”, *Annalen der Physik und Chemie*, **185**:2 (1860) 275–301 (cit. on p. 16).
- [31]*G173-03e1 standard tables for reference solar spectral irradiances: direct normal and hemispherical of 37° tilted surface*. ASTM International (cit. on pp. 18, 43).
- [32]P. Würfel. “The chemical potential of radiation”, *Journal of Physics C: Solid State Physics*, **15**:18 (1982) 3967 (cit. on p. 19).
- [33]T. Kirchartz. “Generalized detailed balance theory of solar cells”. PhD thesis. Forschungszentrum Jülich, 2009 (cit. on p. 19).
- [34]Gordon Lasher and Frank Stern. “Spontaneous and Stimulated Recombination Radiation in Semiconductors”, *Physical Review*, **133**:2A (1964) A553–A563 (cit. on p. 19).
- [35]P. Würfel, S. Finkbeiner, and E. Daub. “Generalized Planck’s radiation law for luminescence via indirect transitions”, *Applied Physics A Materials Science & Processing*, **60**:1 (1995) 67–70 (cit. on p. 19).
- [36]C. Donolato. “A reciprocity theorem for charge collection”, *Applied Physics Letters*, **46**:3 (1985) 270–272 (cit. on p. 19).

- [37]T. Kirchartz, U. Rau, M. Kurth, J. Mattheis, and J.H. Werner. “Comparative study of electroluminescence from Cu(In,Ga)Se₂ and Si solar cells”, *Thin Solid Films*, **515**:15 (2007) 6238–6242 (cit. on pp. 20, 26, 31, 41, 43).
- [38]T. Kirchartz and U. Rau. “Electroluminescence analysis of high efficiency Cu(In,Ga)Se₂ solar cells”, *Journal of Applied Physics*, **102**:10 (2007) 104510 (cit. on pp. 20, 26, 28, 41, 43).
- [39]Thomas Kirchartz, Uwe Rau, Martin Hermle, et al. “Internal voltages in GaInP/GaInAs/Ge multijunction solar cells determined by electroluminescence measurements”, *Applied Physics Letters*, **92**:12 (2008) 123502 (cit. on p. 20).
- [40]K. Vandewal, K. Tvingstedt, A. Gadisa, O. Inganäs, and J. V. Manca. “On the origin of the open-circuit voltage of polymer-fullerene solar cells”, *Nature Materials*, **8**:11 (2009) 904–909 (cit. on pp. 20, 26, 28).
- [41]T. C. M. Müller, B. E. Pieters, T. Kirchartz, R. Carius, and U. Rau. “Effect of localized states on the reciprocity between quantum efficiency and electroluminescence in Cu(In,Ga)Se₂ and Si thin-film solar cells”, *Solar Energy Materials and Solar Cells*, **129** (2014) 95–103 (cit. on pp. 20, 38, 42, 43).
- [42]T. C. M. Müller. “Light Absorption and Radiative Recombination in Thin-Film Solar Cells”. PhD thesis. Forschungszentrum Jülich, 2015 (cit. on p. 20).
- [43]A. Miller and E. Abrahams. “Impurity Conduction at Low Concentrations”, *Physical Review*, **120**:3 (1960) 745–755 (cit. on pp. 20, 21, 77).
- [44]R. A. Marcus. “Exchange reactions and electron transfer reactions including isotopic exchange. Theory of oxidation-reduction reactions involving electron transfer. Part 4.A statistical-mechanical basis for treating contributions from solvent, ligands, and inert salt”, *Discussions of the Faraday Society*, **29** (1960) 21–31 (cit. on pp. 20, 21, 23).
- [45]J. Bisquert. “Hopping Transport of Electrons in Dye-Sensitized Solar Cells”, *The Journal of Physical Chemistry C*, **111**:46 (2007) 17163–17168 (cit. on p. 20).
- [46]C. Deibel and V. Dyakonov. “Polymer-fullerene bulk heterojunction solar cells”, *Reports on Progress in Physics*, **73**:9 (2010) 096401 (cit. on p. 20).
- [47]J. Cottaar, L. J. A. Koster, R. Coehoorn, and P. A. Bobbert. “Scaling Theory for Percolative Charge Transport in Disordered Molecular Semiconductors”, *Physical Review Letters*, **107**:13 (2011) (cit. on p. 20).

- [48]I. I. Fishchuk, A. Kadashchuk, S. T. Hoffmann, et al. “Unified description for hopping transport in organic semiconductors including both energetic disorder and polaronic contributions”, *Physical Review B*, **88**:12 (2013) (cit. on p. 20).
- [49]S. D. Baranovskii. “Theoretical description of charge transport in disordered organic semiconductors”, *physica status solidi (b)*, **251**:3 (2014) 487–525 (cit. on p. 20).
- [50]A. V. Nenashev, J. O. Oelerich, and S. D. Baranovskii. “Theoretical tools for the description of charge transport in disordered organic semiconductors”, *Journal of Physics: Condensed Matter*, **27**:9 (2015) 093201 (cit. on p. 20).
- [51]N. Lu, L. Li, W. Banerjee, et al. “Charge carrier hopping transport based on Marcus theory and variable-range hopping theory in organic semiconductors”, *Journal of Applied Physics*, **118**:4 (2015) 045701 (cit. on p. 20).
- [52]W. F. Libby. “Theory of Electron Exchange Reactions in Aqueous Solution”, *The Journal of Physical Chemistry*, **56**:7 (1952) 863–868 (cit. on p. 21).
- [53]E. U. Condon. “A Theory of Intensity Distribution in Band Systems”, *Physical Review*, **28**:6 (1926) 1182–1201 (cit. on p. 21).
- [54]E. U. Condon. “Nuclear Motions Associated with Electron Transitions in Diatomic Molecules”, *Physical Review*, **32**:6 (1928) 858–872 (cit. on p. 21).
- [55]J. Franck and E. G. Dymond. “Elementary processes of photochemical reactions”, *Transactions of the Faraday Society*, **21**:February (1926) 536 (cit. on p. 21).
- [56]R. A. Marcus. “Electron Transfer Reactions in Chemistry: Theory and Experiment (Nobel Lecture)”, *Angewandte Chemie International Edition in English*, **32**:8 (1993) 1111–1121 (cit. on p. 21).
- [57]R. A. Marcus. “On the Theory of Oxidation-Reduction Reactions Involving Electron Transfer. I”, *The Journal of Chemical Physics*, **24**:5 (1956) 966–978 (cit. on pp. 21, 77).
- [58]R. A. Marcus. “On the Theory of Electron-Transfer Reactions. VI. Unified Treatment for Homogeneous and Electrode Reactions”, *The Journal of Chemical Physics*, **43**:2 (1965) 679–701 (cit. on p. 21).

- [59]H. Eyring. “The Activated Complex in Chemical Reactions”, *The Journal of Chemical Physics*, **3**:2 (1935) 107–115 (cit. on p. 23).
- [60]S. Arrhenius. “Über die Dissociationswärme und den Einfluss der Temperatur auf den Dissociationsgrad der Elektrolyte”, *Zeitschrift für Physikalische Chemie*, **4U**:1 (1889) (cit. on p. 23).
- [61]J. R. Miller, L. T. Calcaterra, and G. L. Closs. “Intramolecular long-distance electron transfer in radical anions. The effects of free energy and solvent on the reaction rates”, *Journal of the American Chemical Society*, **106**:10 (1984) 3047–3049 (cit. on p. 23).
- [62]R. A. Marcus. “Relation between charge transfer absorption and fluorescence spectra and the inverted region”, *The Journal of Physical Chemistry*, **93**:8 (1989) 3078–3086 (cit. on p. 23).
- [63]R. T. Ross. “Some Thermodynamics of Photochemical Systems”, *Journal of Chemical Physics*, **46**:12 (1967) 4590–4593 (cit. on pp. 26, 28).
- [64]G. Smestad and H. Ries. “Luminescence and Current Voltage Characteristics of Solar-Cells and Optoelectronic Devices”, *Solar Energy Materials and Solar Cells*, **25**:1-2 (1992) 51–71 (cit. on pp. 26, 28).
- [65]M. A. Green. “Radiative efficiency of state-of-the-art photovoltaic cells”, *Progress in Photovoltaics: Research and Applications*, **20**:4 (2012) 472–476 (cit. on pp. 26, 28, 43).
- [66]J. Yao, T. Kirchartz, M. S. Vezie, et al. “Quantifying Losses in Open-Circuit Voltage in Solution-Processable Solar Cells”, *Physical Review Applied*, **4**:1 (2015) 014020 (cit. on pp. 26–28, 31, 41–43).
- [67]T. Kirchartz, K. Taretto, and U. Rau. “Efficiency Limits of Organic Bulk Heterojunction Solar Cells”, *The Journal of Physical Chemistry C*, **113**:41 (2009) 17958–17966 (cit. on pp. 26, 28, 48).
- [68]W. Tress, N. Marinova, O. Inganas, et al. “Predicting the Open-Circuit Voltage of CH₃NH₃PbI₃ Perovskite Solar Cells Using Electroluminescence and Photovoltaic Quantum Efficiency Spectra: the Role of Radiative and Non-Radiative Recombination”, *Advanced Energy Materials*, **5**:3 (2015) 1400812 (cit. on pp. 26, 28).
- [69]Y.X. Li, X.D. Liu, F.P. Wu, et al. “Non-fullerene acceptor with low energy loss and high external quantum efficiency: towards high performance polymer solar cells”, *Journal of Materials Chemistry A*, **4**:16 (2016) 5890–5897 (cit. on pp. 26, 28, 30).

- [70]K. Tvingstedt, O. Malinkiewicz, A. Baumann, et al. “Radiative efficiency of lead iodide based perovskite solar cells”, *Scientific Reports*, **4** (2014) 6071 (cit. on pp. 26, 28).
- [71]D. Baran, T. Kirchartz, S. Wheeler, et al. “Reduced voltage losses yield 10% efficient fullerene free organic solar cells with >1 V open circuit voltages”, *Energy & Environmental Science*, **9**:12 (2016) 3783–3793 (cit. on pp. 26, 30).
- [72]W. Zhao, D. Qian, S. Zhang, et al. “Fullerene-Free Polymer Solar Cells with over 11% Efficiency and Excellent Thermal Stability”, *Advanced Materials*, **28** (2016) 4734–4739 (cit. on pp. 26, 28, 30).
- [73]T. Markvart. “Thermodynamics of losses in photovoltaic conversion”, *Applied Physics Letters*, **91**:6 (2007) 064102 (cit. on p. 27).
- [74]D. Baran, M. S. Vezie, N. Gasparini, et al. “Role of Polymer Fractionation in Energetic Losses and Charge Carrier Lifetimes of Polymer: Fullerene Solar Cells”, *The Journal of Physical Chemistry C*, **119**:34 (2015) 19668–19673 (cit. on pp. 28, 30).
- [75]U. Rau and T. Kirchartz. “On the thermodynamics of light trapping in solar cells”, *Nature Materials*, **13** (2014) 103–104 (cit. on p. 28).
- [76]U. Rau, U. W. Paetzold, and T. Kirchartz. “Thermodynamics of light management in photovoltaic devices”, *Physical Review B*, **90**:3 (2014) 035211 (cit. on pp. 28, 41, 53, 63).
- [77]O. D. Miller, E. Yablonovitch, and S. R. Kurtz. “Strong Internal and External Luminescence as Solar Cells Approach the Shockley-Queisser Limit”, *IEEE Journal of Photovoltaics*, **2**:3 (2012) 303–311 (cit. on pp. 28, 48).
- [78]H. Ibach and H. Lüth. *Solid-State Physics: An Introduction to Principles of Material Science*. 5th ed. Springer-Verlag, 2009, 161ff (cit. on p. 29).
- [79]W. Bludau, A. Onton, and W. Heinke. “Temperature dependence of the band gap of silicon”, *Journal of Applied Physics*, **45**:4 (1974) 1846–1848 (cit. on p. 29).
- [80]G.D. Cody. “Urbach edge of crystalline and amorphous silicon: a personal review”, *Journal of Non-Crystalline Solids*, **141** (1992) 3–15 (cit. on p. 29).
- [81]J. Tauc. “Optical properties and electronic structure of amorphous Ge and Si”, *Materials Research Bulletin*, **3**:1 (1968) 37–46 (cit. on pp. 29, 35, 37, 38).

- [82]B. D. Viezbicke, S. Patel, B. E. Davis, and D. P. Birnie. “Evaluation of the Tauc method for optical absorption edge determination: ZnO thin films as a model system”, *physica status solidi (b)*, **252**:8 (2015) 1700–1710 (cit. on p. 29).
- [83]T. M. Mok and S. K. O’Leary. “The dependence of the Tauc and Cody optical gaps associated with hydrogenated amorphous silicon on the film thickness: αI Experimental limitations and the impact of curvature in the Tauc and Cody plots”, *Journal of Applied Physics*, **102**:11 (2007) 113525 (cit. on p. 29).
- [84]G.D. Cody, B.G. Brooks, and B. Abeles. “Optical absorption above the optical gap of amorphous silicon hydride”, *Solar Energy Materials*, **8**:1-3 (1982) 231–240 (cit. on p. 29).
- [85]R.M. Dawson, Y.M. Li, M. Gunes, et al. “Optical Properties of Hydrogenated Amorphous Silicon, Silicon-Germanium and Silicon-Carbon Thin Films”, *MRS Proceedings*, **258** (1992) (cit. on p. 29).
- [86]P. Liu, P. Longo, A. Zaslavsky, and D. Pacifici. “Optical bandgap of single- and multi-layered amorphous germanium ultra-thin films”, *Journal of Applied Physics*, **119**:1 (2016) 014304 (cit. on p. 29).
- [87]N.A. Ran, J.A. Love, C.J. Takacs, et al. “Harvesting the Full Potential of Photons with Organic Solar Cells”, *Advanced Materials*, **28**:7 (2016) 1482–1488 (cit. on p. 30).
- [88]S. M. Tuladhar, M. Azzouzi, F. Delval, et al. “Low Open-Circuit Voltage Loss in Solution-Processed Small-Molecule Organic Solar Cells”, *ACS Energy Letters*, **1**:1 (2016) 302–308 (cit. on p. 30).
- [89]U. Rau and J. H. Werner. “Radiative efficiency limits of solar cells with lateral band-gap fluctuations”, *Applied Physics Letters*, **84**:19 (2004) 3735–3737 (cit. on pp. 33, 48).
- [90]D. Aiken, M. Stan, C. Murray, et al. “Temperature dependent spectral response measurements for III-V multi-junction solar cells”, *Conference Record of the Twenty-Ninth IEEE Photovoltaic Specialists Conference, 2002.* 2002, pp. 828–831 (cit. on p. 36).
- [91]H. Helmers, C Karcher, and A.W. Bett. “Bandgap determination based on electrical quantum efficiency”, *Applied Physics Letters*, **103**:3 (2013) 032108 (cit. on pp. 36–38).
- [92]T.M.H. Tran, B.E. Pieters, M. Schneemann, et al. “Quantitative evaluation method for electroluminescence images of a-Si: H thin-film solar modules”, *Phys Status Solidi-R*, **7**:9 (2013) 627–630 (cit. on pp. 39, 43).

- [93]T. Kirchartz, A. Helbig, W. Reetz, et al. “Reciprocity Between Electroluminescence and Quantum Efficiency Used for the Characterization of Silicon Solar Cells”, *Progress in Photovoltaics: Research and Applications*, **17:6** (2009) 394–402 (cit. on p. 41).
- [94]A.V. Shah, H. Schade, M. Vanecek, et al. “Thin-film silicon solar cell technology”, *Progress in Photovoltaics: Research and Applications*, **12:2-3** (2004) 113–142 (cit. on p. 41).
- [95]R.A. Street. “Recombination in a-Si:H: Defect luminescence”, *Physical Review B*, **21:12** (1980) 5775–5784 (cit. on p. 42).
- [96]R.A. Street. “Luminescence and recombination in hydrogenated amorphous silicon”, *Advances in Physics*, **30:5** (1981) 593–676 (cit. on p. 42).
- [97]R.A. Street, D.K. Biegelsen, and R.L. Weisfield. “Recombination in a-Si:H: Transitions through defect states”, *Physical Review B*, **30:10** (1984) 5861–5870 (cit. on p. 42).
- [98]K. Tvingstedt, K. Vandewal, A. Gadisa, et al. “Electroluminescence from Charge Transfer States in Polymer Solar Cells”, *Journal of American Chemical Society*, **131:33** (2009) 11819–11824 (cit. on p. 42).
- [99]U. Rau. “Superposition and Reciprocity in the Electroluminescence and Photoluminescence of Solar Cells”, *IEEE Journal of Photovoltaics*, **2:2** (2012) 169–172 (cit. on p. 43).
- [100]W. Gong, M.A. Faist, N.J. Ekins-Daukes, et al. “Influence of energetic disorder on electroluminescence emission in polymer:fullerene solar cells”, *Physical Review B*, **86:02** (2012) 024201 (cit. on p. 43).
- [101]T. Kirchartz, J. Nelson, and U. Rau. “Reciprocity between Charge Injection and Extraction and Its Influence on the Interpretation of Electroluminescence Spectra in Organic Solar Cells”, *Physical Review Applied*, **5:5** (2016) 054003 (cit. on p. 43).
- [102]S. De Wolf, J. Holovsky, S.-J. Moon, et al. “Organometallic Halide Perovskites: Sharp Optical Absorption Edge and Its Relation to Photovoltaic Performance”, *The Journal of Physical Chemistry Letters*, **5:6** (2014) 1035–1039 (cit. on pp. 43, 58).
- [103]T. Tiedje, E. Yablonovitch, G. D. Cody, and B. G. Brooks. “Limiting efficiency of silicon solar cells”, *IEEE Transactions on Electron Devices*, **31:5** (1984) 711–716 (cit. on pp. 48, 51).

- [104]M. A. Green. “Limits on the open-circuit voltage and efficiency of silicon solar cells imposed by intrinsic Auger processes”, *IEEE Transactions on Electron Devices*, **31**:5 (1984) 671–678 (cit. on p. 48).
- [105]M. J. Kerr, A. Cuevas, and P. Campbell. “Limiting efficiency of crystalline silicon solar cells enhanced to Coulomb-enhanced auger recombination”, *Progress in Photovoltaics*, **11**:2 (2003) 97–104 (cit. on p. 48).
- [106]A. Richter, M. Hermle, and S. W. Glunz. “Reassessment of the Limiting Efficiency for Crystalline Silicon Solar Cells”, *IEEE Journal of Photovoltaics*, **3**:4 (2013) 1184–1191 (cit. on p. 48).
- [107]C. N. Savory, A. Walsh, and D. O. Scanlon. “Can Pb-Free Halide Double Perovskites Support High-Efficiency Solar Cells?”, *ACS Energy Letters* (2016) 949–955 (cit. on p. 48).
- [108]A. Zakutayev, X. W. Zhang, A. Nagaraja, et al. “Theoretical Prediction and Experimental Realization of New Stable Inorganic Materials Using the Inverse Design Approach”, *Journal of the American Chemical Society*, **135**:27 (2013) 10048–10054 (cit. on p. 48).
- [109]L. P. Yu, R. S. Kokenyesi, D. A. Keszler, and A. Zunger. “Inverse Design of High Absorption Thin-Film Photovoltaic Materials”, *Advanced Energy Materials*, **3**:1 (2013) 43–48 (cit. on p. 48).
- [110]C. N. Savory, A. M. Ganose, W. Travis, et al. “An assessment of silver copper sulfides for photovoltaic applications: theoretical and experimental insights”, *Journal of Materials Chemistry A*, **4**:32 (2016) 12648–12657 (cit. on p. 48).
- [111]T. Yokoyama, F. Oba, A. Seko, et al. “Theoretical Photovoltaic Conversion Efficiencies of ZnSnP_2 , CdSnP_2 , and $\text{Zn}_{1-x}\text{Cd}_x\text{SnP}_2$ Alloys”, *Applied Physics Express*, **6**:6 (2013) 061201 (cit. on p. 48).
- [112]I.-H. Lee, J. Lee, Y. J. Oh, S. Kim, and KJ Chang. “Computational search for direct band gap silicon crystals”, *Physical Review B*, **90**:11 (2014) 115209 (cit. on p. 48).
- [113]Y. J. Oh, I.-H. Lee, S. Kim, J. Lee, and K. J. Chang. “Dipole-allowed direct band gap silicon superlattices”, *Scientific Reports*, **5** (2015) 18086 (cit. on p. 48).
- [114]W.-J. Yin, T. Shi, and Y. Yan. “Superior Photovoltaic Properties of Lead Halide Perovskites: Insights from First-Principles Theory”, *The Journal of Physical Chemistry C*, **119**:10 (2015) 5253–5264 (cit. on p. 48).

- [115]M. Bercx, N. Sarmadian, R. Saniz, B. Partoens, and D. Lamoen. “First-principles analysis of the spectroscopic limited maximum efficiency of photovoltaic absorber layers for CuAu-like chalcogenides and silicon”, *Physical Chemistry Chemical Physics*, **18**:30 (2016) 20542–20549 (cit. on p. 48).
- [116]W. Meng, B. Saparov, F. Hong, et al. “Alloying and Defect Control within Chalcogenide Perovskites for Optimized Photovoltaic Application”, *Chemistry of Materials*, **28**:3 (2016) 821–829 (cit. on p. 48).
- [117]N. Sarmadian, R. Saniz, B. Partoens, and D. Lamoen. “First-principles study of the optoelectronic properties and photovoltaic absorber layer efficiency of Cu-based chalcogenides”, *Journal of Applied Physics*, **120**:8 (2016) 085707 (cit. on p. 48).
- [118]J. Heo, R. Ravichandran, C. F. Reidy, et al. “Design Meets Nature: Tetrahedrite Solar Absorbers”, *Advanced Energy Materials*, **5**:7 (2015) 1401506 (cit. on p. 48).
- [119]T. Kirchartz, F. Staub, and U. Rau. “Impact of Photon Recycling on the Open-Circuit Voltage of Metal Halide Perovskite Solar Cells”, *ACS Energy Letters*, **1**:4 (2016) 731–739 (cit. on p. 51).
- [120]M. A. Green. “Lambertian light trapping in textured solar cells and light-emitting diodes: Analytical solutions”, *Progress in Photovoltaics*, **10**:4 (2002) 235–241 (cit. on p. 52).
- [121]W van Roosbroeck and W. Shockley. “Photon-Radiative Recombination of Electrons and Holes in Germanium”, *Physical Review*, **94** (1954) 1558–1560 (cit. on p. 53).
- [122]F. Urbach. “The Long-Wavelength Edge of Photographic Sensitivity and of the Electronic Absorption of Solids”, *Physical Review*, **92**:5 (1953) 1324–1324 (cit. on p. 57).
- [123]F. Staub, H. Hempel, J.-C. Hebig, et al. “Beyond Bulk Lifetimes: Insights into Lead Halide Perovskite Films from Time-Resolved Photoluminescence”, *Physical Review Applied*, **6**:4 (2016) 044017 (cit. on p. 67).
- [124]A. Alkauskas, Q. Yan, and C. G. Van de Walle. “First-principles theory of nonradiative carrier capture via multiphonon emission”, *Physical Review B*, **90**:7 (2014) 075202 (cit. on p. 67).
- [125]L. Shi, K. Xu, and L.-W. Wang. “Comparative study of ab initio non-radiative recombination rate calculations under different formalisms”, *Physical Review B*, **91**:20 (2015) 205315 (cit. on p. 67).

- [126]G. D. Barmparis, Y. S. Puzyrev, X. G. Zhang, and S. T. Pantelides. “Theory of inelastic multiphonon scattering and carrier capture by defects in semiconductors: Application to capture cross sections”, *Physical Review B*, **92**:21 (2015) 214111 (cit. on p. 67).
- [127]L. Hedin. “New Method for Calculating 1-Particle Greens Function with Application to Electron-Gas Problem”, *Physical Review*, **139**:3A (1965) A796–A823 (cit. on p. 69).
- [128]G. Kresse and D Joubert. “From ultrasoft pseudopotentials to the projector augmented-wave method”, *Physical Review B*, **59**:3 (1999) 1758 (cit. on p. 69).
- [129]M. Shishkin and G. Kresse. “Implementation and performance of the frequency-dependent GW method within the PAW framework”, *Physical Review B*, **74**:3 (2006) 035101 (cit. on p. 69).
- [130]S. Lany. “Band-structure calculations for the 3d transition metal oxides in GW”, *Physical Review B*, **87**:8 (2013) 085112 (cit. on p. 69).
- [131]S. Lany. “Semiconducting transition metal oxides”, *Journal of Physics-Condensed Matter*, **27**:28 (2015) 283203 (cit. on p. 69).
- [132]P. Jackson, R. Wuerz, D. Hariskos, et al. “Effects of heavy alkali elements in Cu(In,Ga)Se₂ solar cells with efficiencies up to 22.6%”, *physica status solidi (RRL) - Rapid Research Letters*, **10**:8 (2016) 583–586 (cit. on p. 73).
- [133]W. Wang, M. T. Winkler, O. Gunawan, et al. “Device Characteristics of CZTSSe Thin-Film Solar Cells with 12.6% Efficiency”, *Advanced Energy Materials*, **4**:7 (2014) 1301465 (cit. on p. 73).
- [134]F. W. de Souza Lucas, A. W. Welch, L. Baranowski, et al. “Effects of Thermochemical Treatment on CuSbS₂ Photovoltaic Absorber Quality and Solar Cell Reproducibility”, *The Journal of Physical Chemistry C*, **120**:33 (2016) 18377–18385 (cit. on p. 73).
- [135]A. W. Welch, L. L. Baranowski, P. Zawadzki, et al. “Accelerated development of CuSbS₂ thin film photovoltaic device prototypes”, *Progress in Photovoltaics: Research and Applications*, **24** (2016) 929–939 (cit. on p. 73).
- [136]A. W. Welch, L. L. Baranowski, P. Zawadzki, et al. “CuSbSe₂ photovoltaic devices with 3% efficiency”, *Applied Physics Express*, **8**:8 (2015) 082301 (cit. on p. 73).

Appendix

Tab. 6.1 Key to the appreciation of molecules

P3HT	Poly(3-hexylthiophene-2,5-diyl)
PCDTBT	Poly[N-9'-heptadecanyl-2,7-carbazole-alt-5,5-(4',7'-di-2-thienyl-2',1',3'-benzothiadiazole)]
IDTBT	Poly[(2,1,3-benzothiadiazole-4,7-diyl)alt(4,9-dihydro-4,4,9,9-tetraoctylbenzo[1'',2'':4,5;4'',5'':4',5']bissilolo[3,2-b:3',2'-b'] dithiophene-2,7-diyl)]
PTB7	Poly[[4,8-bis[(2-ethylhexyl)oxy]benzo[1,2-b:4,5-b']dithiophene-2,6-diyl][3-fluoro-2-[(2-ethylhexyl)carbonyl]thieno[3,4-b]thiophenediyl]]
PDPP3T	Poly[2,5-bis(2-hexyldecyl)-2,3,5,6-tetrahydro-3,6-dioxopyrrolo[3,4-c]pyrrole-1,4-diyl- alt -[2,2':5',2''-terthiophene]-5,5''-diyl]
PC _{61/71} BM	[6,6]-phenyl-C61/71-butyric acid methyl ester
MAPIC	CH ₃ NH ₃ PbI _{3-x} Cl _x

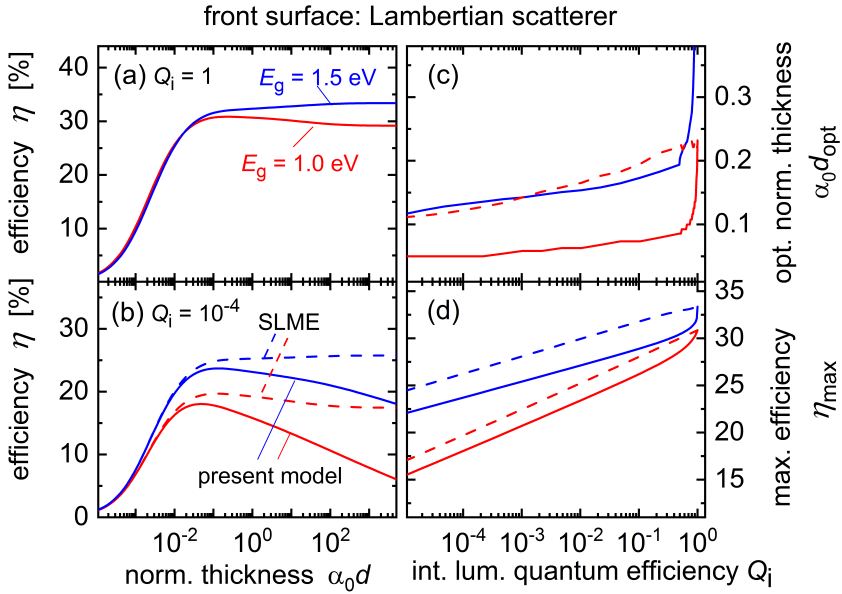


Fig. 6.1 Analogously to Figure 4.5, here with a Lambertian scatterer as front surface and not a flat front surface as shown in Figure 4.5. See Figure 4.2 for more details on the different light trapping concepts.

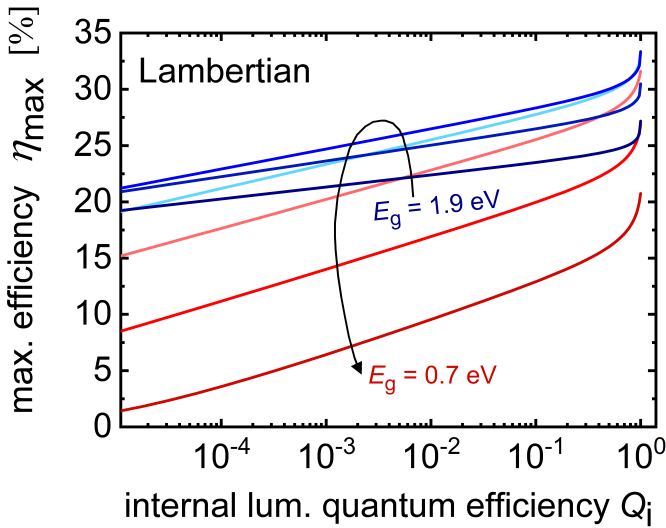


Fig. 6.2 Maximal efficiency as a function of internal luminescence quantum efficiency for band gaps $E_g = 0.7$ eV to 1.9 eV (red to blue) in steps of 0.2 eV, analogously to Figure 4.6. Here with a Lambertian scatterer as front surface.

List of Symbols

A	Absorptance
A_{SQ}	Idealized absorptance in Shockley Queisser model
c	Speed of light in vacuum
ct	Number of occupied charge transfer states
d	Thickness of absorber layer
d_{opt}	Optimal thickness of absorber
E_0	Cut-off energy
E_c	Conduction band energy
E_{ch}	Band tail or Urbach energy
E_{ct}	Energy of the charge transfer state
E_g	Band-gap energy
E_g^{da}	Dipole-allowed electron transition energy
E_g^{PV}	Photovoltaic band-gap energy (defined via Eq. 3.9)
E_g^{SQ}	Shockley-Queisser type band-gap energy
E_v	Valence band energy
E_x	Energy of the exciton state
E_γ	Photon energy
f_{ct}	Occupation probability of the charge transfer state

$f_{ct,0}$	Occupation probability of the charge transfer state in thermodynamic equilibrium
f_r	Fraction of radiative recombination current
f_x	Occupation probability of the exciton state
$f_{x,0}$	Occupation probability of the exciton state in thermodynamic equilibrium
FF	Fill factor of the solar cell
h	Planck constant
H	Heavy-side or step function
J	Electric current
J_0	Saturation current
J_0^{nrad}	Non-radiative saturation current
J_0^{rad}	Radiative saturation current
J_0^{SQ}	Saturation current according to Shockley-Queisser model
J_{sc}	Short-circuit current or photo-generated current
J_{sc}^{SQ}	Photo-generated current according to Shockley-Queisser model
k	Boltzmann constant
k_{gr}	Rate constant of the electron transfer between the charge transfer state and the ground state
k_{np}	Rate constant of the electron transfer between the charge transfer state and the state of free carriers
k_x	Rate constant of the electron transfer between the charge transfer state and the exciton state
n	Refractive index
n_{id}	Ideality factor
n_{rad}	Radiative ideality factor
np	Number of free charge carriers

N_{ct}	Number of charge transfer states
N_{e-}	Number of electrons
N_{ph}	Number of photons
N_x	Number of exciton states
p_e	Photon emission probability
P_{max}	Maximum power output of solar cell
P_{sun}	Total power of sun radiation on solar cell
$P(E_g)$	Distribution of band-gap energies
$P_G(E_g)$	Gaussian distribution of band-gap energies
q	Elementary charge
Q_e^{LED}	External electroluminescence quantum efficiency
Q_e^{PV}	External quantum efficiency
Q_i	Internal luminescence quantum efficiency
$r_{i \rightarrow j}$	Electron transfer rate from state i to state j
R	Total recombination rate
R_j^i	Rate coefficient of the electron transfer rate from i to state j
R^{nrad}	Non-radiative recombination rate
R_0^{nrad}	Non-radiative recombination rate in thermodynamic equilibrium
R^{rad}	Radiative recombination rate
R_0^{rad}	Radiative recombination rate in thermodynamic equilibrium
T	Temperature
T_c	Temperature of solar cell
T_r	Transmittance of solar cell
V_{oc}	Open-circuit voltage
V_{oc}^{rad}	Open-circuit voltage in the radiative limit

V_{oc}^{SQ}	Open-circuit voltage of idealized solar cell/according to Shockley-Queisser model
$W_{gr,np,x}^{in}$	Incoming weighted rate coefficient (defined via Eq. 5.3)
$W_{gr,np,x}^{out}$	Outgoing weighted rate coefficient (defined via Eq. 5.3)
x	Number of occupied exciton states
α	Absorption coefficient
δ	Delta function
$\delta\phi_{x/ct}^{out}$	Excess output photon flux from recombination in exciton/charge transfer state
δj_{np}^{out}	Excess current resulting from electron-hole pairs in the charge transfer state dissociation into free carriers
ΔG^*	Activation energy in Marcus theory
ΔG^0	Difference between free energy in equilibrium configuration of product and reactant in Marcus theory
ΔV_{oc}^{sc}	Short-circuit loss term of open-circuit voltage
ΔV_{oc}^{rad}	Radiative loss term of open-circuit voltage
ΔV_{oc}^{nrad}	Non-radiative loss term of open-circuit voltage
ζ	Occupation metric defined as $\zeta := \log(1/f_x - 1)$
λ	Reorganization energy
η	Conversion efficiency of solar cell
η_{max}	Maximal conversion efficiency
η^{rad}	Efficiency limit in the radiative limit
η^{SQ}	Efficiency limit according to the Shockley Queisser model
η_{coll}	Energy-dependent collection efficiency (defined via Eq. 5.12)
$\bar{\eta}_{coll}$	Average collection efficiency (defined via Eq. 5.12)
η_{capt}	Energy-dependent capture efficiency (defined via Eq. 5.12)

$\bar{\eta}_{\text{capt}}$	Average capture efficiency (defined via Eq. 5.14)
η_{trans}	Energy-dependent transfer efficiency (defined via Eq. 5.12)
$\bar{\eta}_{\text{trans}}$	Average transfer efficiency (defined via Eq. 5.13)
μ_{γ}	Chemical potential of radiation
ν	Normalized excess free charge carriers ($\nu = (np - n_0p_0)/n_0p_0$)
ξ	Normalized excess occupation probability of the charge transfer state
$\rho_{x,\text{ct}}^{\text{gr},x,\text{np}}$	Normalized electron transfer rate constants (defined via Eq. 5.6)
ϕ_{bb}	Black body radiation spectrum
ϕ_{em}	Emission/luminescence spectrum
ϕ_{sun}	Sun spectrum
Φ_{EL}	Integrated/total electroluminescence
$\phi_{\text{ct}}^{\text{in}}$	Incoming photon flux capable to excite an electron into the charge transfer state
$\phi_{\text{ct},0}^{\text{ct}}$	Incoming photon flux capable to excite an electron into the charge transfer state in thermodynamic equilibrium
$\phi_{\text{x}}^{\text{in}}$	Incoming photon flux capable to generate excitons
$\phi_{\text{ct},0}^{\text{in}}$	Incoming photon flux capable to generate excitons in thermodynamic equilibrium
$\varphi_{x/\text{ct}}$	Normalized excess incoming photon flux
χ	Normalized excess occupation probability of the exciton state

List of Publications

B. Blank, T. Kirchartz, S. Lany, and U. Rau. "Selection Metric for Photovoltaic Materials Screening Based on Detailed-Balance Analysis", *Physical Review Applied*, **8**:2 (2017) 024032. (corresponds to Chapter 4)

U. Rau, B. Blank, T. Müller, and T. Kirchartz. "Efficiency Potential of Photovoltaic Materials and Devices Unveiled by Detailed-Balance Analysis", *Physical Review Applied*, **7**:4 (2017) 044016. (corresponds to Chapter 3)

F. de Souza Lucas, A. Welch, L. Baranowski, P. Dippo, H. Hempel, T. Unold, R. Eichberger, B. Blank, U. Rau, L. Mascaro, and A. Zakutayev. "Effects of Thermochemical Treatment on CuSbS₂ Photovoltaic Absorber Quality and Solar Cell Reproducibility", *The Journal of Physical Chemistry C*, **120**:33 (2016) 18377-18385.

B. Blank, C. Ulbrich, T. Merdzhanova, C. Zahren, B. E. Pieters, A. Gerber, and U. Rau. "Analysis of the light-induced degradation of differently matched tandem solar cells with and without an intermediate reflector using the Power Matching Method", *Solar Energy Materials and Solar Cells*, **143** (2015) 1-8.

C. Ulbrich, C. Zahren, A. Gerber, B. Blank, T. Merdzhanova, A. Gordijn, and U. Rau. "Matching of Silicon Thin-Film Tandem Solar Cells for Max-

imum Power Output", *International Journal of Photoenergy*, (2013)
314097.

Acknowledgements

After the great time I had at the institute working on my thesis, I want to say thank you to everyone who helped me along the way. In particular I would like to thank:

The Bosch-Forschungsstiftung for the trust in my competences and for financing my research, and especially for the fun and informative meetings with the other scholarship holders.

Prof. Rau for your excellent academic guidance. It was a great pleasure to discuss the inside and outside world of solar cells with you, your deep physical understanding was of great help for me. Thank you for genuinely listen to my ideas even if they turned out to be non-sense at the end. More importantly, I want to sincerely thank you for the freedom you granted me to pursue whatever I had in mind - even if it had little to do with my thesis work. I believe at some point you must have regretted telling me: "Es geht mir bei Doktorarbeiten nicht um wissenschaftliche Erkenntnisse, sondern um Persönlichkeitsentwicklung." The discussions about politics and the rest of the world apart from solar cells were just as enlightening as our scientific ones. Thank you!

Prof. Kirchartz for always having time to teach me anything from photons and phonons to huge solar modules and never laughing at my questions. Thank you for your support and your endurance in our lengthy discussions. I also admire your passion for academic topics, it

was a great motivation for me. It was great to hear your point of view on academic life and see the world through your eyes every once in a while.

Prof. Deibel for the correction of my thesis, the pleasant atmosphere during my defense and for always answering my mails within seconds.

TCM² for the excellent initial training in the lab and help with ASA. It was great having you there during the first year of my thesis, even though your empty desk really intimidated me in the beginning :).

Stephan for the smile you put on my face every single day that we shared the office. Thank you for accepting me into your holy office after Caro left ;) Also, thank you for the great time we spend together and for being a true womanizer :D.

The "Organic Group" for your hospitality to the doctoral student without a home. It was a pleasure to be part of the "journal club" and see beyond the scope of my work.

Yael for the great, open and deep conversations we had. A special thanks for your help with my presentations, your remarks were frequently real eye-openers.

Markus for your support in the optics lab. Your expertise and patience with the little photons were of great help to me.

David for the last months in the common office, for sharing your thoughts with me and listening to mine.

Bart for helping me to improve my writing skills - even though I am still far from being at your level. Thank you for helping me to sort out many modeling problems that I ran into.

Florian for the great time we had together every day on our way to the institute and back. A huge thank you also goes to everyone that gave me a ride during my time in Jülich. Thank you for helping me avoid the strenuous ride with public transportation to Bugra, Tina, Marzella, Tsveti, Michael, Ulli, Jan, David, and some "strangers" from the research center that gave me rides in the middle of the night, when nobody from the institute was there anymore.

Thank you to the "Kicker" people, who made my break over and over again, especially to Gunnar for his unforgettable style of play, hilarious comments and always being up for an extra session. Special thanks go to everyone who was behind me in the highscore list :P

Dr. Köster for making HITEC what it was for me, a great platform to connect with PhD students from different institutes and a great opportunity to gain valuable experience for life and my professional career.

I want to thank all PhD students at the institute (and even some PhDs from other institutes).¹ It was a blast with you there and I really enjoyed coming to the institute and sharing the good and bad times with you. It helped me immensely that there was always somebody who seemed to be going through the same ups and downs as I was :) I will never forget the summer schools and conferences that we went to together. My thank you goes also to all the technicians.¹ You did a fantastic job, I would have been completely screwed without you.

Last but not least, I want to thank my family. Thank you Paolo for proof-reading and even more important pushing me over the finish line :D, thank you Raél for letting me sleep the night before my defense and thank you to my parents who weren't really fond of the idea of me doing a PhD but were and are always there for me.

¹I started to name you here but I was afraid that I would forget someone and that I'd regret it later. So I decided to go the easy way and not name anyone.

Band / Volume 508

Solar driven water electrolysis based on silicon solar cells and earth-abundant catalysts

K. Welter (2020), iv, 165 pp

ISBN: 978-3-95806-495-9

Band / Volume 509

Electric Field Assisted Sintering of Gadolinium-doped Ceria

T. P. Mishra (2020), x, 195 pp

ISBN: 978-3-95806-496-6

Band / Volume 510

Effect of electric field on the sintering of ceria

C. Cao (2020), xix, 143 pp

ISBN: 978-3-95806-497-3

Band / Volume 511

Techno-ökonomische Bewertung von Verfahren zur Herstellung von Kraftstoffen aus H₂ und CO₂

S. Schemme (2020), 360 pp

ISBN: 978-3-95806-499-7

Band / Volume 512

Enhanced crosshole GPR full-waveform inversion to improve aquifer characterization

Z. Zhou (2020), VIII, 136 pp

ISBN: 978-3-95806-500-0

Band / Volume 513

Time-Resolved Photoluminescence on Perovskite Absorber Materials for Photovoltaic Applications

F. Staub (2020), viii, 198 pp

ISBN: 978-3-95806-503-1

Band / Volume 514

Crystallisation of Oxidic Gasifier Slags

J. P. Schupsky (2020), III, 127, XXII pp

ISBN: 978-3-95806-506-2

Band / Volume 515

Modeling and validation of chemical vapor deposition for tungsten fiber reinforced tungsten

L. Raumann (2020), X, 98, XXXVIII pp

ISBN: 978-3-95806-507-9

Band / Volume 516

Zinc Oxide / Nanocrystalline Silicon Contacts for Silicon Heterojunction Solar Cells

H. Li (2020), VIII, 135 pp

ISBN: 978-3-95806-508-6

Band / Volume 517

Iron isotope fractionation in arable soil and graminaceous crops

Y. Xing (2020), X, 111 pp

ISBN: 978-3-95806-509-3

Band / Volume 518

Geophysics-based soil mapping for improved modelling of spatial variability in crop growth and yield

C. Brogi (2020), xxi, 127 pp

ISBN: 978-3-95806-510-9

Band / Volume 519

Measuring and modelling spatiotemporal changes in hydrological response after partial deforestation

I. Wiekenkamp (2020), xxxvii, 276 pp

ISBN: 978-3-95806-512-3

Band / Volume 520

Characterization of Root System Architectures from Field Root Sampling Methods

S. Morandage (2020), xxii, 157 pp

ISBN: 978-3-95806-511-6

Band / Volume 521

Generation Lulls from the Future Potential of Wind and Solar Energy in Europe

D. S. Ryberg (2020), xxvii, 398 pp

ISBN: 978-3-95806-513-0

Band / Volume 522

Towards a Generalized Framework for the Analysis of Solar Cell Performance based on the Principle of Detailed Balance

B. J. Blank (2020), iv, 142 pp

ISBN: 978-3-95806-514-7

Weitere *Schriften des Verlags im Forschungszentrum Jülich* unter
<http://wwwzb1.fz-juelich.de/verlagextern1/index.asp>

Energie & Umwelt / Energy & Environment
Band / Volume 522
ISBN 978-3-95806-514-7

Mitglied der Helmholtz-Gemeinschaft

